DYNAMIC BEHAVIOR OF REINFORCED CONCRETE FRAMES WITH INFILL WALLS

A Thesis Submitted to
the Graduate School of Engineering and Sciences of
İzmir Institute of Technology
in Partial Fulfillment of the Requirements for the Degree of

MASTER OF SCIENCE

in Structural Mechanics

by
Mehmet Alper ÇANKAYA

June 2011

İZMİR

We approve the thesis of **Mehmet Alper ÇANKAYA**

Assist. Prof. Dr. Cemalettin DÖNMEZ
Supervisor

Assoc. Prof. Dr. Murat Altuğ ERBERİK
Committee Member

Assist. Prof. Dr. Gürsoy TURAN
Committee Member

27 June 2011

Prof. Dr. Gökmen TAYFUR
Head of the Department of Civil Engineering

Prof. Dr. Durmuş Ali DEMİR
Dean of the Graduate School of Engineering and Sciences

ACKNOWLEDGEMENTS

This research project was financially supported by Scientific and Research Council of Turkey (TÜBİTAK). I would like to express my sincere gratitude for the support provided.

I would also like to express my gratitude to Izmir Institute of Technology (IYTE) without its infrastructure thesis work would have been a distant reality.

It is an honor for me to have worked with my supervisor Assist. Prof. Dr. Cemalettin DÖNMEZ. He has made available his knowledge and helped me throughout this project and thesis study.

I would like to thank the members of thesis defense committee Assoc. Prof. Dr. Murat Altuğ ERBERİK and Assist. Prof. Dr. Gürsoy TURAN for their advices and helps in reviewing my thesis.

I would also like to thank my colleagues at the Department of Civil Engineering and all of those who helped me in anyway during the completion of the project.

Lastly, I owe my deepest gratitude to my parents and family who have given me the opportunity of an education and support throughout my life.

ABSTRACT

DYNAMIC BEHAVIOR OF REINFORCED CONCRETE FRAMES WITH INFILL WALLS

Current practices utilize infill walls as insulation or partition material but not as a structural material. The main reason for this choice is the complexity of the partition wall-frame interaction behavior. Therefore infill walls typically ignored in the structural designs. However, existence of partition walls heavily effect stiffness, strength and behavior of structures.

The main purpose of the presented study is the investigation of the dynamic parameters of reinforced concrete frames with and without infill walls. Moreover, lateral strength, stiffness and energy dissipation properties of the frames are also studied. In order to achieve the purpose four planar, one-bay, four story RC frames with 1/5 scale are designed, constructed and tested. In the frames main parameters are selected as presence of partition walls and ductile/non-ductile reinforcement detailing. Experiments are consisted of static and dynamic tests. In static tests each frame subjected to lateral loads that were applied at the each story level to provide a lateral loading increasing with height. Lateral load levels were controlled by the drift levels in the first story. Dynamic tests were performed at the end of each deformation level and modal analysis methods are utilized. Analyses have shown that existence of partition walls in the frame increased the natural frequencies of the frames. However, reinforcement detailing did not have a significant effect on natural frequencies. It is also observed that the natural frequencies of the frames decreased with increasing damage level. On the other hand, presence of partition walls effected the damaged behavior of the frames and drift is observed to concentrate to the first story with the increasing level of damage. And finally stiffness, strength and energy dissipation properties of frames with partition walls are observed to be dramatically higher than the frames without partition walls.

ÖZET

DOLGU DUVARLI BETONARME ÇERÇEVELERİN DİNAMİK DAVRANIŞI

Günümüzde dolgu duvarlar tipik olarak izolasyon ve bölme duvarı olarak kullanılmaktadırlar. Dolgu duvar-çerçeve etkileşimindeki göreli karmaşıklıktan dolayı da çoğunlukla yapısal tasarım esnasında hesaplamalarda yer almazlar. Ancak dolgu duvarlar bulundukları yapının rijitliğini, yanal dayanımını ve dinamik özelliklerini önemli ölçüde değiştirmektedir.

Bu çalışmanın ana amacı dolgu duvarlı/duvarsız betonarme çerçevelerin dinamik parametrelerinin araştırılması ve dinamik davranış üzerindeki etkisinin incelenmesidir. Ayrıca bu çalışmada çerçevelerin yanal kapasite, sıkılık ve enerji sönümleme özellikleri de incelenmiştir. Bunun için 1/5 ölçekli, tek açıklıklı ve dört katlı dört adet betonarme çerçeve tasarlanmış, üretilmiş ve test edilmiştir. Çerçevelerdeki dolgu duvarların varlığı/yokluğu ve sünek/gevrek donatı detayı değişkenler olarak seçilmiştir. Statik testler sırasında tüm çerçeveler tersinir yanal yüklemelere maruz bırakılmıştır. Yükleme her kat seviyesinden yapılmış ve bina yüksekliğinde ters üçgen şeklinde bir dağılım oluşturulmuştur. Herbir yanal yükleme seviyesi birinci katta önceden belirlenmiş ötelenmeleri oluşturacak şekilde elde edilmiştir. Dinamik testler ise herbir yükleme grubundan sonra uygulanmış ve elde edilen veriler modal analiz yöntemiyle işlenmiştir. Analizler sonucunda dolgu duvarlı çerçevelerin doğal frekanslarının arttığı gözlemlenmiştir. Ancak donatı detayının gevrek veya sünek olarak değişmesi doğal frekanslarda önemli bir değişime sebebiyet vermemiştir. Diğer taraftan dolgu duvarın varlığı hasar görmüş çerçevenin davranışını değiştirdiği gibi ötelenmelerin de birinci katta yoğunlaşmasına neden olmuştur. Son olarak dolgu duvarlar çerçevenin yanal dayanım, rijitlik ve enerji sönüm kapasitelerinde dikkate değer artışlara neden olmuşlardır.

TABLE OF CONTENTS

LIST OF FIGURES

LIST OF TABLES

Figure **Page**

CHAPTER 1

INTRODUCTION

1.1. General

Brick wall as a structural member lost its structural importance in modern times and is in use as partition and/or insulation material in various forms. Decision of its use and design is mainly under the control of the architects. Typically structural engineers do not consider partition walls as a structural member of the buildings in their calculations. Therefore interaction of partition wall with the bounding frame is usually ignored in design. The aim of the study presented in this thesis is the experimental investigation of the structural frame/partition wall interaction in RC frames for the purpose of defining implications of hybrid system on dynamic behavior and identification of the dynamic parameters.

Partition walls are composed of relatively stiff, brittle and strong bricks and the weak mortar. Strength of combination strongly depends on the weak mortar. The quality control of the partition walls is very low in most applications. Mortar is generally hand mixed at the site and main parameter of mix design is the workability. Bricks are produced at the brick kilns. There is a rich variety of raw materials and geometries and no well defined boundaries about its geometrical and mechanical properties. TS EN 771-1 is the standard that defines the requirement about the bricks in Turkey but quality control is typically low. Other aspect of the brick walls strength is the workmanship of the construction which is highly dependent on the available labor quality. As a whole it is very difficult to quantify the quality and mechanical properties of partition walls.

Partition walls function as vital elements for the service of the structures. Even if the loss of the partition does not cause any structural problems, it might stop the service. Also it could cause serious life safety implications. Therefore, understanding the behavior of partition walls in extreme conditions is very important.

Inherent geometry of the partition walls leads to a weak out of plane and strong in plane stiffness and strength. Due to the high in plane stiffness, partition walls could resist high loads at very small deformations. When partition walls are integrated with

the RC frames, high in plane stiffness results to high force levels in the walls at small drift levels, however, its brittle character causes loss of its resistance before the structural frame reach to its capacity. This condition can effect the mode of failure in the structure. Structural frame and partition wall interaction can induce brittle shear failures by converting RC columns to short columns; moreover partition walls may strengthen the upper stories of a building and may result with soft story mechanism at the first story which is an undesired event under earthquake loading. Opposite to these disadvantages, some researchers (Fajfar and Dolsek, 2008) mention that if partition walls are properly evaluated in design process and distributed throughout the structure, it is generally advantageous for the seismic response of structure.

Due to difficulty in rationalizing the interaction with the frame and partition walls, they are not considered as a part of the horizontal load resisting of system in the conventional design processes of frame structures. Turkish Earthquake Code '07 assumes that partition walls do not make any contribution to the behavior of structural frames. There are references to the partitions only in two sections (Section 2.3 and 7F). One of them is about the strength irregularity between the floors and other is the usage of partitions for strengthening purposes. Some studies show that disregarding the effect of partitions on the structural behavior is not always safe (Negro and Colombo, 1996). A rational approach to estimate when it is safe to disregard and when it is not, must be developed. Moreover, uses of such simplified design approaches do not estimate the level where the damage in the masonry infill wall occurs, this might be important in terms of non-structural damages.

1.2. Background Study

Effects of partition walls have been investigated by many researchers over the last fifty years. However, there is no consensus provided yet. Most of the work done is concentrated on lateral stiffness, strength and energy dissipation concepts.

Mehrabi et al. (1996) tested twelve 1/2 scale, single story, and one bay frame specimens. In this study, two types of frames were designed. These were weak frames with non-ductile reinforcement detailing and strong frames with ductile reinforcement detailing. Strong frames had an aspect ratio of 1/1.5 while the weak frames had 1/1.5 and 1/2. Material types of the partition walls were also evaluated as parametric

variables. Therefore, two different types of partition walls were employed. These are strong and weak partition walls. Strong partition wall was referred to the partition wall with hollow concrete masonry blocks and weak partition wall was referred to the partition wall with solid concrete masonry blocks. As the last parametric variable, monotonic and cyclic loading histories were chosen. It is reported that, the first major cracks in the partition walls took place at a drift ratio between 0.17% and 0.46%. This cracking level of partition walls were called as serviceability limit in the study. Another observation was made about the lateral load level. According to study, the frames with partition walls exhibit a higher maximum lateral load level than that of bare frames. On the other hand, at lateral resistance level of 80% drop from the maximum resistance, drift ratio varied 1% to 2% for all the frames. This level of drift was considered as ultimate limit state of frames with infill walls. It is also reported that the specimens with weak frames and strong partition walls exhibited brittle shear failures in columns. However, these cases occurred at relatively large drift levels, which were mostly beyond 1%. The fundamental disadvantages of this kind of severe shear cracks in columns are the instability risk and irreparable damage. Lastly, it is mentioned that specimens with weak frame and strong partition walls exhibited a good energy dissipation compared to the weak frame with weak partitions. As a conclusion, it is emphasized that if the frame is properly designed for strong seismic loads, partition walls have a beneficial influence on its performance. It is also noted that, partition walls may be used to improve the performance of existing non-ductile frames.

Negro and Colombo (1996) performed a series of pseudo-dynamic tests on a full scale, 4 stories RC building which was detailed with ductile reinforcement. Three different partition wall configurations were applied on the same frame. First test was performed on the bare frame, second test was performed on uniformly infilled frame and third test was performed by leaving the first story empty to lead to a soft-story mechanism. Results of experimental tests indicated that, uniformly distributed partition walls caused a 50% increase in base shear while structure with soft story had a small increase of base shear than that of the bare frame. Moreover, the bare frame hysteresis curves exhibited stable dissipative loops with decreasing amplitude from bottom to top stories. It is also reported that after the first large amplitude cycle, pinching was developed in the hysteresis curves. As the reason of the pinching effect in the hysteresis curves, material non-linearity is shown. In the hysteresis curves of uniformly infilled frame, amplitudes of cycles also exhibited similar dissipative loops with the bare frame.

However, severe stiffness and strength degradations could be observed in the hysteresis curves of uniformly infilled frame unlike the bare frame. For the structure with soft story, energy dissipation is almost limited to the first story movement. In the study, inter-story drift ratios are also investigated. Bare frame inter-story drift at the first story was obtained to be more than twice than that of the uniformly infilled frame. Maximum inter-story drift ratio reached a value of 3.5% for the same story in soft story case. In the study, dominant frequencies of frames are calculated by stiffness matrices. Before the each dynamic test, first mode frequencies were found to be 1.78, 3.30 and 1.66Hz for the bare, uniformly infilled and soft-story frames respectively. This shows that the presence of non-structural partition walls causes a change of dominant frequencies of system. Related with the frequency change, a stiffness change also occurs. The study is concluded by evaluation of the increase in stiffness, strength and energy dissipation as positive sides of the partition walls. However, irregular distribution of partition walls is shown as a reason of the unacceptable high ductility demands in frame.

Mosalam et al. (1997) conducted a series of quasi-static experimental investigation of non-seismic designed, steel frames, with partition walls. In this study number of bays, opening conditions and relative strength of infill and mortar were the variable parameters. According to test results, compressive strength of infills has an important effect on the mode of failure of infill panels. Stronger partition blocks caused mortar cracking and weaker blocks caused corner crushing. Results also showed that, even though the ultimate capacity for the two-bay specimen was almost twice the capacity of the single-bay specimen, the initial stiffness was just 1.7 times greater. It was also observed that, initial stiffness of a frame with partition was reduced almost 50% after partition wall cracking.

Lee and Woo (2001) investigated the seismic performance of a, 1/5 scale, 2 bay, 3 story RC frame. The study is conducted on the same frame by organizing the partition wall configuration as bare frame (BF), partially infilled frame (PIF) and fully infilled frame (FIF). The tests were consisted of two categories. These were dynamic and static test categories. Dynamic tests were performed to determine the realistic responses of an RC frame with partition wall and non-seismic detailing under simulated ground motions. The implemented peak ground acceleration levels were varied between 0.12g to 0.4g during the dynamic tests. Natural frequencies of the FIF, PIF and BF models were detected by the free vibration tests. These were obtained as 0.06s, 0.17s and 0.23s of the FIF, PIF and BF respectively. For the 0.4g base accelerations, first story inter-

story drift ratios of FIF, PIF and BF models were obtained as 0.19%, 0.51% and 1.68% respectively. On the other hand, from the obtained hysteresis curves maximum stiffness was obtained as 117 kN/mm for the FIF model. It was 31.4 kN/mm and 4.21 kN/mm for PIF and BF models respectively. Similarly, FIF model experienced the highest base shear. According to study, FIF model absorbed the highest energy than other two models. Between the other two frames, PIF model absorbed less energy than BF. This is explained by yielding of BF model. Afterwards, static test were performed to obtain the ultimate capacities of the BF and PIF models. Moreover, pushover analysis was also performed by a computer program solely for the bare frame, in order to compare BF pushover curves. Initial stiffness of analytical result was found to be higher when ultimate strength was lower than the test results. The reason of change in the pushover curve parameters is explained by the high damages occurred in the frame after the earthquake simulation tests. During the pushover tests, roof drift of PIF model reached 43.1mm which is equal to 1.94% drift ratio. This value reached 2.1% for the BF model which was obtained by analysis. A base shear comparison is also reported. According to the results reported, PIF model reached base shear levels that were 2.5 times greater than BF model. Study is concluded with a discussion of advantages and disadvantages of masonry infill. Reduction of global lateral displacement capacity and dependence of the quality to the workmanship are reported as the disadvantages. And in comparison to the increase in strength with partition walls the small increase in earthquake inertia forces is reported to be the advantage.

Al-Chaar et al. (2002) conducted an experimental program to investigate the behavior of non-ductile frames with and without partition walls. For this purpose five 1/2 scale, one story frames with varying number of bays were tested. These frames were subjected to in-plane monotonic loading program and were reached to a maximum of 9% story drift ratios. Moreover, two types of infill materials were used. These were concrete masonry unit (CMU) and brick infill. It is reported that, shear cracks in columns first observed about 1% of drift ratio in single bay models. However, same event occurred at a drift ratio less than 1% in the frames with multiple bays. It is also reported that first major cracks in the infill walls was observed at a drift ratio less than 1% for all of the frames. An important observation was made from the obtained load-deflection curves. In the frames with multiple bays a serious load reduction was occurred after the peak capacity of each frame is being exceeded. Stiffness of the single bay frames were reported to be 24 and 18 times stiffer than the bare frames while

multiple bay frames were 35 and 40 times stiffer respectively. Lastly, observed modes of failures were reported. Bare frame failed from a brittle failure due to the shear cracks occurred in the beam column joint zones and top/bottom regions of columns. Frames with CMU partition walls experienced frictional (sliding-based) and corner crush failure modes. It was caused by the low compressive strength/high shear strength ratio of CMU walls. On the other hand, failure mode of one bay frame with brick infill wall occurred in the compression strut form. However, failure mode of multiple bay frame with brick infill wall differed from compression strut model. Frictional failure mode was observed in the multiple bay frame with brick infill walls. As the reason of the change, collective behavior of bays as shear wall is shown in the multiple bay frame with brick infill walls.

Pujol and Fick (2010) conducted tests on a three story full scale flat plate structure which was designed to resist gravity loads only. The purpose of the study was to investigate the possible positive and negative effects of the partition walls. Therefore, the study was concentrated on the response of full scale RC frame with and without partition walls. In this report response was assessed by strength, stiffness and displacement capacity of the system. For this purpose tests were performed in two categories. First, the structure was loaded by in-plane cyclic loading by six hydraulic actuators as a bare frame. Four different displacement levels were applied. These were 0.22%, 0.45%, 1.5% and 3% roof drift ratios respectively. When roof drift ratio reached 2.8%, punching shear failure occurred in a column-slab connection region of the third story floor and then at 3% drift ratio test was stopped. At this stage maximum base shear was obtained as 68.1 tons. In second phase, brick partition walls added into the two bays out of four bays of the frame. Considering the presence of partition walls, loading program was modified. According to this program, two cycles were applied at each target drift and small displacement increments were chosen for consequent loading cycles. It is reported that the first cracks in the partition walls and the separation between the columns and partition walls were first observed at a roof drift ratio of 0.15%. At 1%, crack widths reached 10mm and cracks became visible in all of the story panels. Test was stopped at a drift ratio of 1.75% because of the concerns about the stability of the slab where a punching shear failure occurred during the first test. It is mentioned that partition walls increased the initial stiffness of frame system by 500% and the base shear by 100%. These increases sustained up to roof drift ratios as high as 1.5%. At the end, it is concluded that partition walls can be expected to help control

inter-story drift, provided that measures are taken to prevent out-of-plane failure of the infill and the shear failure of the columns.

1.3. Objective and Scope

An experimental study is conducted at the Structural Mechanics Laboratory of Izmir Institute of Technology (IYTE). The main objective is to investigate the dynamic behavior of gravity only and seismically detailed RC frames with and without partition walls when subjected to pseudo-static loading. Other objectives are to examine the stiffness and strength behavior of RC frames with partition walls, to observe the interaction between frame and infill wall under pseudo-static loading, and the energy dissipation characteristics.

Experimental program consisted of testing of four 4-story frames. Frames were designed considering two parameters: reinforcement detailing and the presence of infill walls. Reinforcement detailing was based on providing or not providing the ductility to members of the frame. Brittle reinforcement detailing was based on the old insufficient Turkish practice and ductile reinforcement detailing was based on the Turkish Earthquake Code, 2007. Considering the physical limits of the laboratory and the goals of the study frames were designed to be 1/5 scale, one bay, four story structures.

Frames were subjected to in-plane pseudo-static loading with increasing intensity. Loading levels were controlled by the inter-story drift of the first floor and frames were loaded to have two full cycles at every drift level. After each cycle group static loading was stopped and system was subjected to impact and snap-back excitations in order to obtain the dynamic parameters of the systems.

1.4. Organization

Chapter 1: Introduction

General information for the study is presented and aim and the scope are stated. Also a brief literature review on the experimental and analytical studies of RC frames with and without partition walls is presented.

Chapter 2: Experimental study

Presentation starts with the details of RC frames such as dimensions, reinforcement detailing. The mechanical and geometrical properties of materials that the specimens are constructed follow. Later static and dynamic test setups are explained in detail. Chapter ended with a presentation of the testing procedure.

Chapter 3: Static Behavior

Chapter starts with the details of the static loading program. Load-deformation relations and observed damages follow. Afterwards behavior history of each frame is discussed in detail.

Chapter 4: Dynamic Behavior

Validity of experimental modal analysis methods are discussed, estimated frequency and modal shape information of each frame at each loading group using the experiment modal analysis procedures are presented.

Chapter 5: Conclusion and Discussion of Results

Results of the experimental study are summarized. Conclusions of the current study and the recommendations for future studies are presented.

CHAPTER 2

EXPERIMENTAL STUDY

2.1. Introduction

Four RC frames are tested. The test setup, specimen dimensions and material properties of the frames will be presented in this chapter. Discussion starts with the presentation of reinforcement and construction details. Material properties follow. The loading and measurement set up are presented afterwards. Chapter is closed with the description of the testing procedures.

2.2. Test Specimens

The physical limitations of the laboratory and static/dynamic dual purpose of the specimens enforced a 1/5 scale, one bay, four story planar frames. The main parameters of the study were the reinforcement details of the frames and the presence of the infill walls. Two different reinforcement detailing was chosen. These were typical seismically insufficient gravity detailing in Turkish practice and the ductile detailing according to Turkish Earthquake Code ’07. Insufficient details were introduced through longitudinal reinforcement splice lengths, stirrup locations, intervals and hook geometry. Infill walls were built with hollow clay tiles. Four frames were constructed based on the defined parameters. An overview of RC frames with general dimensions is presented in Figure 2.1. Geometry, construction details and the reinforcement of the frames are presented in Section 2.3. Mechanical properties of the materials used are presented in Section 2.4.

In order to obtain the response under pseudo-static cyclic loading and dynamic parameters of the system at every damage stage (cycle), the vertical load on the system is applied in the form of external masses to the system. Physical size limitations and safety concerns limited the amount of external mass added to the system. Mass amount reached to about 10% of axial load capacity in the first story columns of the specimens. The external mass layout detail can be found in Section 2.3. Considering the limitations

of the laboratory and loading behavior, an inverse triangular load profile is chosen and applied to the frames. The details of the loading setup and instrumentation for this purpose are presented in Section 2.5 and 2.6 respectively. Finally testing procedures are presented in Section 2.7.

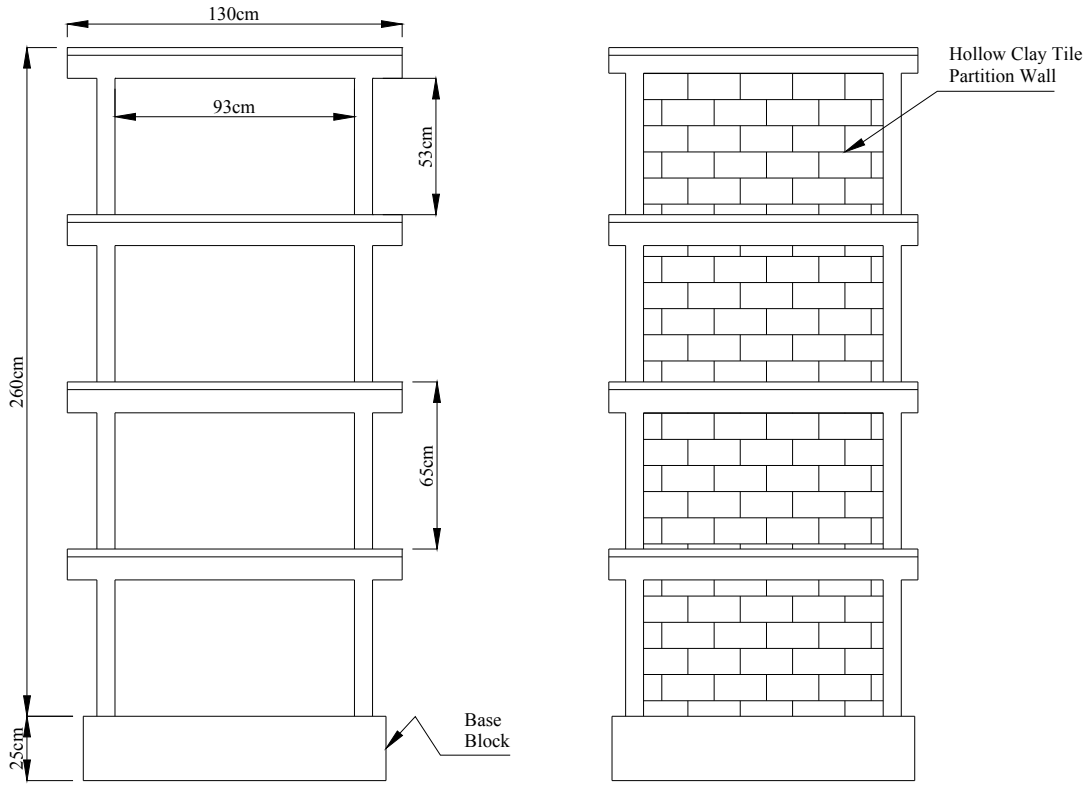

Figure 2.1. Overview of RC frames used in the tests.

2.3. Dimensions and Details of the RC Frames

Frames were designed to have slab portions at floor levels to support the added external masses, Figure 2.2. Also in order to attach the frames to the strong floor of the laboratory a thick base slab was needed, Figure 2.3. Frame was scaled in 1/5 for the geometric proportions. Regular materials were used and their shapes were not subjected to scaling. Reinforcement ratios and maximum grain size in concrete followed the code requirements. Due to the geometry of the frame, concrete was poured in upright position in a story by story order. Necessary limited volume of each batch of concrete was mixed

in the laboratory utilizing a concrete mixer. Partially constructed frame cage and the formwork are shown in Figure 2.4.

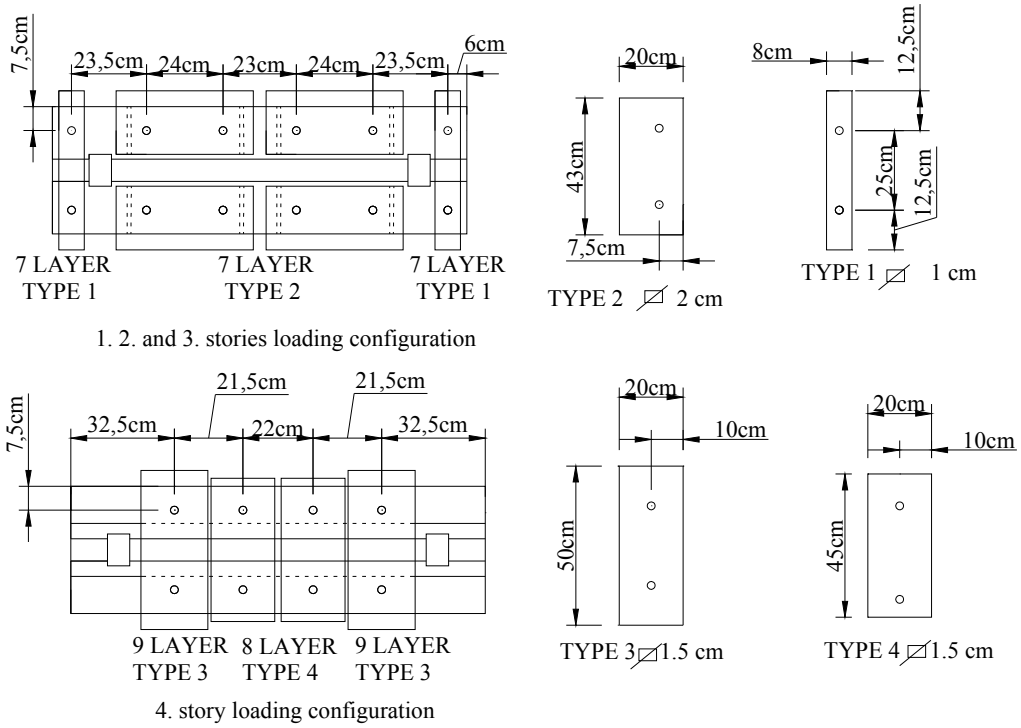

Figure 2.2. Layout of external loads on RC frames

Columns of the frames have a rectangular section, 7x10 cm. Originally beam sections were designed to have a “T” geometry with 5x12 cm web, 40x3 cm flanges. First frame was constructed with the original dimensions. Due to the concrete casting difficulties, segregation was observed. Therefore, beam dimensions were modified to 7x12 cm web and 40x3.5 cm flanges for other three frames. Column cross section and modified beam cross section of constructed frames are shown in Figure 2.3.

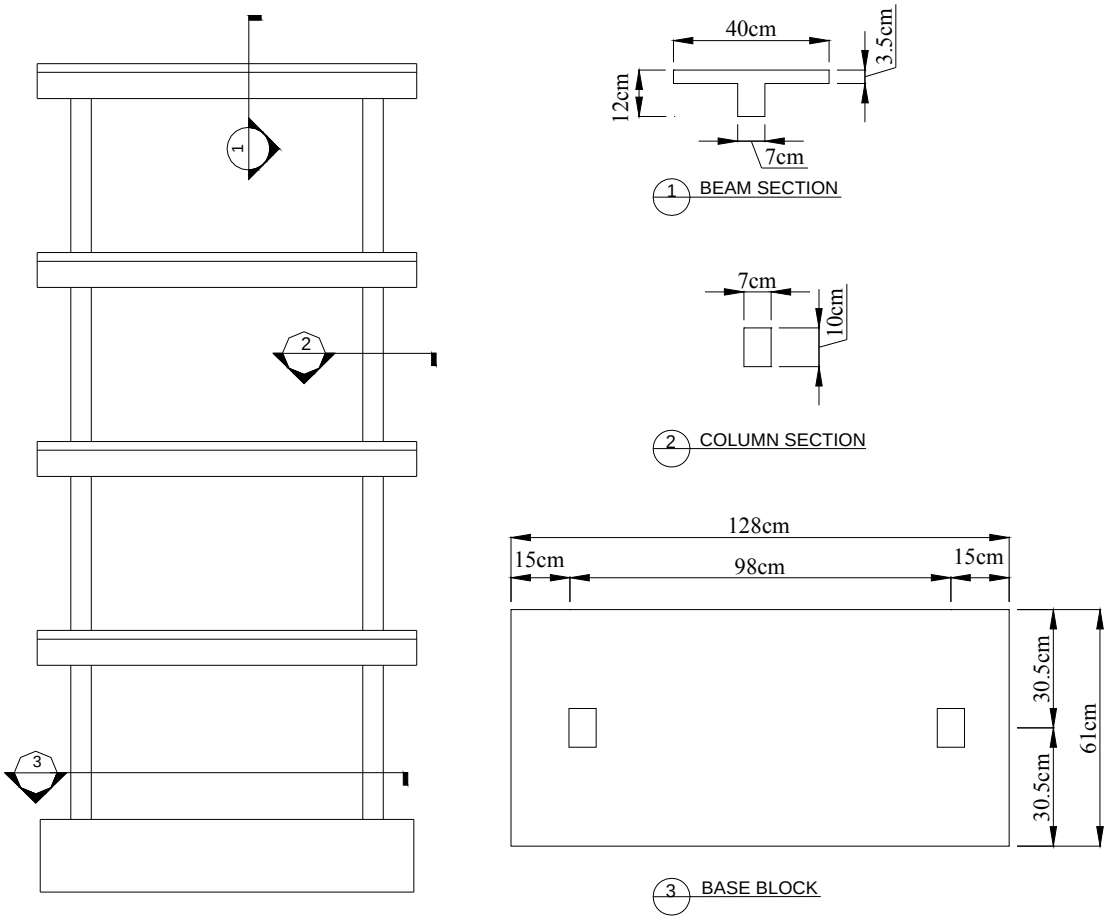

Figure 2.3. Column, beam and base block dimensions of the frames

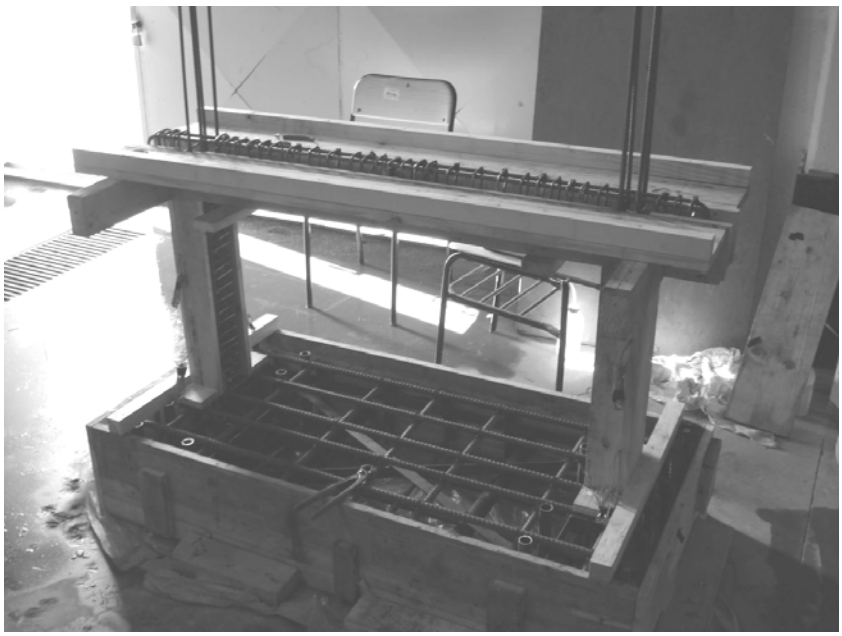

Figure 2.4. First floor cage and the formwork

Ductility of the frames was controlled by appropriate longitudinal/transverse reinforcement detailing and also by sufficient splice length for longitudinal column reinforcement. Columns and beams of all the frames were detailed with $4\phi 8$ deformed bars as longitudinal reinforcement and $\phi 5$ cold drawn plain bars, as transverse reinforcements. The location and spacing of the reinforcement are presented in Figure 2.5 and Figure 2.6 for ductile and brittle cases respectively.

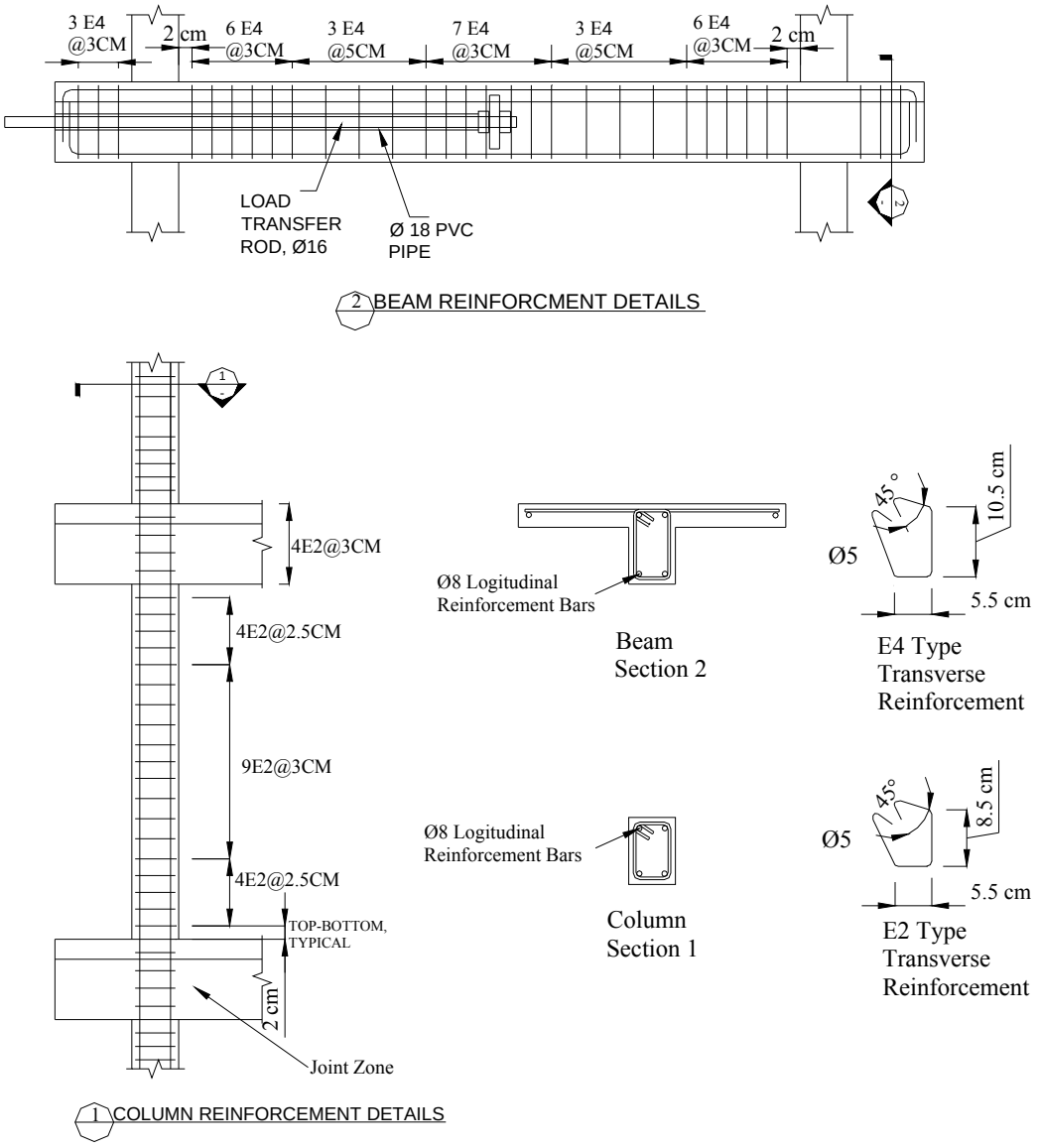

Figure 2.5. Frames with ductile reinforcement details and cross sections

As it can be observed from the figure longitudinal reinforcement of frames with ductile reinforcement detail had a single regular splice at the third floor level. On the

other hand frames with brittle reinforcement detail had splices at each floor with 25ϕ development length. Stirrups of the frames with ductile frames had less than d/2 spacing and 135º hooks. Stirrups within the joint regions were also provided. Frames with brittle reinforcement detailing had a stirrup spacing of d/2 or greater and had 90º hooks. No stirrups were provided at the joint regions.

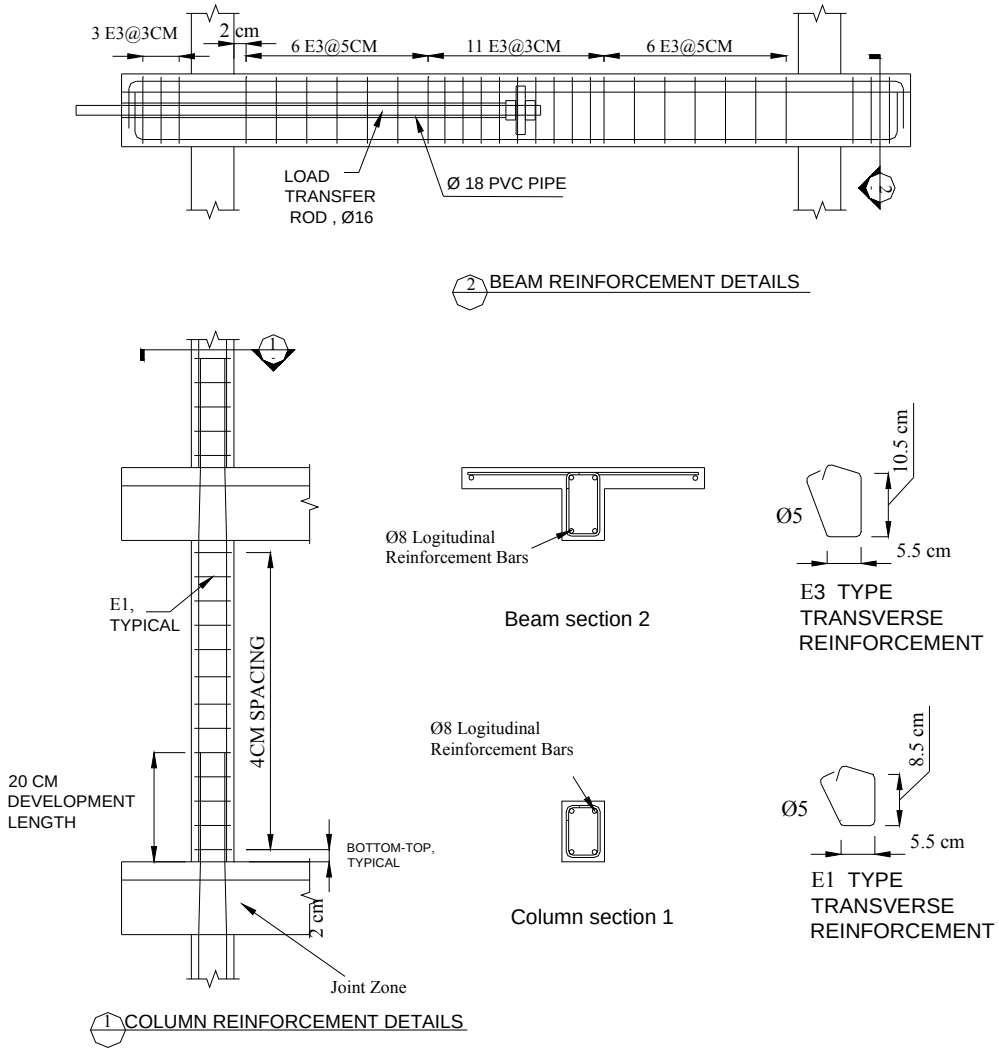

Figure 2.6. Frames with brittle reinforcement details and cross sections

Frames one and three were the frames with brittle reinforcement detailing with and without infill walls, respectively. Frames two and four were the frames with ductile reinforcement detailing with and without infill wall, Table 2.1.

Table 2.1. Frame definitions

FRAME NO	*VARIABLES*	
	Presence of Infill Walls	*Reinforcement Detailing*
1	No	Brittle
2	No	Ductile
3	Yes	Brittle
4	Yes	Ductile

Spans of the third and fourth frames were filled with hollow clay tile partition walls. Hollow clay tiles were obtained from a local supplier. Void ratio of the tiles used was about 0.5. Original size of the tiles was 13x18.5x28cm rectangular prisms. Due to the scaling, original size of the tiles were not suitable for the test frames. In order to obtain suitable tile sizes, 5.7x10x13cm rectangular prisms were cut from the original tiles. A picture of the original geometry and the cut out piece is presented in Figure 2.7. During the construction of third frame partition walls, mortar was mixed with portions 4:4:15 of cement:lime:sand respectively and for partition walls of fourth frame, mortar was mixed with portions 4:4:16 of cement:lime:sand respectively.

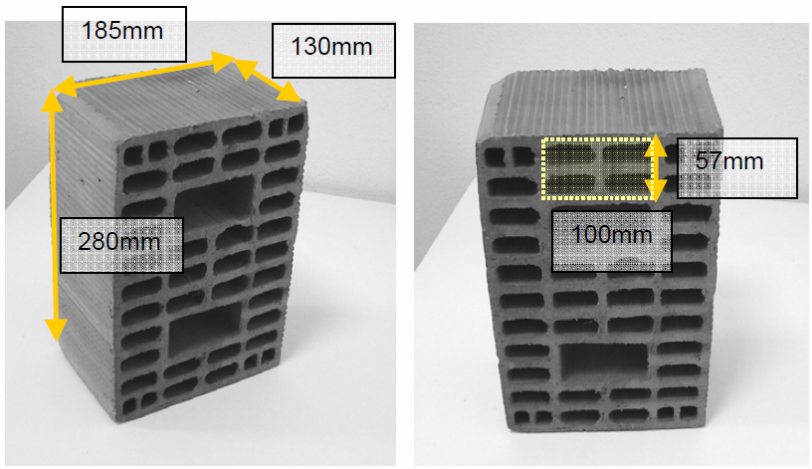

Figure 2.7. Sizes of the original hollow clay tiles and the pieces that were cut for the test purposes

2.4. Material Properties

The mechanical properties of the materials used in the experiments were obtained through material tests. Three material groups were tested: concrete, reinforcement steel and hollow clay tiles. Compressive strength of concrete was obtained by taking standard cube and cylinder specimens. Except the last frame three sets of three specimens were prepared for the frames. Two sets out of these three sets were cured in water tank and the third set was kept with the frame to have same curing conditions. One of the sets that were kept in the water tank was tested at 28^{th} day. Other two sets were tested at the day of the experiment. Six specimens were taken for the last frame. All the specimens were tested in the day of experiment. Compression tests were organized to reach to failure load in a duration of 2-2.5 minutes. Whenever applies strength values of the cube specimens were converted to equivalent cylinder values by multiplication of coefficient 0.87. Mean compressive strength results of the specimens are presented in Table 2.2.

Table 2.2. Test results of mean compressive strength of concrete groups.

DURATION	*FRAME SPECIMEN SET*			
	1	*2*	*3*	*4*
Concrete at 28^{th} Day (MPa)	27.7	26.1	27.7	-
Day of Experiment, Specimens Kept by the Frame (MPa)	42.6 (117^{th} day)	36.1 (117^{th} day)	37.1 (150^{th} day)	-
Day of the Experiment, Specimens Kept in Water Tank, (MPa)	40.1 (117^{th} day)	34.9 (117^{th} day)	35.4 (150^{th} day)	24.7 (79^{th} day)

Two types of reinforcing steel were used. $\phi 8$ deformed bars were used as longitudinal reinforcement of beams and columns and $\phi 5$ cold drawn plain bars were used as shear reinforcements. Mechanical properties of reinforcements were obtained by testing six coupons. Coupons were 30cm long and selected from the batch randomly. Test results showed that $\phi 8$ steels were S420 type defined by in TS500. Yield stresses obtained for each $\phi 8$ specimen is presented in Table 2.3 and a typical stress-strain graph is presented in Figure 2.8

Table 2.3. Measured yield stresses of $\phi 8$ deformed bars

	STEEL SPECIMEN NO					
	1	*2*	*3*	*4*	*5*	*6*
Yield Stress (MPa)	470	465	469	465	480	471

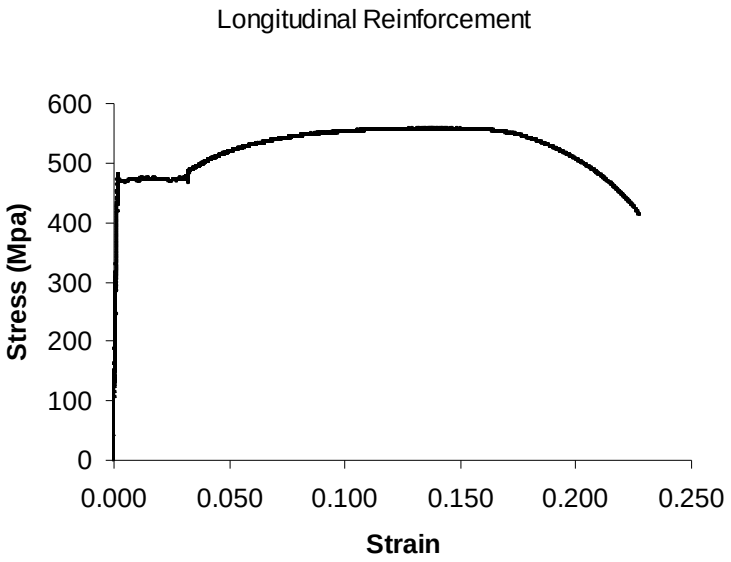

Figure 2.8. Stress-strain graph of $\phi 8$ longitudinal reinforcement steel

Tests results show that $\phi 5$ cold drawn plain bars had about 420MPa yield strength but their ultimate strain was below the code defined for cold drawn bars. Test results also show that there were two types of plain bars with different ultimate strain values. These were 2% and 6% which were below the 10% TS500 defined limits. During the tests no stirrup failure was observed, therefore it is accepted that ultimate strain limitation of the shear reinforcement did not impair the test results. Yield stresses of shear reinforcement are given in Table 2.4, stress-strain relation of both types are presented in Figure 2.9.

Table 2.4. Measured yield stresses of $\phi 5$ cold drawn plain bars

	STEEL SPECIMEN NO					
	1	*2*	*3*	*4*	*5*	*6*
Yield Stress (MPa)	419	419	430	417	421	423

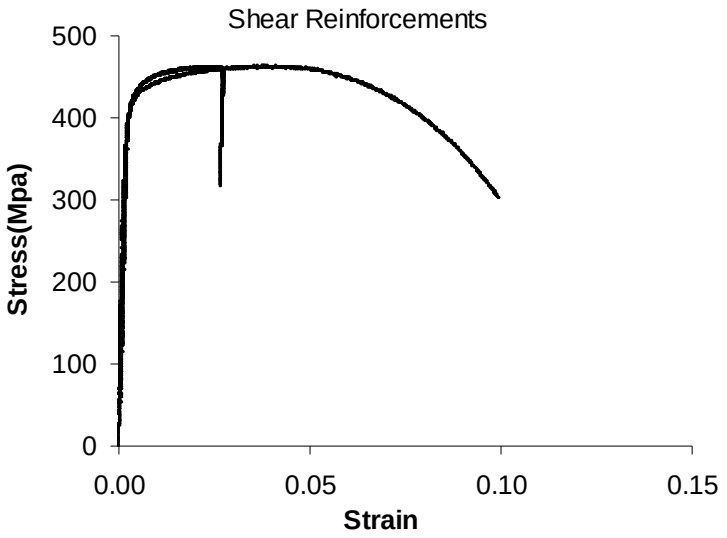

Figure 2.9. Stress-strain relation of the two types of $\phi 5$ cold drawn plain bars

Compression strength of the 3rd frame partition wall was determined by testing three samples of hollow clay tile prisms. Each prism contained two hollow clay tiles combined with mortar. Dimensions of the test specimen are presented in Figure 2.10. The prisms were subjected to axial loading along to the holes of the tiles. Strength of each sample computed on the basis of gross area. Compressive strengths were obtained as 3.6, 5.4 and 5MPa. Also the bare clay tiles were tested along and perpendicular to the holes. Samples were tested for each group. These tests resulted in strengths of 9.9, 12.4, 10.9 MPa along the holes and 6.4, 5.5, 6.1MPa perpendicular to holes. On the other hand, shear strengths of infills in the frames with the infill walls were determined by loading a wall panel in diagonal. Three panel samples for each frame were tested. Dimensions of these specimens are presented in Figure 2.10. Shear strength of the specimens were computed by dividing the failure load to the product of length of diagonal and the thickness of the panel. These tests resulted to 0.16, 0.22 and 0.47 MPa

for the 3rd and 0.86, 0.84 and 0.57 MPa for the 4th frames. Difference in the shear strength values of shear tests can be explained by variation in mortar strengths.

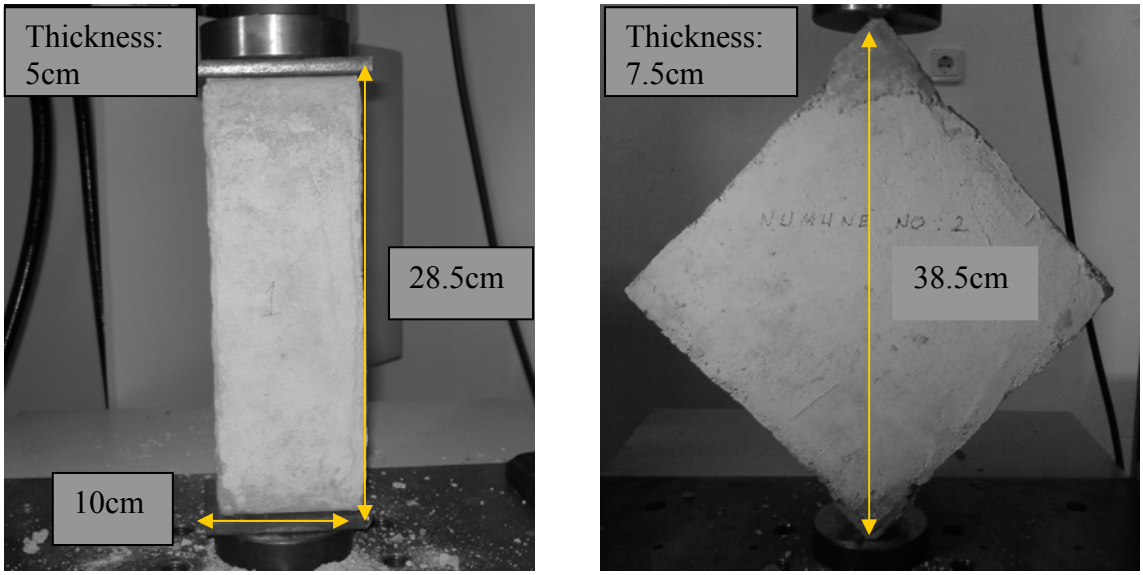

Figure 2.10. Typical dimensions of partition wall samples

2.5. Test Setup

Test setup was developed to serve for both static and dynamic experimental programs. As a result, a detachable in plane loading system was designed and constructed. Due to the heavy masses at the floor levels, a safety frame was also designed and constructed. Out of plane stability of the frames were provided by an external steel frame which was located on the safety frame. Details of the static and dynamic test setups are discussed below.

2.5.1. Static Test Setup

In order to observe the behavior of the frames under cyclic loading, a pseudo-static loading program was developed. Inverted triangle load distribution was selected as the loading profile. For this purpose a system of simply supported steel beams were designed. The loading system made it possible to apply loads proportional to the height of the loading level from the base, Figure 2.13. The load distribution mechanism was connected to the concrete frames through the ϕ16mm steel rods. In order to distribute

the loads evenly to both sides and to avoid any premature failure at the connection region, these steel rods were extended to center of the beam in a ϕ18mm PVC pipe and connected to a bearing plate within the beam, Figure 2.5.

Dynamic testing of the frames necessitated detachment of the pseudo-static loading system at every loading cycle of the frames, Figure 2.11. For this purpose the hydraulic jack was designed to connect with two hinges at both ends. During the static tests jack was stabilized by a support plate, Figure 2.12. When it was needed to perform dynamic test, connections of the load distribution mechanism to the frame and the support struts of the jack was disconnected.

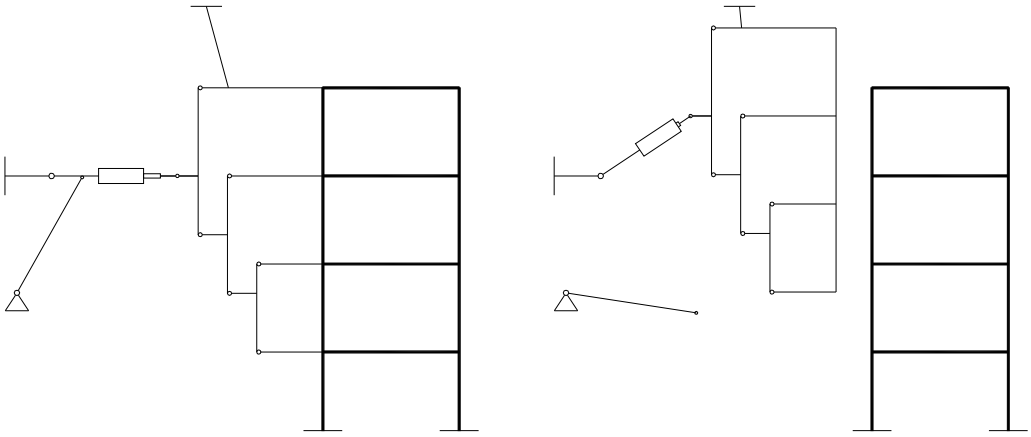

a) Lateral loading mechanism connected to the frame

b) Lateral loading mechanism disconnected

Figure 2.11. Positions of the static loading system for static and dynamic tests

On the other hand, to provide stability for out-of-plane motions; another support frame was designed which was constructed in contact with the safety frame, Figure 2.14. In order to minimize friction between the frame and support frame, teflon on teflon bearings were used at both faces of 4th story beam. Moreover, an in-plane hanging system was also designed and constructed to provide back up support to the loading mechanism in any case of emergency situation, Figure 2.12 and Figure 2.13. Same frame was also used to hold the loading mechanism while it was detached from the RC frames during dynamic testing. Details of the hanging, support and loading frames are presented in Appendix A.

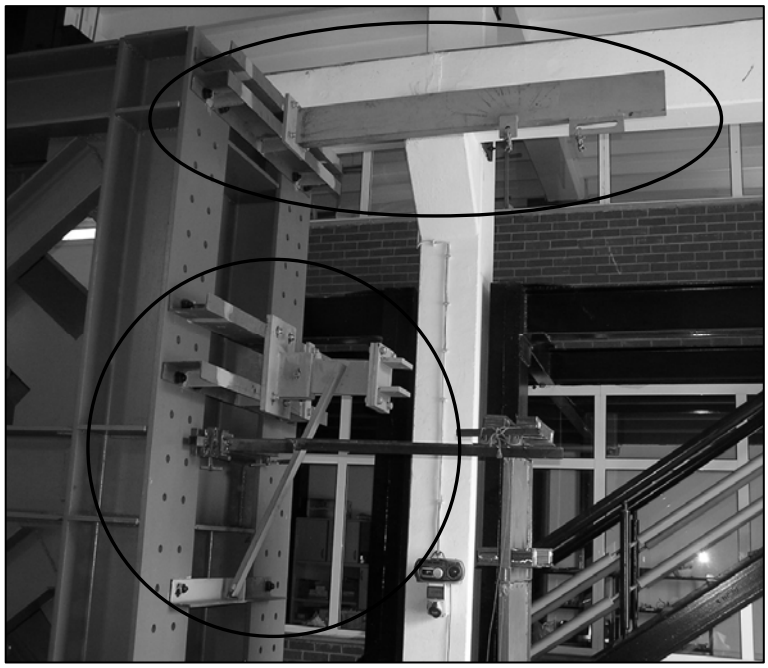

Figure 2.12. In-plane hanging frame (top) and hydraulic cylinder attachment at loading system (bottom)

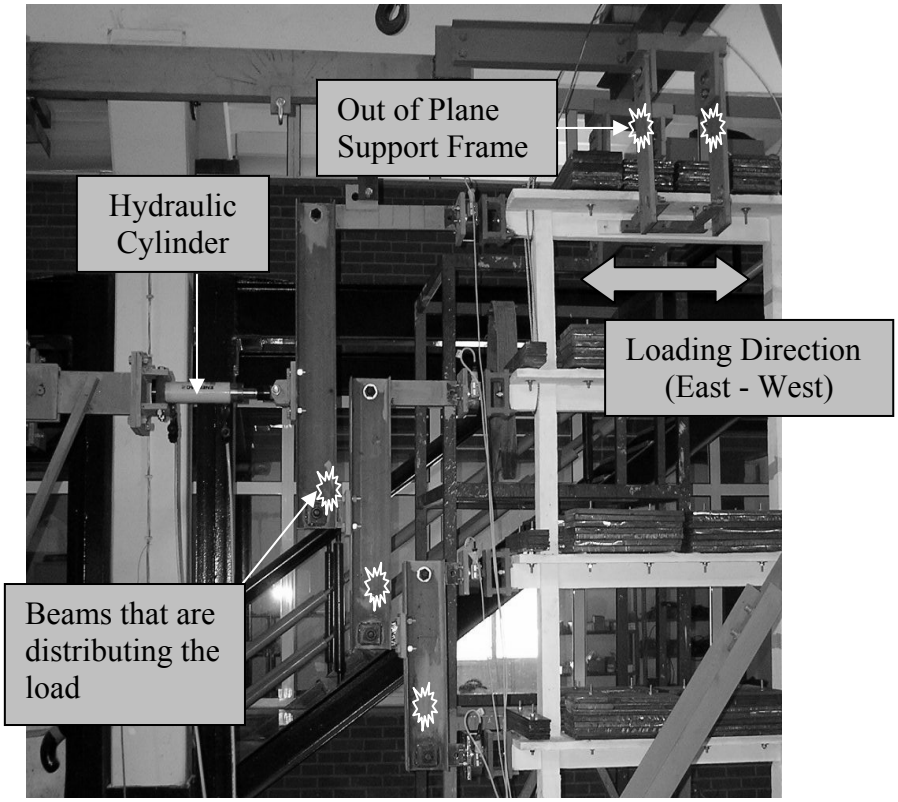

Figure 2.13. Lateral load distribution mechanism connected to hydraulic cylinder and the support frame

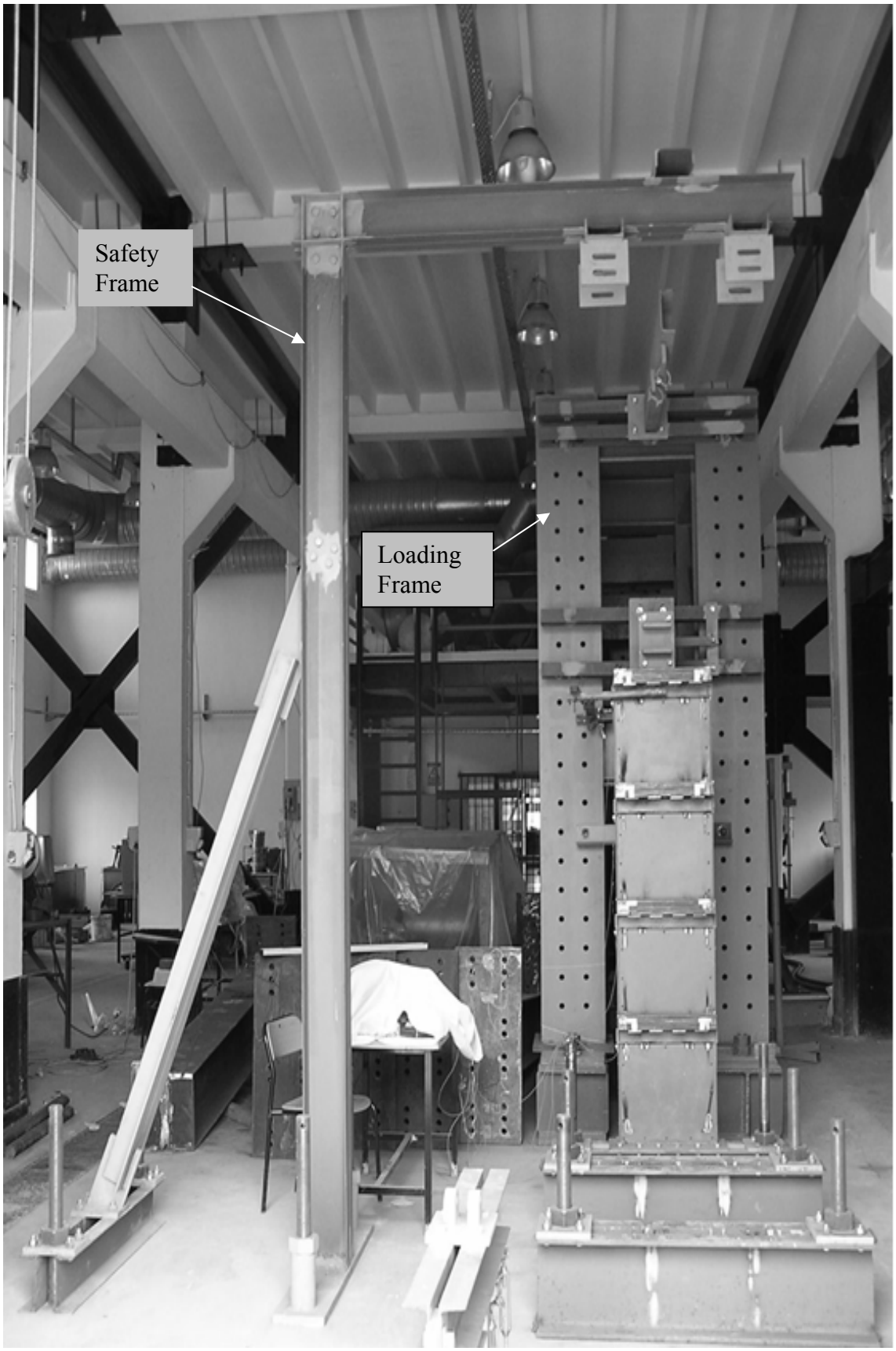

Figure 2.14. Loading and Safety frames

In order to have realistic frequencies for the frames during dynamic testing, masses were needed at floor levels. Therefore additional masses were applied to floor levels. Masses were tried to be distributed as uniformly as possible along the beam span at each story. About a mass of 420 kg was positioned at the first three stories per story and 330 kg was positioned at the last story. Steel plates were used to provide the necessary build up. In order to avoid the interference of the applied masses to the stiffness of the beams and have satisfactory attachment, masses were needed to be stationary but at the same time should be isolated from the beams. For this purpose at the first three levels six stacks of steel plates were positioned on two support lines. The connections of the plates to the frame slab were secured by ϕ10mm threaded rods through the holes in plates and the slab. Fourth level masses are applied through four stacks of plates with the same approach. Geometry, layout and the number of additional masses are presented in Figure 2.2.

2.5.2. Dynamic Test Setup

The purpose of the dynamic tests was to obtain the dynamic parameters of the frames at different damage levels. Modal testing is a common method to obtain the dynamic parameters of a system and selected as the first method to be applied. For modal testing purposes frames were excited with an impact hammer at the top level and system response was recorded through 9 accelerometers distributed along the height of the system. Mass of the impact hammer used was 11.6 kg. Considering that impact test will not provide necessary energy to force the frame into nonlinear territory, a second testing procedure was prepared. In this procedure frames were pulled by a cable at the top level to the drift levels well beyond their linear response. Later cable was cut to obtain dynamic response in the frame by the accelerometers along the height of the frame. Second type of test was called as snap-back tests. Snap-back test setup is presented in Figure 2.15.

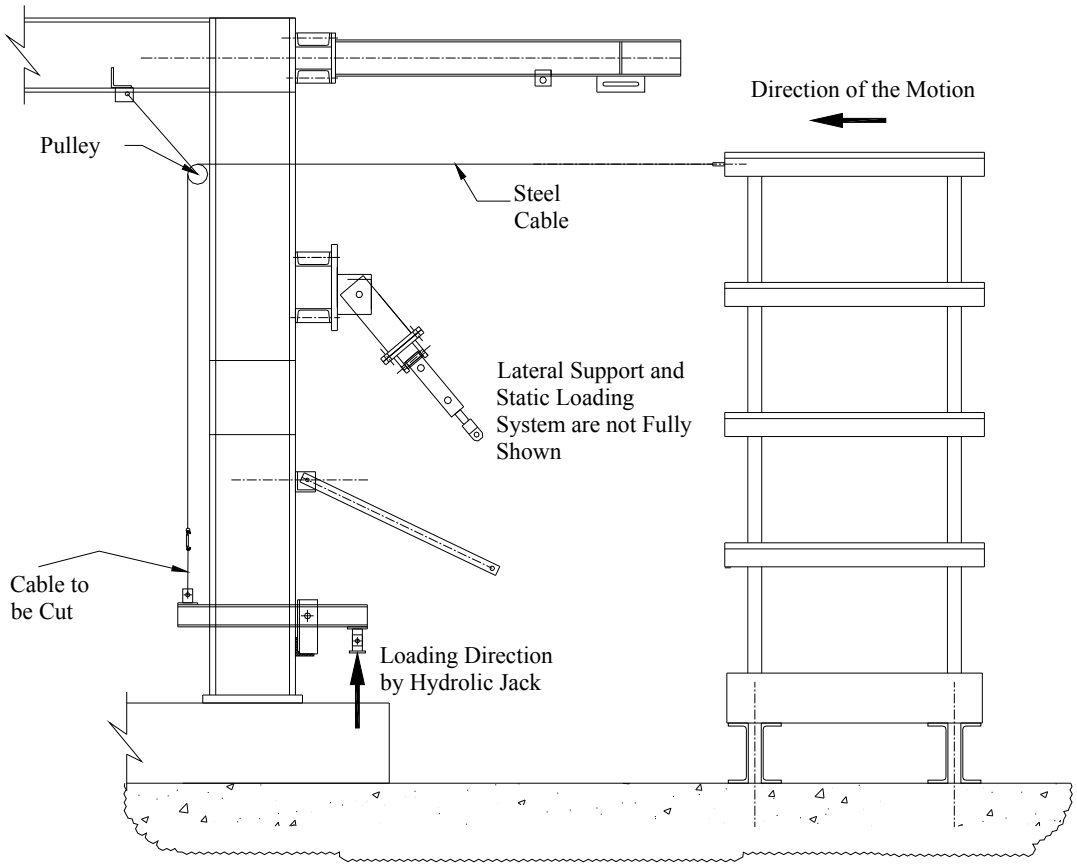

Figure 2.15. Snap-back test setup

2.6. Instrumentation of Frames

Static and dynamic dual character of the tests required two independent instrumentation sets. Static instrumentation was consisted of four resistive linear position transducers (RLPT), three linear variable displacement transducers (LVDT), four load cells and sixteen strain-gauges. Dynamic instrumentation was consisted of seven uniaxial accelerometers, two triaxial accelerometers and an accelerometer on the impact hammer. Sensors were organized through two independent data acquisition units. The instrumentation layouts of the frames were shown schematically in Figure 2.16.

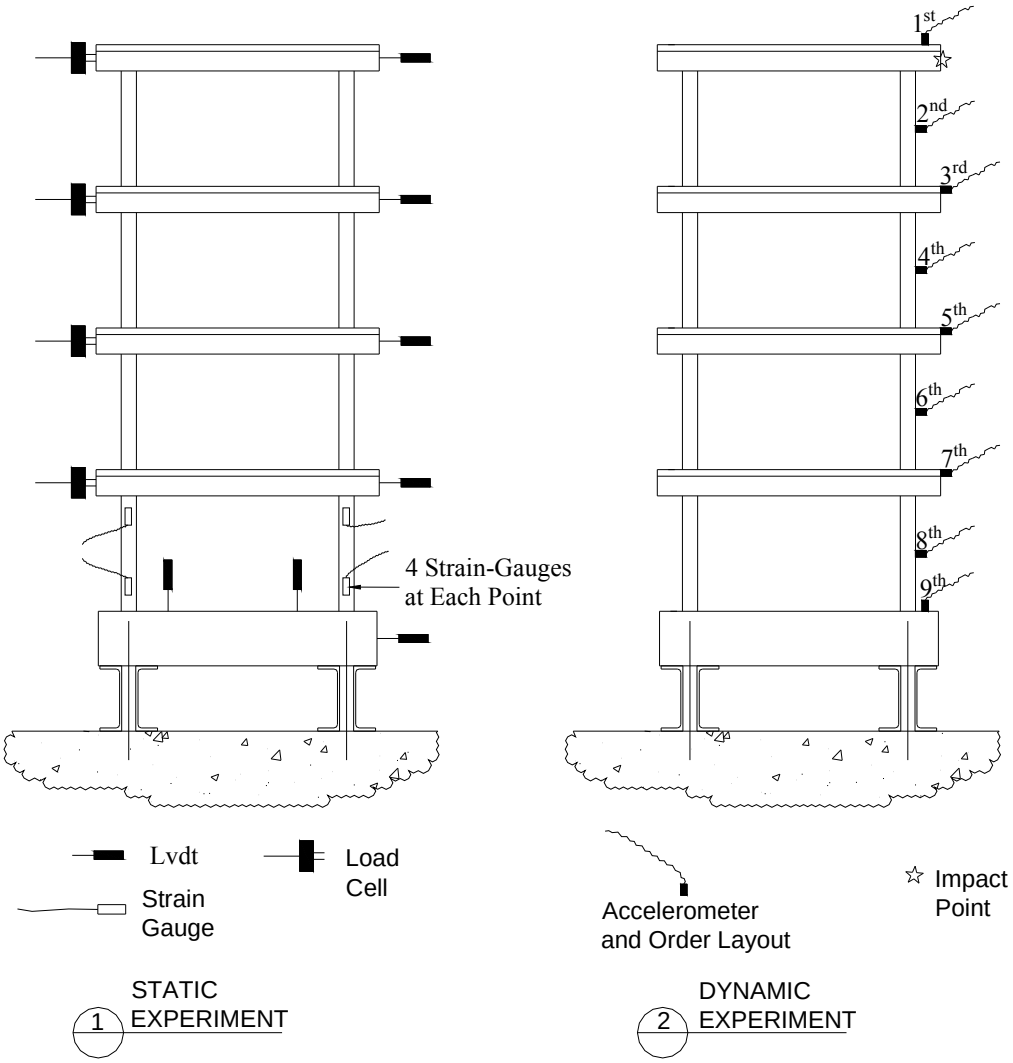

Figure 2.16. Schematic layout of the static and dynamic sensors on the frames

2.6.1. Instrumentation for Static Tests

Based on the ranges of the sensors, two of LVDTs and two of RLPTs were set to measure the story drift of the floors. In order to measure the possible rigid body motion at the base block of the specimens, two RLPTs and one LVDT are used, Figure 2.16. Detailed technical information about LVDTs and RLPTs are presented in Appendix B. Attachment detail of LVDTs' and RLPTs' on reference frame and RC frame is shown in Figure 2.17.

Load cells were positioned at every floor level to measure the applied load by the loading frame to the system. Typical mounting detail of load cells is presented in Figure 2.17. Technical specifications about load cells are also presented in Appendix B.

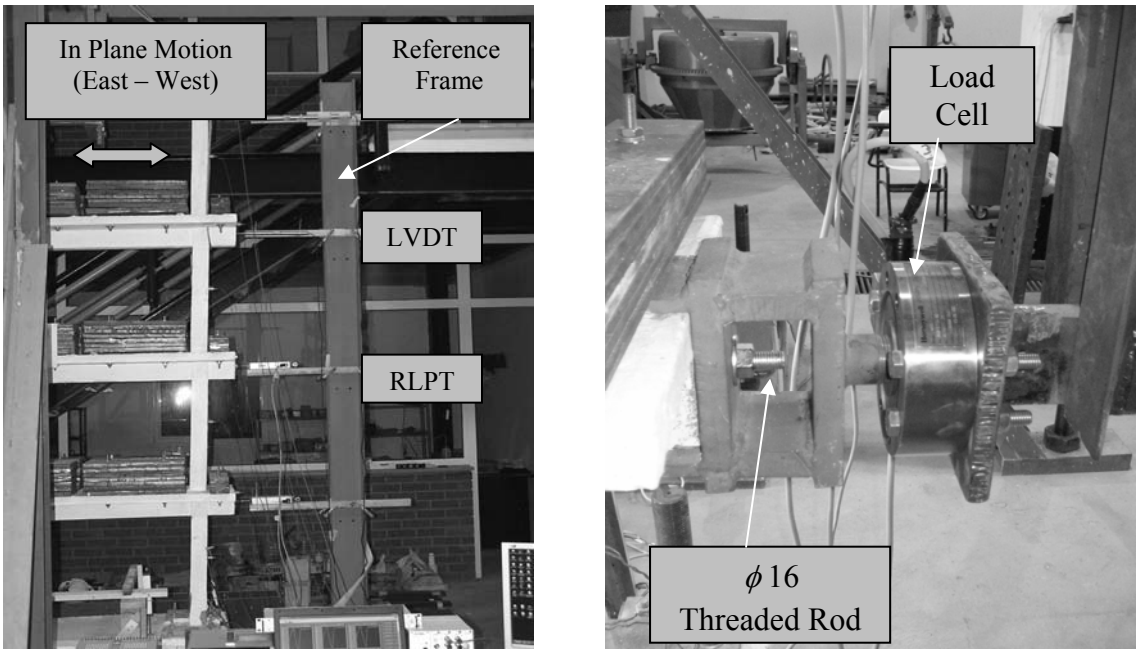

Figure 2.17. Attachment of LVDTs on the reference frame, left. Connection of load cells to lateral loading mechanism and RC frame, right.

In an attempt to resolve the internal moment and shear forces of the frames strain gages were installed at the first story level. Total sixteen strain-gauges were mounted to the longitudinal reinforcements of first story columns. Types of strain-gauges were chosen based on the reinforcement detailing. In this context, post yield strain-gauges were installed on the longitudinal reinforcements of ductile second and fourth frame. Strain-gages were installed at 7cm from the face of the beams/base block. Specifications of strain-gauges are presented in Appendix B.

2.6.2. Instrumentation for Dynamic Tests

Response of the system excited by the impact hammer and snap-back mechanism were monitored by nine accelerometers. The distribution of the accelerometers was selected to obtain a modal shape with good precision. For this purpose accelerometers were positioned at floor levels, mid height of the columns and

on the base block. The accelerometers at the base block and the top floor level were selected to be triaxial to observe the out of plane response at these locations. Specifications of the accelerometers are also presented in Appendix B. Typical mounting detail of the accelerometers to the frames is illustrated in Figure 2.18. Accelerometers were mounted on the faces of the columns and the beams by hot glue. Accelerometers at the fourth story and the base block were mounted on the horizontal surfaces directly.

Figure 2.18. Typical attachment of accelerometers on mid height of the columns and slabs

2.6.3. Data Acquisition Device

Two National Instruments, SCXI-1000 type modular system were used for data gathering. Data acquisition box that was used for dynamic data contains three modules. Two of which were accelerometer modules and an analog to digital converter module. Sensor modules were SCXI-1531 accelerometer conditioners. These modules provide eight BNC channels for accelerometers. Each input channel has individually programmable settings of 4-pole Bessel low-pass filter and input voltage. Settings may vary among 2.5, 5, 10 or 20 kHz and 10, 1 or 0.1 V, respectively. Sensor modules get

the signal and condition it. Analog to digital (A/D) module receives data from the sensor modules and directs to the computer through a USB connection. A/D module provides 16-bit resolution and multiplex 200 kS/s sampling rate. Data acquisition box that was used for static tests contained four modules. Similar to the first box, one of the modules was the SCXI-1600 analog to digital converter. Two other modules were SCXI-1314 strain-gauge modules. These modules provided total sixteen strain-gauge channels. The last module was a SCXI-1100 voltage module. This module was a 32 channel voltage based gauge module. Measurements of the LVDTs, RLPTs and the load cells were followed through this module. All the channels were multiplexed into a single software-programmable gain instrumentation amplifier and jumper-selectable low-pass filter. Connection to SCXI-1100 module was provided by BNC-2095 module. BNC-2095 has 32 labeled BNC connectors, one for each input channel of the SCXI-1100. BNC-2095 also includes circuitry for configurable signal referencing.

2.7. Testing Procedure

Static test of each RC frame specimen was consisted of several cyclic loading groups and each cyclic loading group contained two sub-cycles. In order to observe the effects of different damage levels on frames, gradually increasing amounts of drifts were provided by lateral loading mechanism, Figure 2.13. Loading level was controlled by the inter-story drift ratio of the first story. Maximum inter-story drift ratios reached during the tests were 1.95%, 3.4%, 1.8% 1.95% for the first story respectively from 1st to 4th specimens. Considering the brittle behavior and presence of heavy masses at floor levels, maximum drift ratios of each loading group and number of loading groups were decided during the experiment in order to prevent a sudden collapse of the frame.

Impact hammer and snap-back tests constituted the dynamic tests. Dynamic tests were performed at the end of each static loading group. In order to excite low frequencies of RC frame, soft plastic was chosen as a hammer tip. Frames were excited from the fourth floor level for each excitation and data acquired via 9 accelerometers. Snap-back tests were performed to obtain dynamic data beyond linear zone of frame specimens. To obtain these data, frame specimens were pulled by the designed snap-back mechanism. The pulling process was chosen to be half of the displacement level at

the fourth story in the preceding cycle and the disposable steel piece was cut. Each dynamic test consisted of five impact excitation and three snap-back excitations.

CHAPTER 3

STATIC TESTS

3.1. Introduction

Details of the static testing and the results will be presented. Discussion starts with the presentation of the load history applied to each frame. Load deformation curves and the observed damage follow. Afterwards, analysis of the test results to observe the change in stiffness, strength and energy dissipation will be presented.

3.2. Loading Program

Considering that for frame structures highest drift demands are typically taking place in the lower stories, loading of the frames was controlled through the inter-story drift of first story. Loading history of each frame will be presented in terms of displacements and forces applied to story levels. Applied loading profile of the frames is verified through control of the profile by drawing the ratio of the applied loads at floor levels at the peak values of the each cycle.

Loading history of all frames was organized to apply target drift demands twice. Each repetition subset is considered as cycle groups. The displacement loading histories of all the frames were independent of the time and presentation will be done with consideration of the peak values only. The planned loading scheme could not be applied as planned in the first frame due to the testing difficulties and calibration need of the test setup. As it can be observed in Figure 3.1, first and the last cycle groups contain more than two complete cycles. The presented drift values in Figure 3.1 and Figure 3.2 are the absolute displacements of each story relatively to ground. The displacement loading history of the second, third and fourth frames consisted of six cycle groups and for the first stories they have reached to maximum of ±20mm, ±10.5mm and ±11.5mm displacement values, respectively.

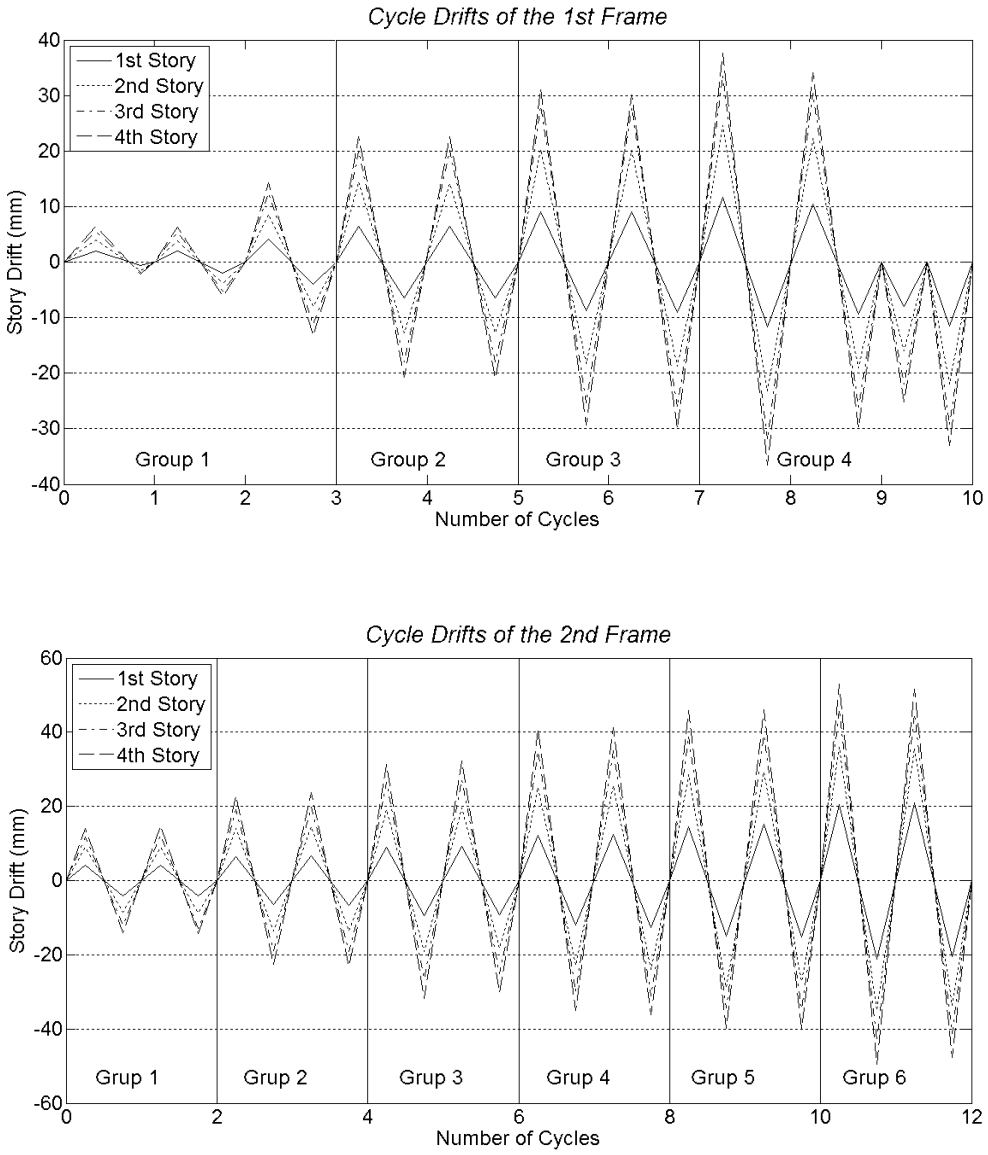

Figure 3.1. Absolute story drifts of the first and second frames

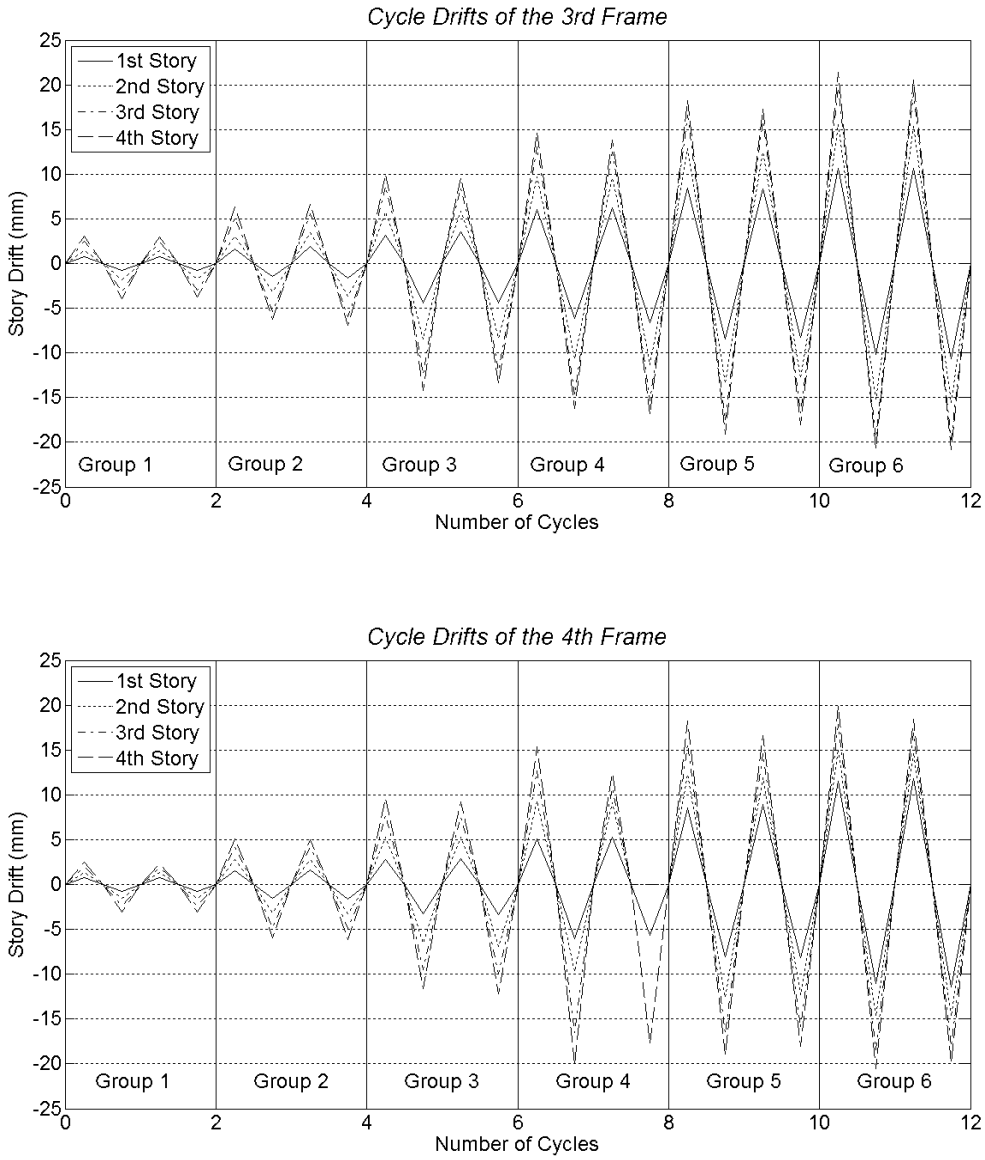

Figure 3.2. Absolute story drifts of the third and fourth frames

In order to show the demand for each story, inter-story drift ratios are calculated and presented in Figure 3.3 and Figure 3.4. It should be noted that rotations in the beam-column joints of the frames are not measured. Therefore, except the first story values inter-story drifts reported in the figure are not the exact values. On the other side, it is obvious that exact values are greater than or equal to the reported values.

Inter-story drift ratios were chosen to be in incremental fashion. These were 0.7%, 1.1%, 1.5%, 1.9% and 0.7%, 1.1%, 1.5%, 2%, 2.5%, 3.4% on the first stories of first and second frames respectively, Figure 3.3 Initial inter-story drift ratios were chosen to initiate the cracks on columns. Following drift levels were selected to have

similar incremental values. Decision to end the experiments was made either due to the safety reasons or by reaching the practical limits of the drift values.

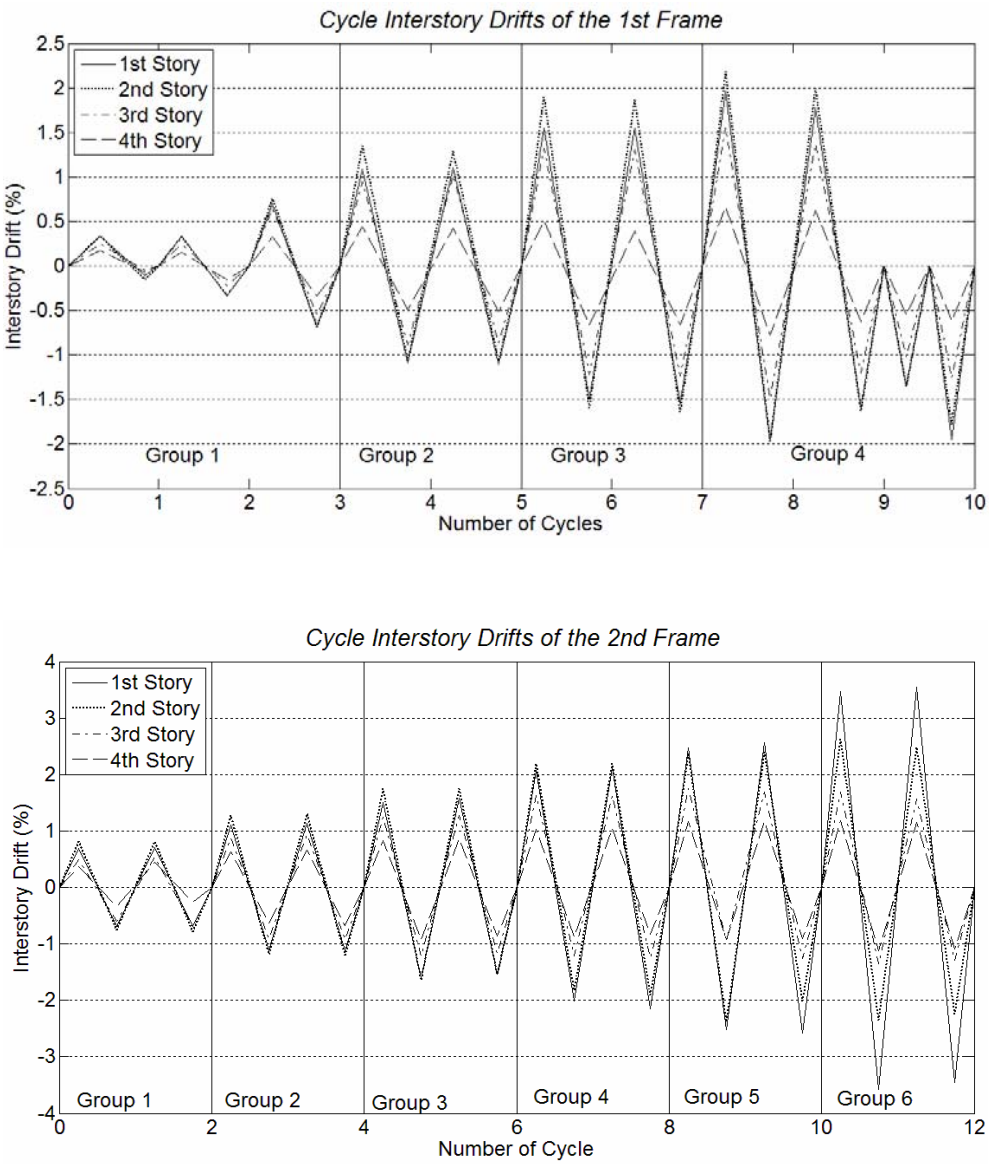

Figure 3.3. Inter-story drift ratios of the first and second frames

A similar incremental approach was chosen for the third and fourth frames. Selected drift levels were 0.1%, 0.3%, 0.7%, 1%, 1.4%, 1.8% and %0.1, %0.3, %0.5, %0.9, %1.4, %1.9 on the first stories of the third and fourth frames respectively, Figure 3.4. First and second cycle group drift ratios selected to be smaller for the purpose of observing the behavior of partition walls. In the following cycle groups, increments of the drift ratios were kept similar to the frames without partition walls.

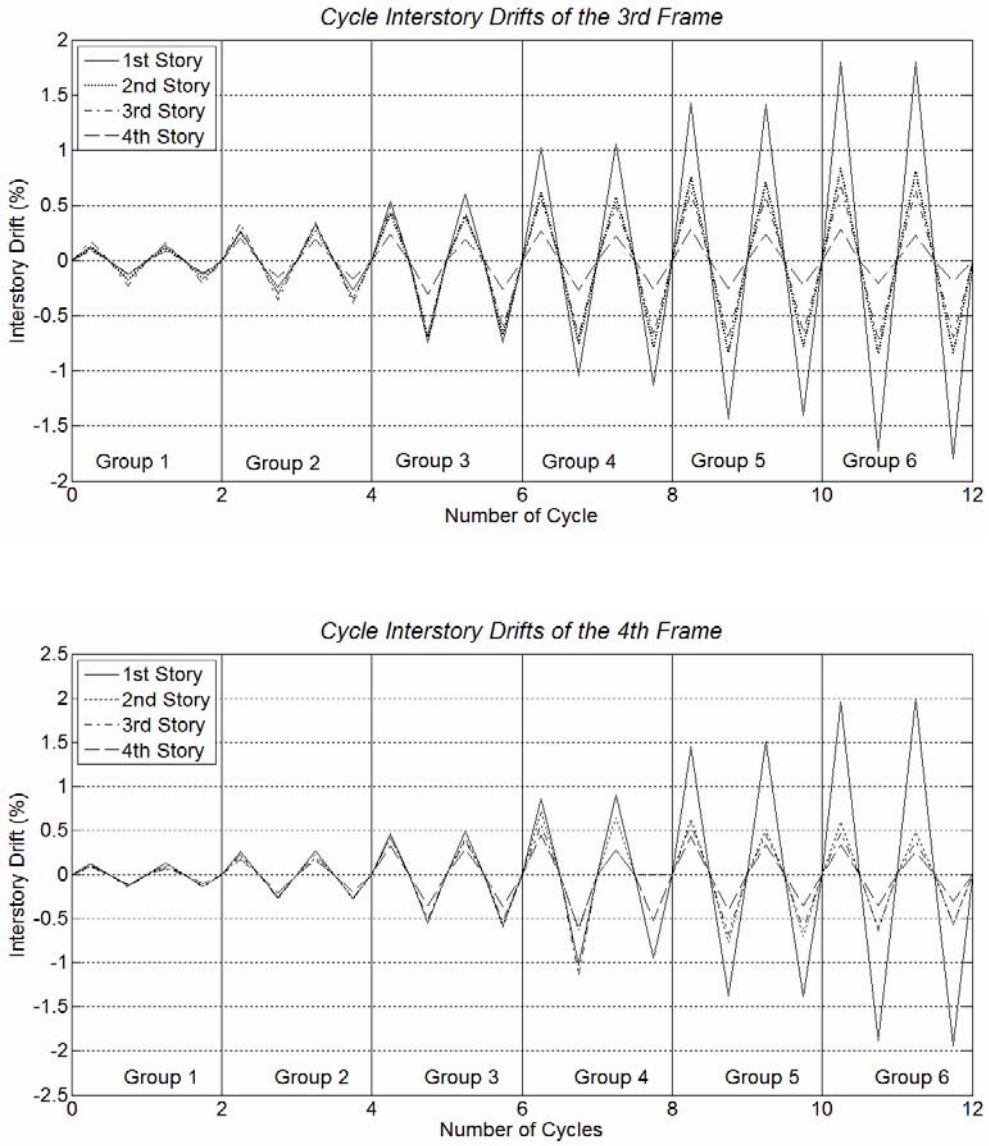

Figure 3.4. Inter-story drift ratios of the third and fourth frames

The loads applied at the story levels were measured by use of the load cells at the story levels. The loads corresponding to applied displacement history are presented in Figure 3.5 and Figure 3.6. As mentioned before the static loading frame was detached from the RC frames to perform the dynamic tests. Therefore the time flow of the static tests was interrupted. Considering this situation the horizontal axis of the graph in the figure is called the composite time. It means that time given on the axis is not consecutive in absolute time but rather the duration of the each group is added on top of each other. Loading and unloading of frames were conducted by a manually controlled hydraulic jack. Thus, unloading of frames was very fast. When the frames reached the

target drifts of each loading cycle group, the maximum loading on frames were maintained to make crack observations on the frames.

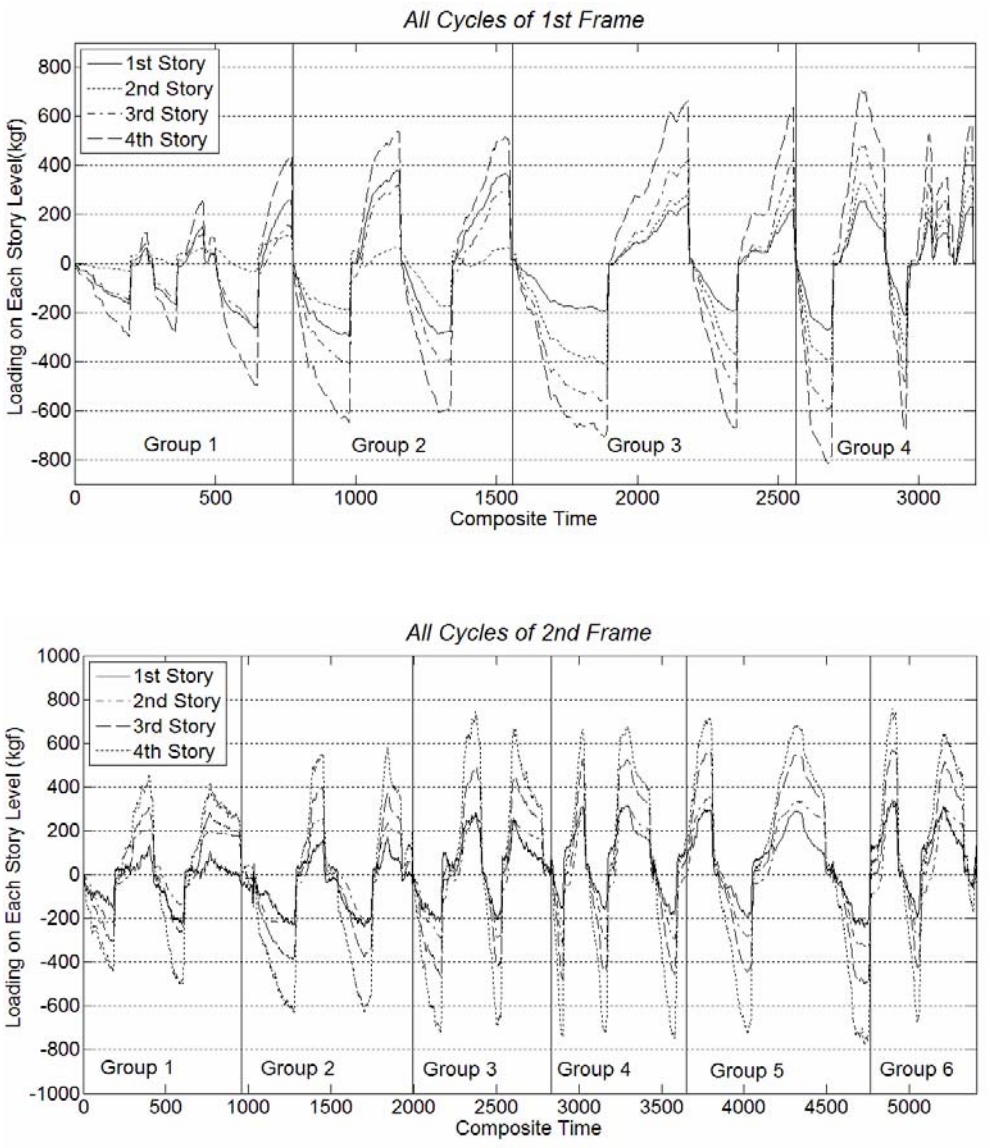

Figure 3.5. The applied loading history to the first and second frames

Loading of the frames were done along east-west axis. Peak values of the loads in east and west directions reached to values of (1712, -2000), (1972, -1763), (4998, -4635), (6000, -5739) kgf for the frames one to four respectively, Figure 3.5 and Figure 3.6. All of the maximum loading values were reached in the first cycle of each cycle group.

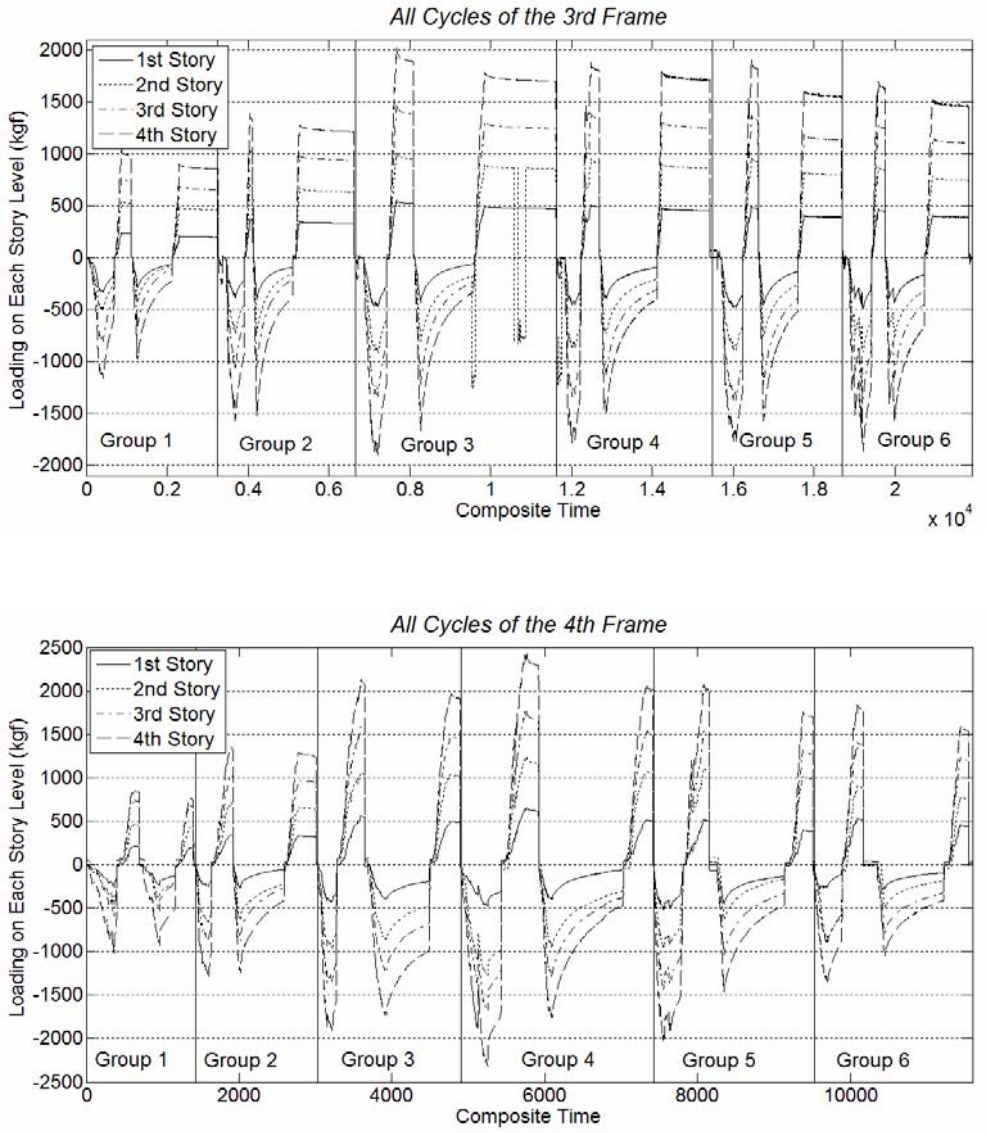

Figure 3.6. The applied loading history to the third and fourth frames

As it was mentioned, inverse triangular load distribution was intended to be applied in the experiments. The shape of loadings on the frames is presented by preparing a graph of loading for each cycle group of the frames by normalization of loadings at story levels to four units at the top and accordingly in the other levels. In Figure 3.7 and Figure 3.8, loading profiles of the frames are presented.

During the first and second cycle groups of the first frame, load distribution was not applied as originally planned. This problem was noticed and resolved during the experiment by calibrating the tightness of the hinges of the load distribution mechanism. After calibration, load distribution of the first frame turned to an acceptable profile. As

it can be seen from the figures of the other frames, load distribution was applied successfully in the rest of the tests.

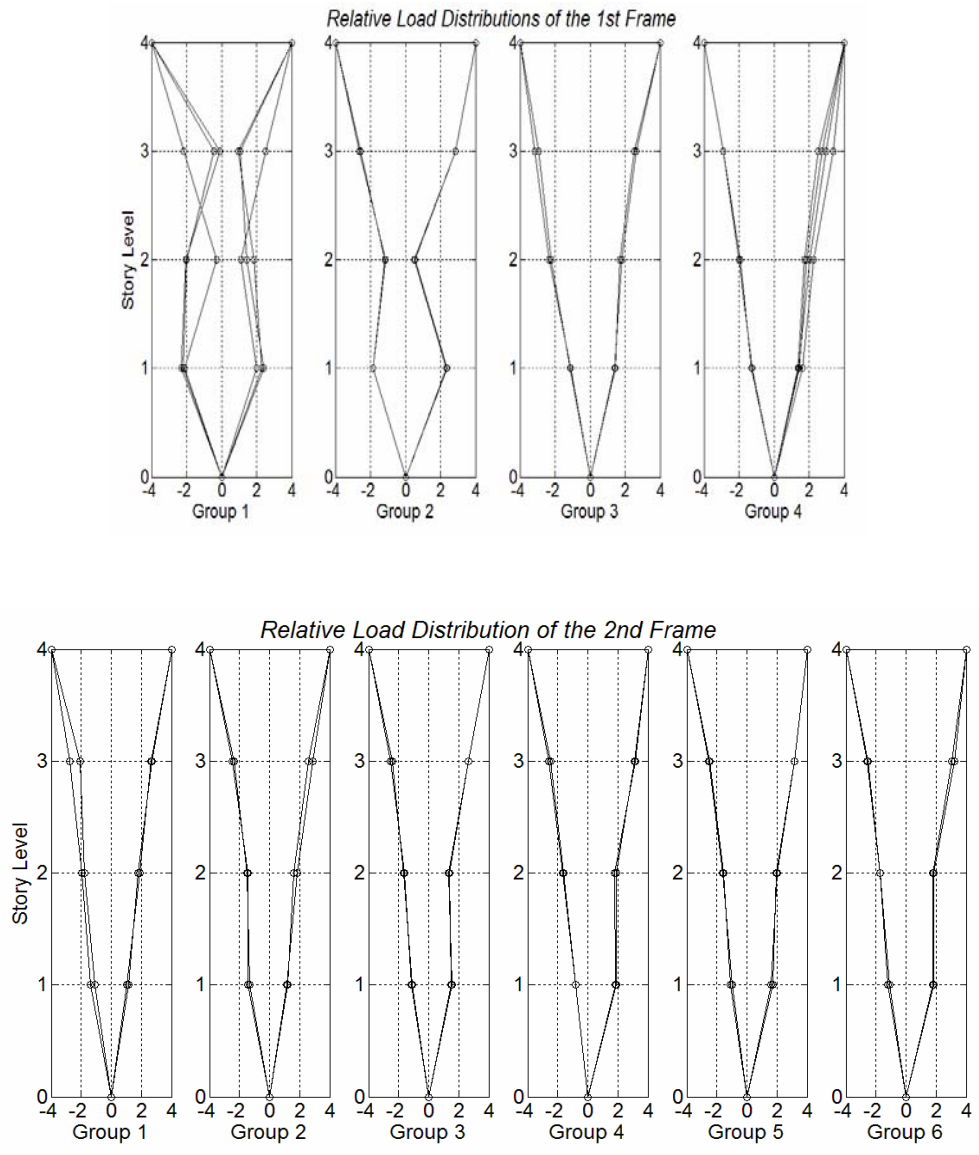

Figure 3.7. Normalized load distribution of the bare frames

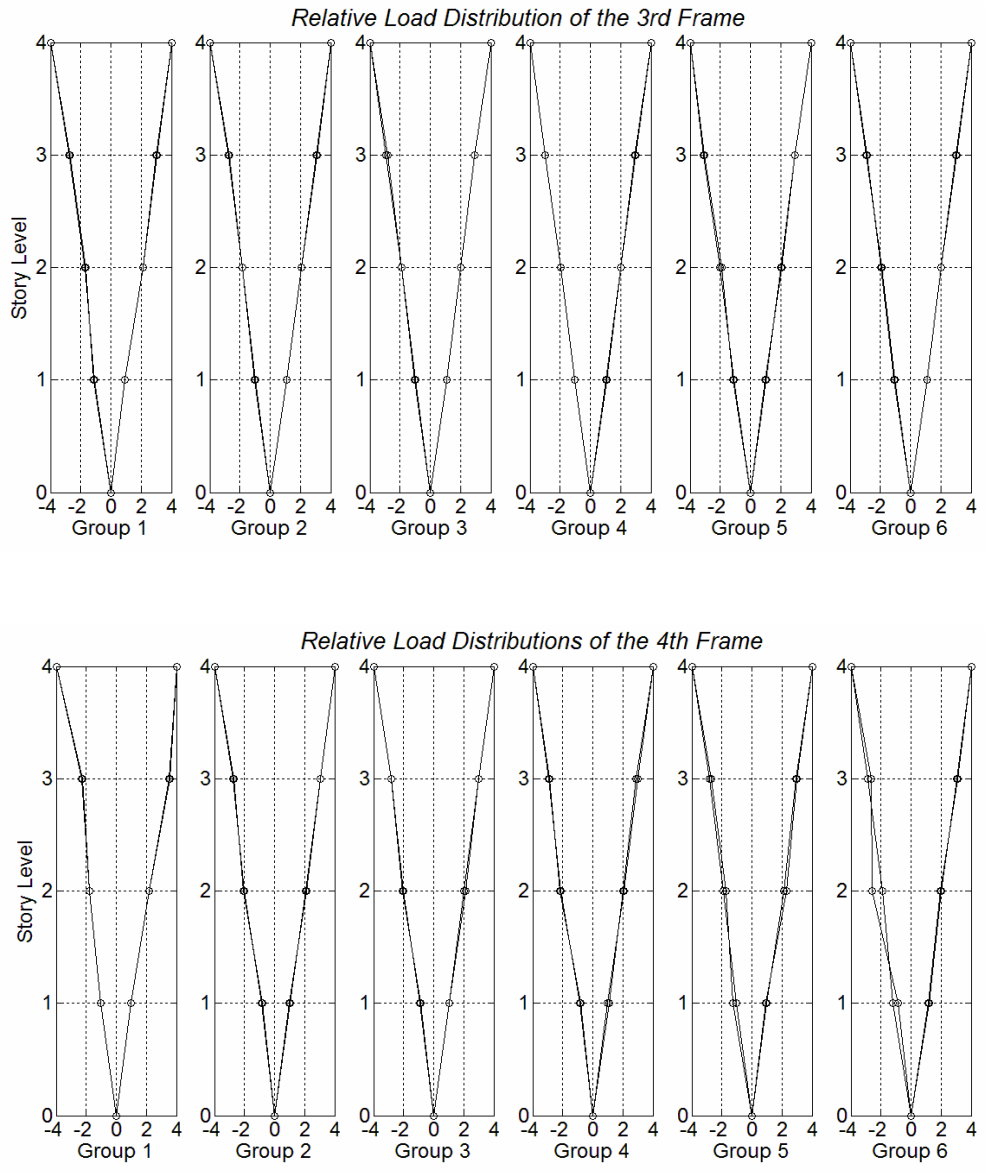

Figure 3.8. Normalized load distribution of the frames with infill wall

3.3. Observed Displacement Relations and Damages

Observed load-displacement relations and damages of the frames are going to be explained in this Section.

3.3.1. Frame #1

Hysteresis curves of the first frame are presented in Figure 3.9. In order to avoid a crowded graph, curves are grouped by story level and loading groups as defined in Section 3.2. Horizontal axes of the curves are the inter-story drift and the vertical axes are the force resisted at story level.

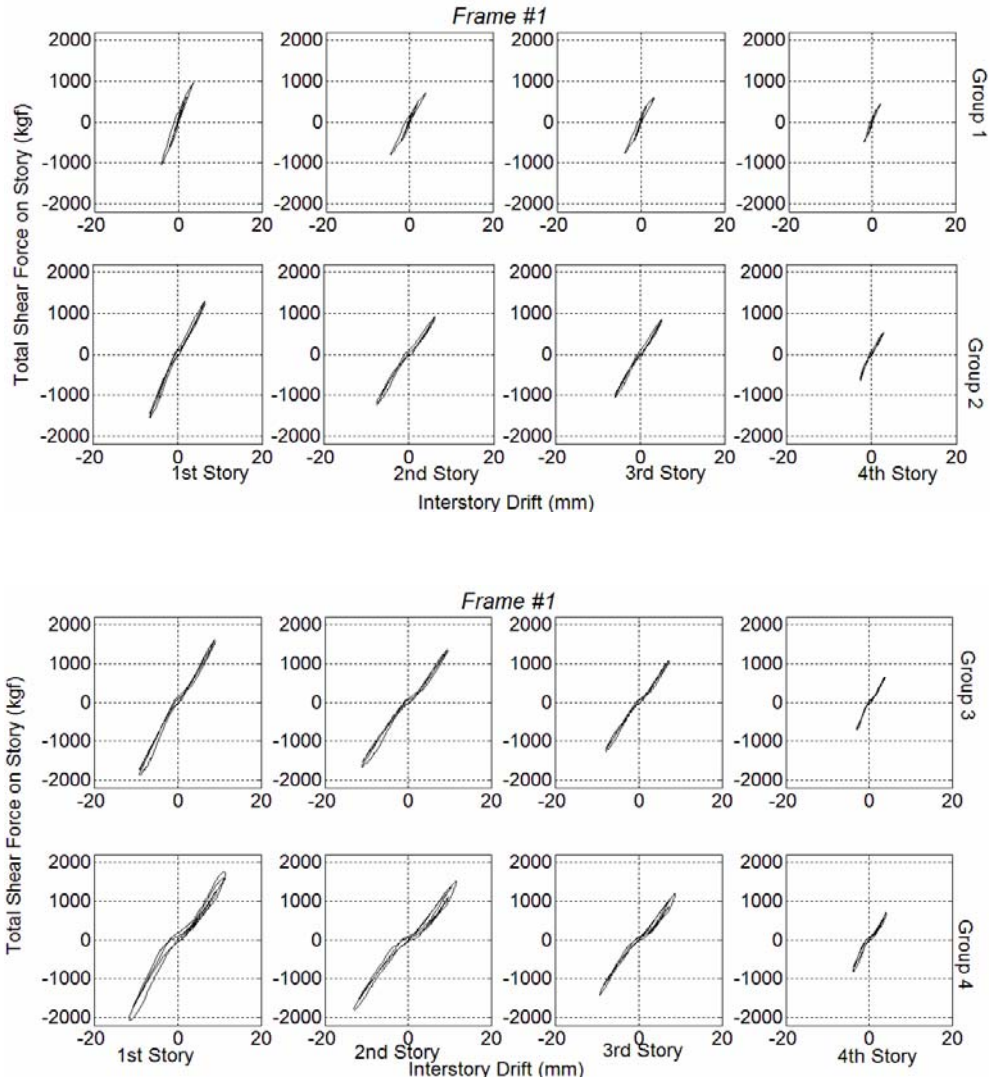

Figure 3.9. Hysteresis curves of frame #1, grouped by stories and cycle groups

In the first loading group, inter-story drift of the first story a reached maximum of ±4mm (0.7%) with 1050 kgf total lateral loading. Even though both columns exceeded their flexural cracking capacity and cracked, hysteresis curves of first loading

group can be accepted as linear lines. At this loading stage, drift of the fourth floor reached a maximum of -14.3mm and +13.2mm in west and east directions respectively.

In the second loading group, inter-story drift of the first story reached a maximum of ±6.5mm (1.1%) with 1450 kgf total lateral loading. At this stage of loading, hysteresis curves could still be accepted linear. Flexural cracks of first story columns were expanded to the span of columns. On the beam-column joint zones, shear cracks were appeared along the faces that are parallel to loading direction, Figure 3.10. Moreover flexure and flexure-shear cracks appeared on beams. Drift value at the fourth floor reached a maximum of 22.6mm.

Figure 3.10. Flexural cracks at the east face (left) and shear cracks at the north face (right) of the first story east column at the end of the second loading group

In the third loading group, inter-story drift of the first story reached a maximum of ±9mm (1.5%) with 1725 kgf total lateral loading. As it can be observed from the hysteresis curves, pinching started in the system. Increased widths of cracks support this observation. Pinching also indicates that bond deterioration of rebars started. Some of the flexural cracks were transformed to the flexure-shear cracks on the first story columns. Reach of the existing cracks also extended both in the first story beam and columns. New flexural and shear cracks also formed on the first story columns, Figure 3.11. New flexure and shear cracks were observed on the beam and columns of second

story. In the beam-column joints of second story shear cracks were appeared similar to the first story beam-column joints. Finally, at this loading stage, drift of the fourth floor reached a maximum of 31.1mm.

Figure 3.11. Cracks at the north face of the first story east column, at the end of the third loading group

In the fourth loading group, inter-story drift of the first story reached a maximum of ±11.5mm (1.9%) with 2000 kgf total lateral loading. During the experiment when the drift of the first story reached to a value of 11mm, it was observed that, connection rods of the last story beam-additional masses were bearing on the support frame. Therefore loading values of the first cycle about ±11mm were not reflecting the real resistance of the frame. In order to avoid the contact, second cycle of this loading group was limited to ±10mm drift. The contact problem was solved for the second loading cycle. Afterwards an 8mm and 11.5mm drift half cycles were performed. In the last half cycle, frame resistance was dropped compared to first 11.5mm cycles. Since the system did not reach to previous loading levels in the last cycle, in order to prevent a possible sudden collapse experiment was stopped at this stage. The existing cracks on the columns increase their reach and from location to location combined with each other. Shear cracks occurred along the faces that were

parallel to the loading direction of the third story beam-column joint zones. In the second loading cycle drift of the fourth floor reached a maximum of -34mm and +29.3mm for west and east directions respectively, in the last half loading cycle along the east direction drift of fourth floor reached a maximum of 33mm.

Loading halted at this level. A detailed crack pattern of first frame is presented in Appendix C. It should be noted that north face crack pattern of first and second story west columns was not available due to the access problems during the tests.

3.3.2. Frame #2

Frame #2 hysteresis curves are shown in Figure 3.12. Similar to the first frame, curves are grouped by the story levels and the loading groups.

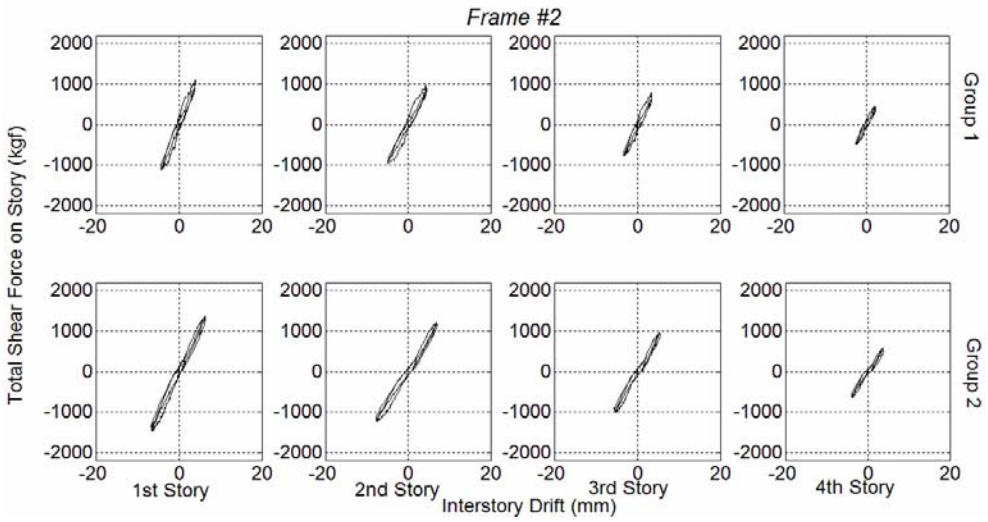

Figure 3.12. Hysteresis curves of Frame #2, grouped by stories and cycle groups

(cont. on next page)

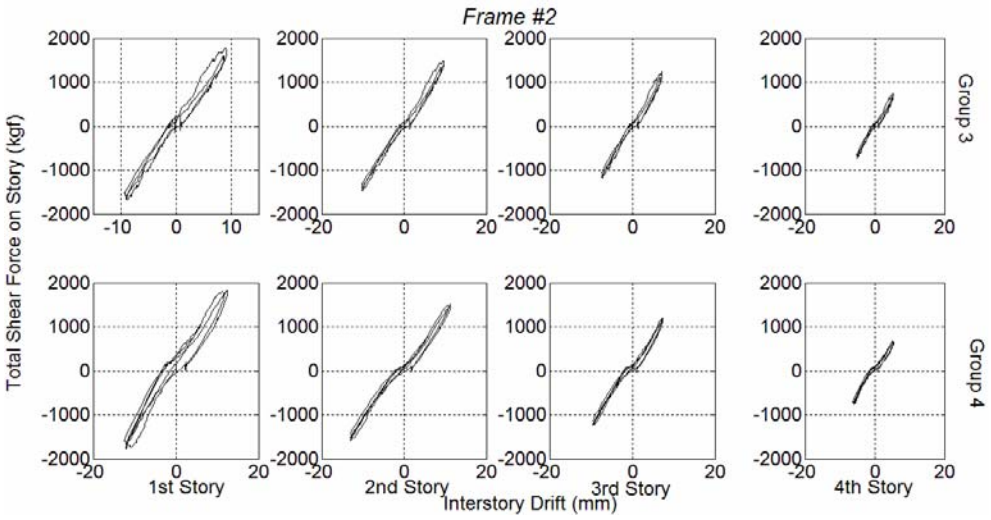

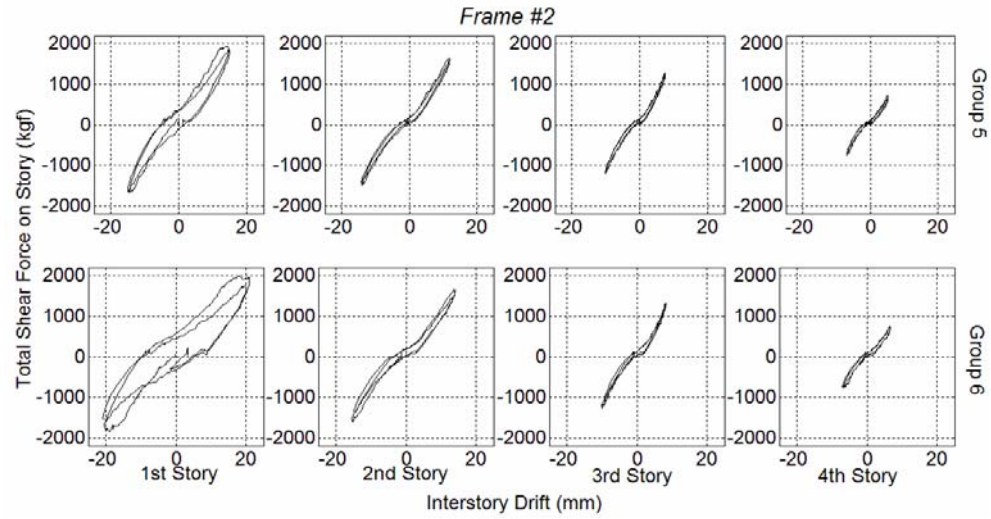

Figure 3.12. (Cont.)

In the first loading group, inter-story drift of the first story reached a maximum of ±4mm (0.7%) with 1120 kgf total lateral loading. Similar to the first frame even though the column section exceeded its flexural cracking capacity and had cracks, hysteresis curves can be accepted as linear lines, Figure 3.13. In addition to the flexural cracks, a shear crack initiation was also observed in the joint zone at the north face of first story east column, Figure 3.13. At this stage of loading, absolute drift of the fourth floor reached a maximum of 14mm.

Figure 3.13. Flexural cracks at the east face (left) and shear crack initiation at the south face (right) of the first story east column, at the end of the first loading group

In the second loading group, inter-story drift of the first story reached a maximum of ±6.5mm (1.1%) with 1445 kgf total lateral loading. At this stage of loading, hysteresis curves could still be accepted linear. On the east and west face of first story columns, widespread flexural cracks were observed, Figure 3.14. Shear cracks were expanded towards to the both sides of the faces that were parallel to loading at the joint zones. Initiation of new flexural and shear cracks was also observed on the beam and columns of second story, Figure 3.14. Moreover, on the first and second story beams some of the flexural cracks were transformed to the flexural-shear cracks. On the third story column, flexural cracks were appeared similar to the flexural cracks on the first and second story columns. At this stage, drift of fourth story reached a maximum of ±23mm.

In the third loading group, inter-story drift of the first story reached a maximum of ±9mm (1.5%) with 1739 kgf total lateral loading. As it can be observed from the hysteresis curves, pinching starts in the system at this loading stage. Length and width of the flexural cracks on the first story columns expanded and some of them transformed to flexural-shear cracks. Moreover, in the first story beam-column joint zones lengths of shear cracks increased and also new shear cracks were appeared

parallel to existing shear cracks in same location of first story columns, Figure 3.15. In addition to this, flexural cracks enlarged on the first story beam. At this stage of loading, drift of the fourth story reached a maximum of +31.8mm.

Figure 3.14. Spreading of flexural cracks at the east face of the first story east column (left) and new shear crack in the joint zone of second story north face east column (right) at the end of the second loading group

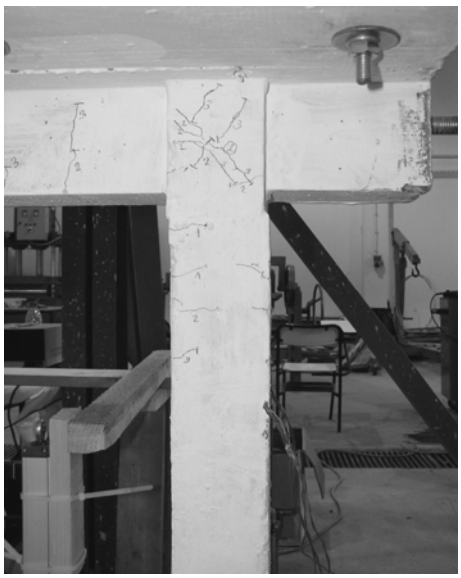

Figure 3.15. Shear cracks on the first story south face east column at the end of the third loading group

In the fourth loading group, inter-story drift of the first story reached a maximum of ±12mm (2%) with 1830 kgf total lateral loading. Opposite to the first frame, the second frame lateral load resisting capacity did not reduce at the imposed inter-story drift levels of the first story. This result was expected based on the difference between reinforcement details. On the hysteresis curves pinching became clear due to the increasing crack discontinuities and potential bond deterioration of the rebars. On the other hand, compression failures of concrete were observed in the compression zones of the first story columns, Figure 3.16. In addition to these, flexural cracks of first story beam were transformed to the flexural-shear cracks and new cracks were also observed. At this loading stage, drift of the fourth story reached a maximum of 40.8mm.

In the fifth loading group, inter-story drift of the first story reached a maximum of ±15mm (2.5%) with 1935 kgf total lateral loading. Lateral strength of frame continued to increase. As typically observed, load resistance of the second loading in cycle groups decreased. Instead of new cracks, mostly existing cracks expanded and the concrete crushing regions of first story columns were advanced, Figure 3.17. At this loading stage drift of the fourth story reached a maximum of 45.8mm.

Figure 3.16. Crushing of concrete on the first story, east face of east column, end of the fourth loading group

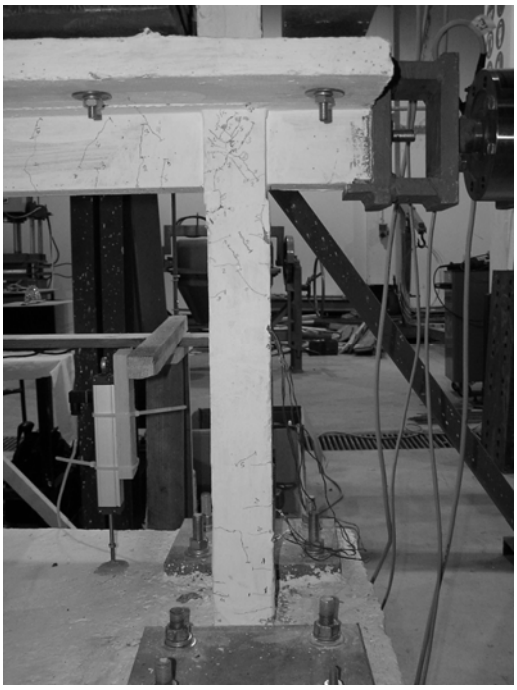

Figure 3.17. First story east column south face at the end of the fifth loading group

In the sixth loading group, inter-story drift of first story reached a maximum of ±20mm (3.4%) with 1972 kgf total lateral loading. Maximum lateral load carrying capacity did not change significantly compared to previous loading group. While inter-story drift ratio increased about 1% in the first story, stationary levels of the lateral load show the existence of plastic mechanisms in the first story. On the other hand, existing crack length and width expansion is also observed similar to the fifth loading group. At this loading stage, drift of the fourth story reached a maximum of 53mm.

Loading was halted at this level. A detailed crack pattern of second frame is presented in Appendix C.

3.3.3. Frame #3

Frame #3 hysteresis curves are shown in Figure 3.18. Similar to the previous frames, curves are grouped by the story levels and the loading groups as defined in Figure 3.2.

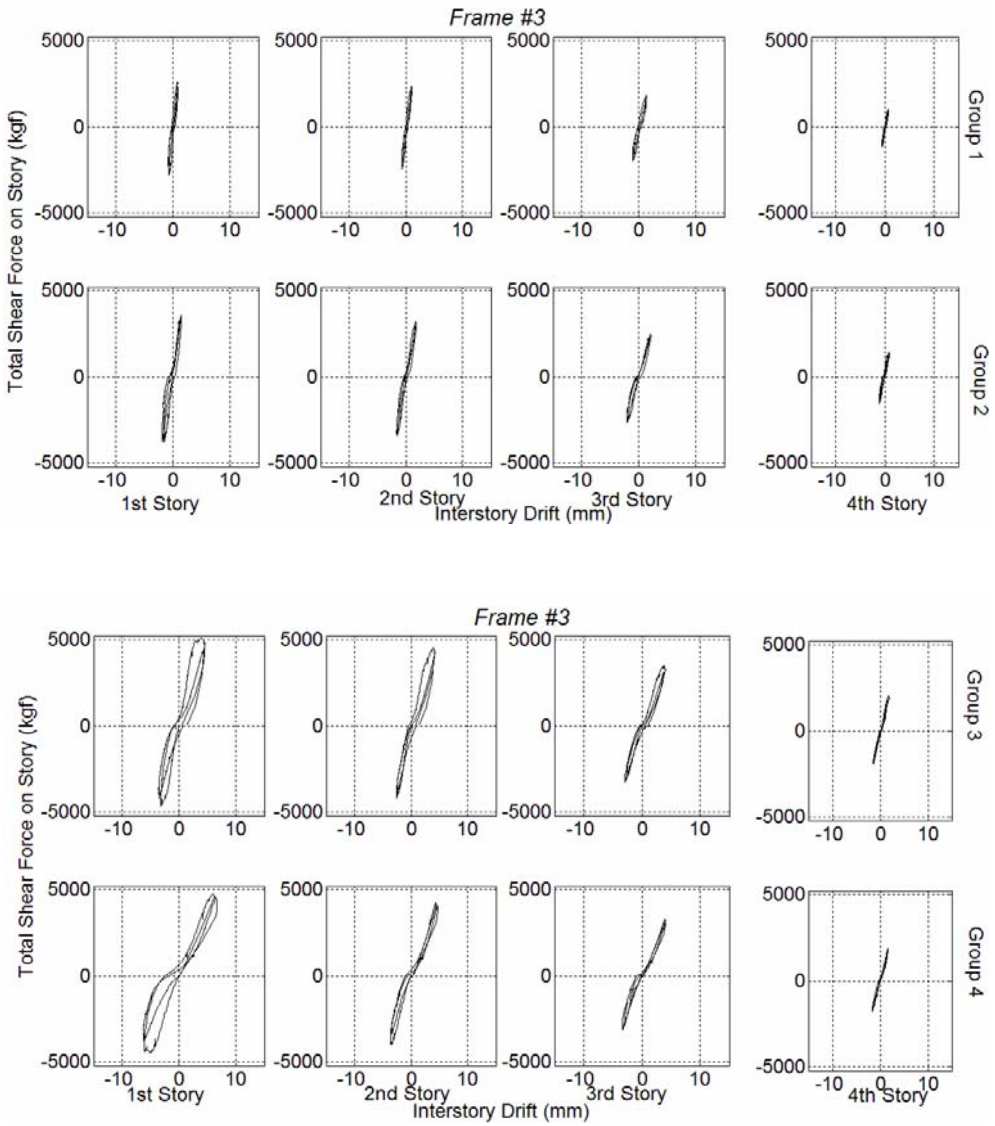

Figure 3.18. Third frame hysteresis curves are shown basis on the story and cycle group separation

(cont. on next page)

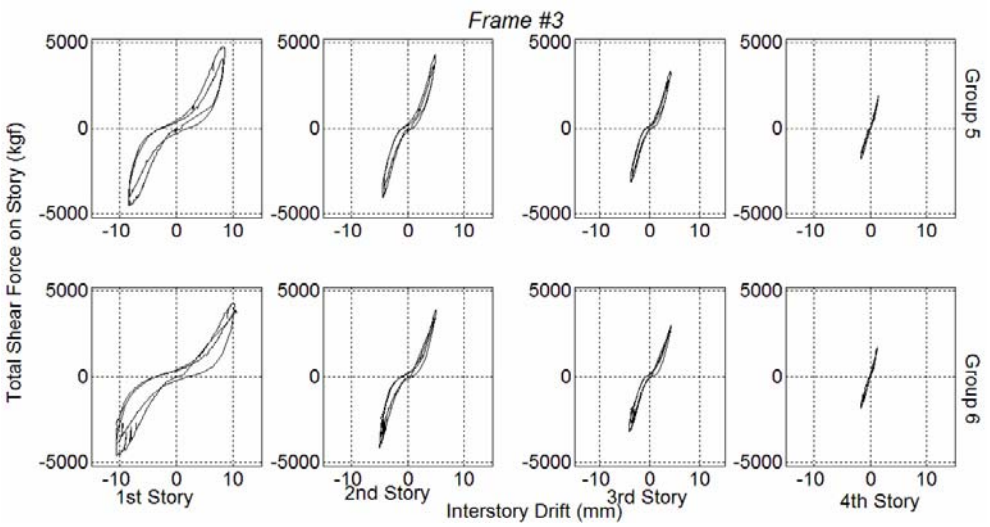

Figure 3.18. (Cont.)

Unlike the first loading groups of first and second frames, the target inter-story drift of the first story is chosen to be ±0.7mm (0.1%) for having an opportunity to observe the behavior of partition walls. Even at this low drift levels cracks occurred in the system. In the first and second story partition walls, diagonal cracks were observed, Figure 3.19. Separations occurred in the interfaces of partition walls and frame elements of first and second stories. Moreover, flexural cracks were also appeared in the first story west column, Figure 3.19. In this loading group a maximum of 2800 kgf total lateral load was reached on the first story. Finally the drift of the fourth story reached a maximum of 3.9mm.

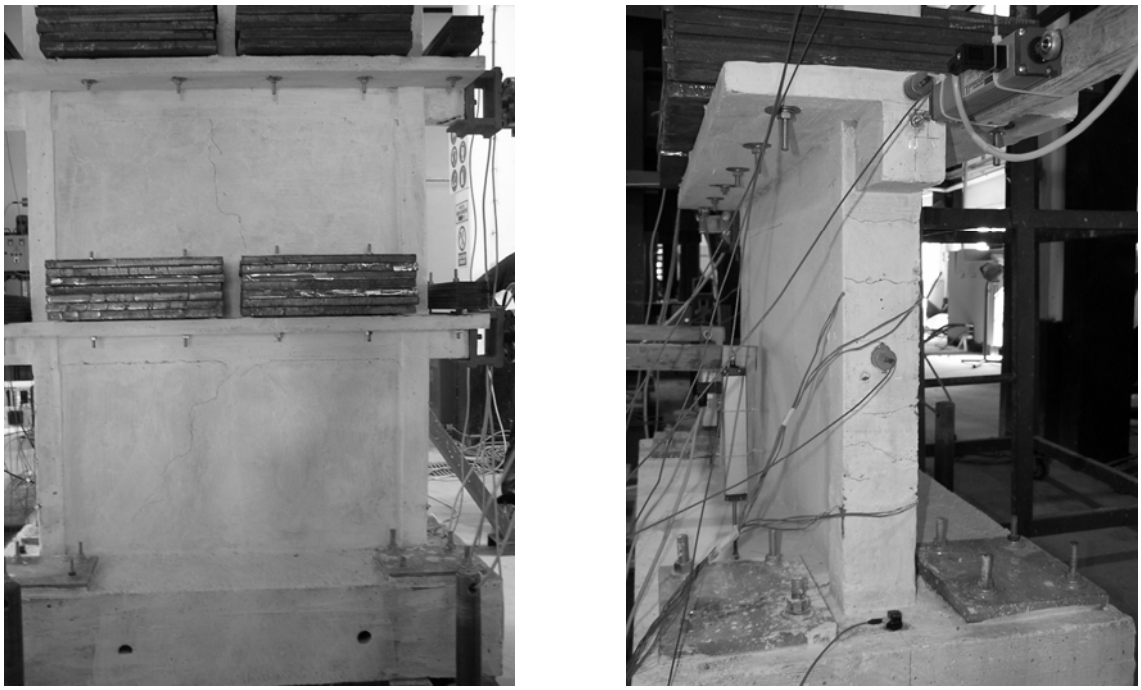

Figure 3.19. Diagonal cracks in the first and second story partition walls (left) and flexural cracks of the first story west column (right), at the end of first loading group

In the second loading group, inter-story drift of the first story reached to maximum values of -1.6mm (0.3 %) and +1.4mm (0.2 %) in west and east directions respectively. Maximum total lateral loading reached to a value of 3787 kgf. New flexural cracks were observed in the beam-column joint zone of the first story east column. Moreover, in the same region of the west column the existing flexural crack transformed to a flexural-shear crack. In the both columns of the second story, new flexural cracks were observed, Figure 3.20. On the other hand, in addition to existing diagonal cracks in the partition walls of first and second stories, new shear cracks were appeared, Figure 3.20. The interface between third story partition wall and the east column separated. Pinching in the hysteresis curves started. Drift of the fourth floor reached to maximum of 6.3mm in this cycle group.

In the third loading group, inter-story drift of the first story reached to maximum values of -3.2mm (0.5%) and +4.4mm (0.7%) in west and east directions respectively. Maximum lateral loading reached to a value of 5053 kgf. At this stage, number and width of flexural cracks that were located in the first and second story columns increased. Moreover, shear cracks were observed at different locations in the columns of first and second stories especially in the regions that were under pressure by partition

walls. Flexural and shear cracks were also observed in the beams of the first and second stories, Figure 3.21. On the other hand, in the first story partition wall, instead of new cracks, existing shear cracks extended further and new sub crack developed in the line with the existing main crack direction. At this loading group, drift of the fourth story level reached to a maximum of 14.2mm.

Figure 3.20. Spreading of flexural cracks in the west column (left) and shear cracks in the partition wall (right) of the second story, at the end of second loading group

Figure 3.21. Flexural and shear cracks in the first story beam at the south face, at the end of the third loading group

In the fourth loading group, inter-story drift of first story reached a maximum of ±6mm (1.0%) with 4739 kgf total lateral loading. As it can be observed from the hysteresis curves, strength degradation in the frame had started in this stage. Some of the flexural cracks in the first and second story columns turned into the flexural-shear cracks and new shear cracks appeared in the joint zones while the existing cracks were spreading. In the first story beam new flexural and flexural-shear cracks were observed as well. Moreover in the second story beam new shear cracks occurred in the locations that were under pressure by partition wall. At this stage of loading, first and second story partition wall plaster at the north face started to spall, Figure 3.22. At this loading group drift of the fourth story reached to a maximum of 16.3mm.

Figure 3.22. Spalling of the partition wall plaster in the second story north face

In the fifth loading group, inter-story drift of first story reached to a maximum of ±8.3mm (1.4%) with 4759 kgf total lateral load. Even though no increase takes place, frame sustained the maximum lateral loading levels in this loading group too. In the first and second stories, residual deformations in columns became visible with bare eye, Figure 3.23 and Figure 3.24. Instead of new crack development in the frame members, lengths and widths of existing cracks increased. In this loading group with the further

increase of the deformations plaster spalling was observed in the partition walls. At this loading stage, drift of the fourth story reached a maximum of 19mm.

Figure 3.23. Residual deformation of the first story columns and the partition wall

Figure 3.24. Residual deformation of the second story columns and the partition wall

In the sixth loading group, inter-story drift of first story reached to a maximum of ±10.7mm (1.8%) with 4330 kgf total lateral loading. Compared to the previous loading group, strength degradation occurred. At this stage of loading, no new cracks

were observed in the first and second stories but existing cracks developed further. Moreover, new flexural cracks were appeared in the third story columns. Similar to the previous loading group, spalling of the wall plaster continued in the first and second story partition walls, Figure 3.25. Finally, at this loading stage, drift of the fourth story reached to a maximum of 21.3mm.

Loading was stopped at this level. A detailed crack pattern of third frame is presented in Appendix C.

Figure 3.25. Damage of the first story at the end of the sixth loading group south face

3.3.4. Frame #4

Hysteresis curves of the Frame #4 are shown in Figure 3.26. Similar to the previous frames, curves are grouped by the story levels and the loading groups as defined in Figure 3.2.

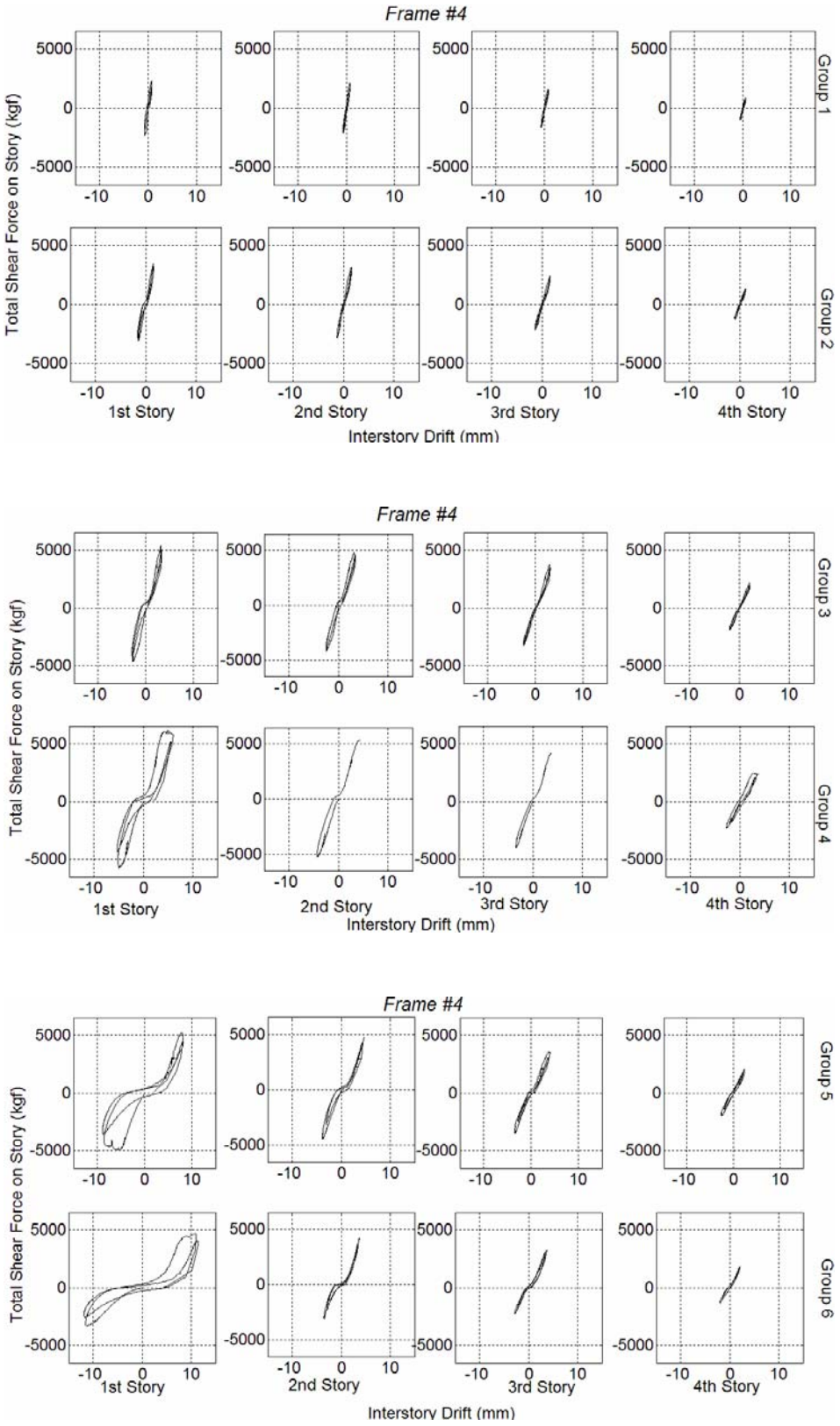

Figure 3.26. Fourth frame hysteresis curves are shown basis on the story and cycle group separation

In the first loading group, inter-story drift of first story reached a maximum of ±0.7mm (0.1 %) with 2288 kgf total lateral loading. Similar to the previous frame, even at this small drift values damage was observed in the partition walls and the frame elements of system. Hairline thick horizontal cracks were appeared at the lower one-third height of the first story partition wall. As an extension of the same crack, a flexural crack was observed in the west column of the first story. Another flexural crack initiated in the joint zone of same column. Moreover, this loading stage also resulted with hairline cracks at joint zones of first story columns and the neighboring partition wall. Finally, drift of the fourth level reached to a maximum of 3mm.

In the second loading group, inter-story drift of first story reached a maximum of ±1.5mm (0.3%) with 3396 kgf total lateral loading. Hysteresis curves can be defined to be accepted as linear. Flexural cracks were appeared in both columns of the first story including the beam-column joint zones. In the joint zones of second story, initiation of flexural cracks was observed. Except the locations where partition wall apply compression to the frame, separation of the partition wall-perimeter frame reached about 1 mm in the first story, Figure 3.27. Finally, at this loading stage, drift of the fourth floor reached to a maximum 5.9mm.

In the third loading group, inter-story drift of first story reached a maximum of 2.7mm (0.5%) and +3.2mm (0.5%) with 5359 kgf total lateral loading. At this stage, hysteresis curves started deviating from linear behaviors and pinching and energy dissipation starts. The number of the flexural cracks increases in the first and second story columns and become more common. Moreover shear cracks were observed in the joint zones of first and second stories, Figure 3.28. In addition to this, flexural and flexural-shear cracks were also observed in the first story beam. On the other hand, instead of new cracks formation in the partition walls, width of the existing cracks increased. At this stage of loading, drift of the fourth floor level reached to a maximum of 11.6mm.

Figure 3.27. Damage in the first story at the end of the second loading group, south face

Figure 3.28. Damage in the joint zone of the first story at the end of third loading group, east column

In the fourth loading group, inter-story drift of first story reached to a maximum of -5mm (0.9%) and +5mm (0.9%) with 6082 kgf total lateral loading. In the beam-column joint zone that was under compression by the partition wall, three cracks with 2 mm width appeared. Cracks were observed to be more or less parallel to each other. At this stage, excessive deformation in the first story column became distinct. On the other

hand, no new cracks were formed in the partition walls. Finally, the drift of the fourth level reached to a maximum of 20mm.

In the fifth loading group, inter-story drift of first story reached a maximum of ±8.3mm (1.4%) with 5247 kgf total lateral loading. Compared to previous group, strength of the frame degraded. In both loading directions, heavy damage due to shear was observed in the beam-column joint zones where the partition wall applies compression, Figure 3.29. Drift of the fourth level reached to a maximum of 19mm. It should be noted that this was the same drift value with the previous loading group of the fourth level.

In the sixth loading group, inter-story drift of first story reached to a maximum of ±11.2mm (1.9%) with 4704 kgf total lateral loading. Degradation in the strength advanced. The heavy shear damages that are occurred in the joint zones of first story were expanded and the concrete in this region started to crush, Figure 3.30. Due to the sustained heavy damages in the first story, the upper stories started to move together as a rigid body. Even though inter-story drift of the first story reached to a level of 1.9%, drift of the fourth story reached to a maximum of 20.5mm only. This value was in the vicinity of the value reached in the fourth loading group.

Loading was stopped at this level. A detailed crack pattern of fourth frame is presented in Appendix C.

Figure 3.29. Damage in first story west column (left) and east column (right) at the end of the fifth loading group, south face

Figure 3.30. Damage of the first story at the end of the sixth loading group, south face

3.4. Properties of Load-Displacement Relations

3.4.1. Strength and Stiffness of RC Frames

In this experimental study, cyclic pseudo-static loading was applied to observe the cyclic behavior of the test frames in the nonlinear range. Frames were pushed to the deflection limits till the safety start to become an issue. In order to obtain the lateral load boundaries of the frames, envelope curves of the recorded hysteresis relations are created for the each cycle of the loading groups. For each frame, envelope curves are obtained for the first story force-displacement relations by connecting the peak points of the measured hysteresis relations. Envelop curves permits the observation of the strength degradations between the first and second loading cycles of the each loading group within the frames. Curves also provided an opportunity to compare the peak force-displacement responses of the frames among each other, Figure 3.31. In the figure first cycles of each loading group are presented. Frames with partition walls reached ultimate loading before 1% inter-story drift of first story while same event occurred at 1.9% for first and 3% for second frames. This observation is a significant sign of deformation capacity reduction of frames with partition walls.

Figure 3.32 presents the envelope curves of the first frame specimen. Horizontal axis of the figure is the total lateral force applied to the system and vertical axis is the inter-story drift ratio of the first story. As it can be observed from the figure, envelope curve of the second loading cycles of each loading group exhibit less strength than that of first loading cycles. Between the cycles of the maximum lateral loading group, strength degradation reached to 17%, Figure 3.36. Strength of the second envelop curve diminished rapidly in the last cycle, as a sign of being close to the failure limits. Also as it was expected frame softens with increasing deformation.

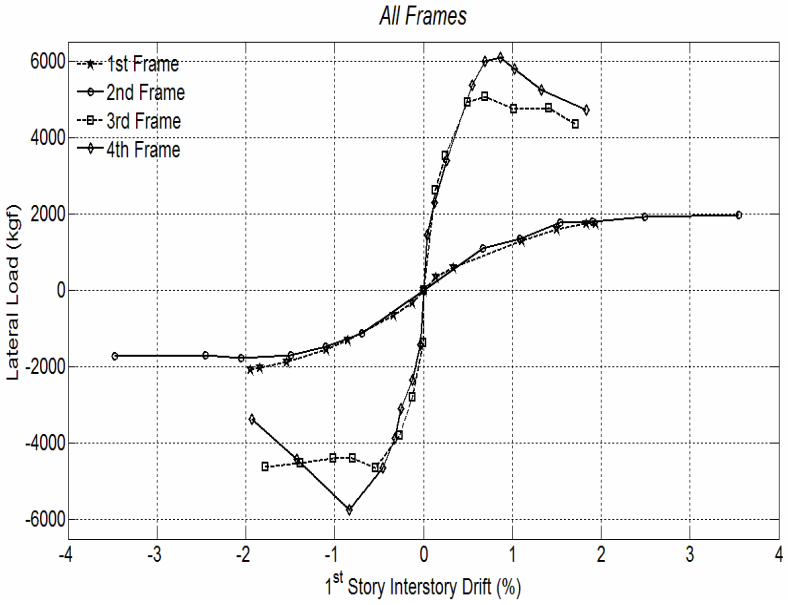

Figure 3.31. Envelope curves of all frames

Figure 3.33 presents the envelope curves of the second frame specimen. Note that second frame reinforcement was designed considering the seismic requirements.

It can be observed from the figure that frame show a ductile behavior. It sustains the lateral load levels without any degradation between ±1.7% to ±3.4% inter-story drift ratios for the first floor. No major strength degradation occurred within the loading groups before the last group at which first floor reached to a drift ratio 3.4%. This value also corresponds to the maximum lateral loading of the frame. At this loading group, a degradation of 15% in strength was observed between the envelop curves of the loading cycles, Figure 3.36.

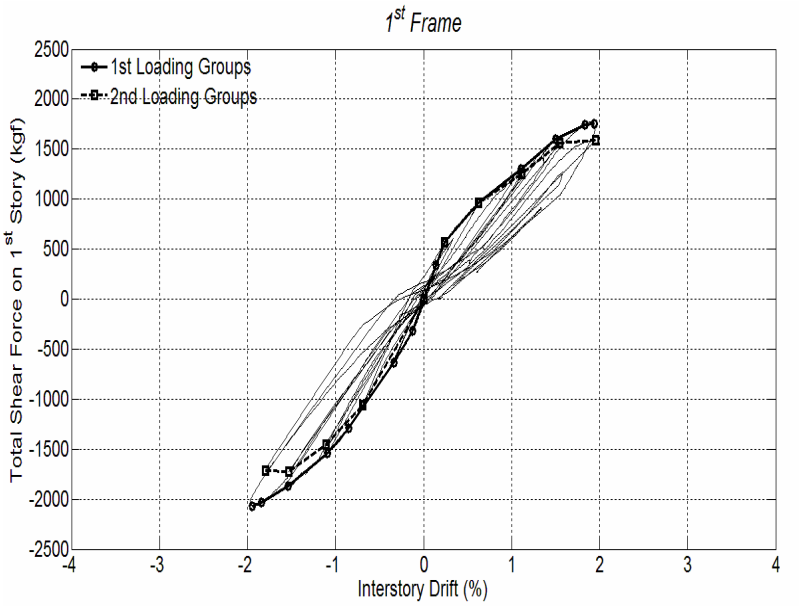

Figure 3.32. Hysteresis and the corresponding envelope curves of the first story, 1st frame

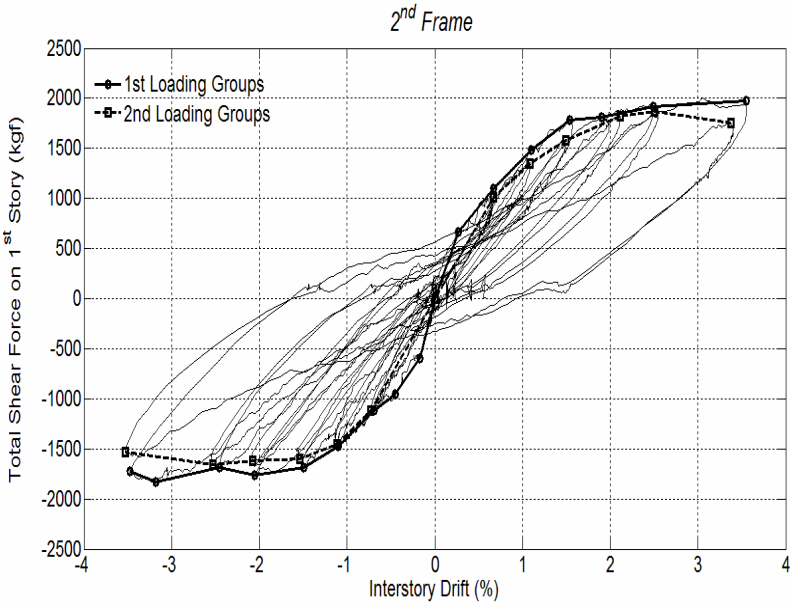

Figure 3.33. Hysteresis and the corresponding envelope curves of the first story, 2nd frame

Figure 3.34 presents the envelope curves of third frame in a similar fashion to previous frames. Compared to the first and second frames, third frame reached a much higher maximum strength level at a much smaller deformation value due to the presence of partition walls. On the other hand, degradation of the second loading cycle started at

an earlier stage with much pronounced decreases. Even though system reached to higher strength values at an earlier drift level, it managed to keep its capacity up the end of the loading. At certain points during the test, loading stopped to observe the behavior of the system. If the force-deformation coordinates of [(-3000kgf,-9mm), (-4200kgf, -8mm), (-3500kgf, -7mm)] are observed, small hysteresis loops could be seen. These loops indicate that if the loading is kept stationary, system creeps and loses some of its strength. Upon loading, system returned to current envelope curve. During the tests, it was observed that this behavior was due to the sliding of the partition wall along the existing cracks. As it was presented, in the third loading group system reached to its maximum strength. At this stage, strength degradation ratio was about 11.5% between first and second loading cycles of the loading group, Figure 3.36.

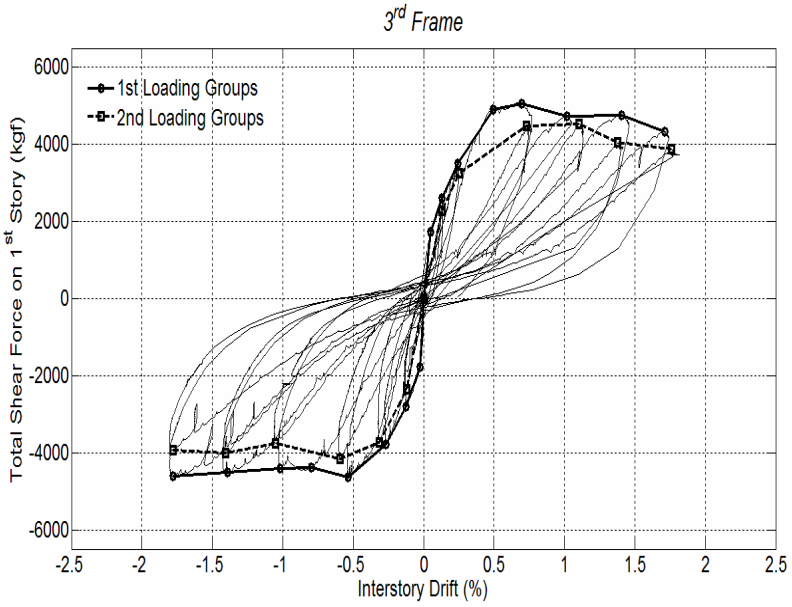

Figure 3.34. Hysteresis and the corresponding envelope curves of the first story, 3rd frame

Envelope curves of the fourth frame are presented in Figure 3.35. Lateral strength of fourth frame was about 17% higher than the third frame. But different than the third frame, capacity degraded quickly after reaching the maximum value. Moreover, in the loading group of maximum lateral loading, strength degraded about 23% between first and second cycles, Figure 3.36. The difference in behavior was result of the failure mode of the partition walls. After having cracked more or less along a single line, third frame partition wall keep sliding back and forth about this single line

of the crack without causing a major damage to the perimeter frame. On the other hand partition wall of the fourth frame kept its integrity with relatively minor cracks and forced the perimeter frame to fail. As a result, even though fourth frame have reinforcement detailed for the ductile behavior, it failed about the same drift levels with the third frame.

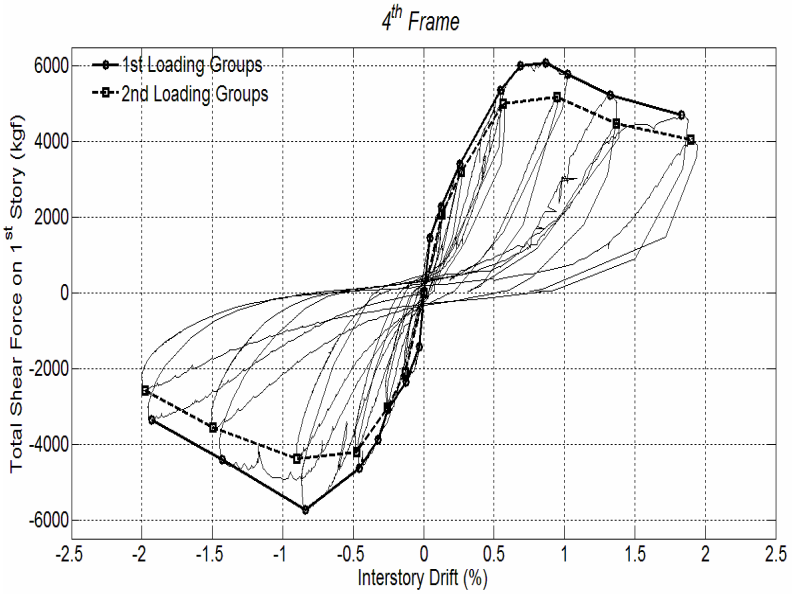

Figure 3.35. Hysteresis and the corresponding envelope curves of the first story, 4th frame

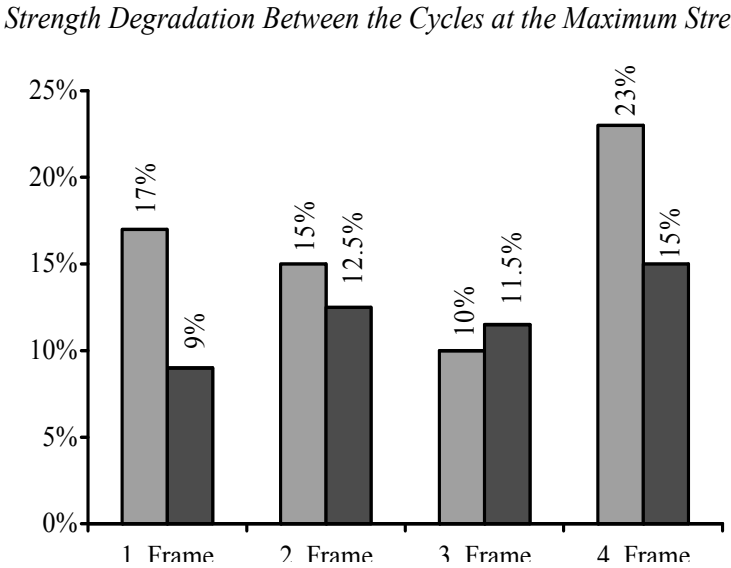

Figure 3.36. Strength degradations for the maximum lateral loading group for west and east directions

In order to observe the effect of test parameters on the softening of each frame stiffness values of the each loading cycle are calculated. Stiffness of the frame at each full cycle is determined by connecting the tips of the force-displacement curves at each extreme with a line and obtaining its slope. Based on the obtained values, stiffness degradation of each frame with reference to maximum inter-story drift ratios in the 1st story reached in that cycle is obtained. Presentation of change in stiffness in the first and second cycles of each loading group is done by creating a normalized stiffness graph against inter-story drift ratio of the 1st story. In each of these graphs, maximum stiffness among the loading cycles is normalized to 100%.

Change of stiffness in the frames between first and second loading cycles are presented in Figure 3.37. For the first frame, it can be observed that first cycles always exhibit a higher stiffness value than the second cycles. Moreover, as the inter-story drift ratio increases, stiffness decreased. First frame stiffness value is obtained as 310 t/m in the first cycle of first loading group.

Similar to the first frame, second frame stiffness decreased in second cycles of each loading cycle groups compared to the first cycles. Stiffness again decreased with increasing inter-story drift. If hysteresis curves are observed, a clear softening in stiffness in the continuing loading groups can be clearly seen. Stiffness of the second frame reached a maximum 275 t/m value in the first cycle of first loading group.

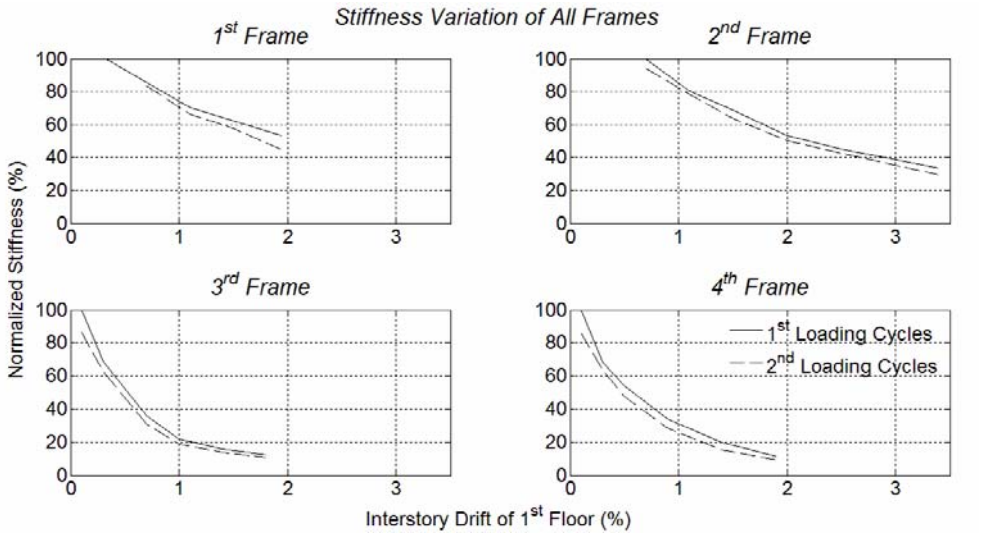

Figure 3.37. Normalized stiffness change of all frames separately

Similar to the previous frames softening of stiffness of the third frame can be seen from the hysteresis curves. Absolute value of the stiffness was much higher than the bare frames. And even though inter-story drift ratios were lower than the bare frames, higher stiffness degradation observed in the third frame compared to the first two bare frames, Figure 3.38. Second cycles had lower stiffness values in each stage of loading groups. Third frame reached a maximum 3435 t/m stiffness value in the first cycle of first loading cycle group.

Fourth frame exhibited a similar behavior for stiffness degradation with the third frame. In the first cycle of first loading group stiffness reached to a maximum 3110 t/m value. Again second loading cycles always exhibited lower stiffness values than the first loading cycles.

At this point it should be noted that, decrease in stiffness of third and fourth frames are sharper than the stiffness of first and second frames due to the presence of partition walls, Figure 3.38.

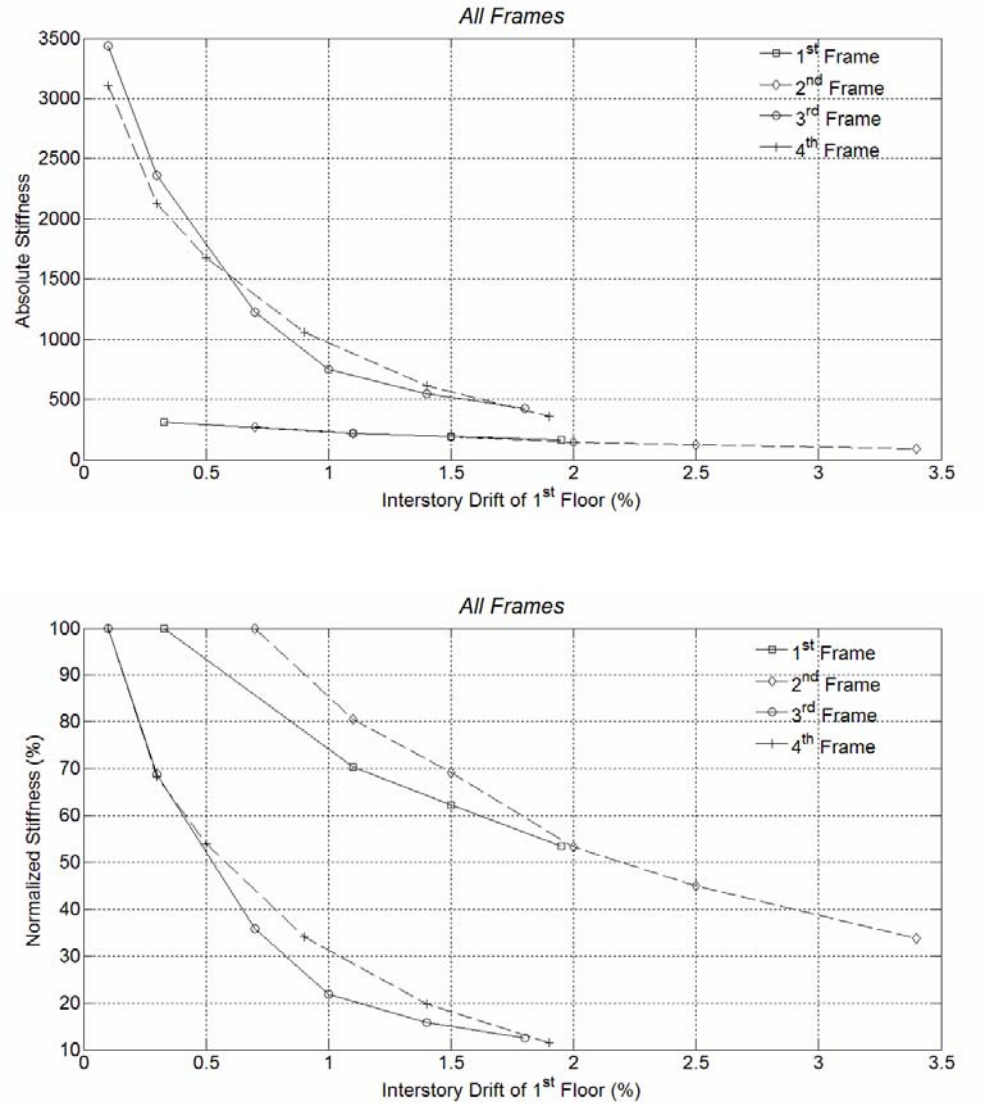

Figure 3.38. Absolute and normalized stiffness change of all frames together

3.4.2. Energy Dissipation

Energy dissipated by frames through hysteresis is defined by the area within the hysteresis curves of the frames. In order to observe the energy dissipation characteristics of the test frames, dissipated energy values of each cycle is calculated and presented in Figure 3.39. Cumulative energy dissipation of each frame against the inter-story drift ratios of first story can be observed from the figure. Dissipated energy values of all stories are calculated and summed with each other for that cycle of loading group. In order to compare the dissipated energy between the first and the second loading cycles of each loading group, energy dissipated in the second loading cycles are also presented.

Cumulative dissipated energy of the first frame is presented in Figure 3.39a. While first story reached 1.95% inter-story drift ratio at the first story, system dissipated a total of 14 kg.m energy in the first loading cycles. Second loading cycles dissipated only 33% of energy dissipated in the first loading cycles. It can be observed that for all of the frames second loading cycles dissipated less energy than the first loading cycles. The amount of dissipated energy is observed to be higher at the upper inter-story drift ratios due to increasing deformation of system which force systems to sustain larger damages in the nonlinear regions.

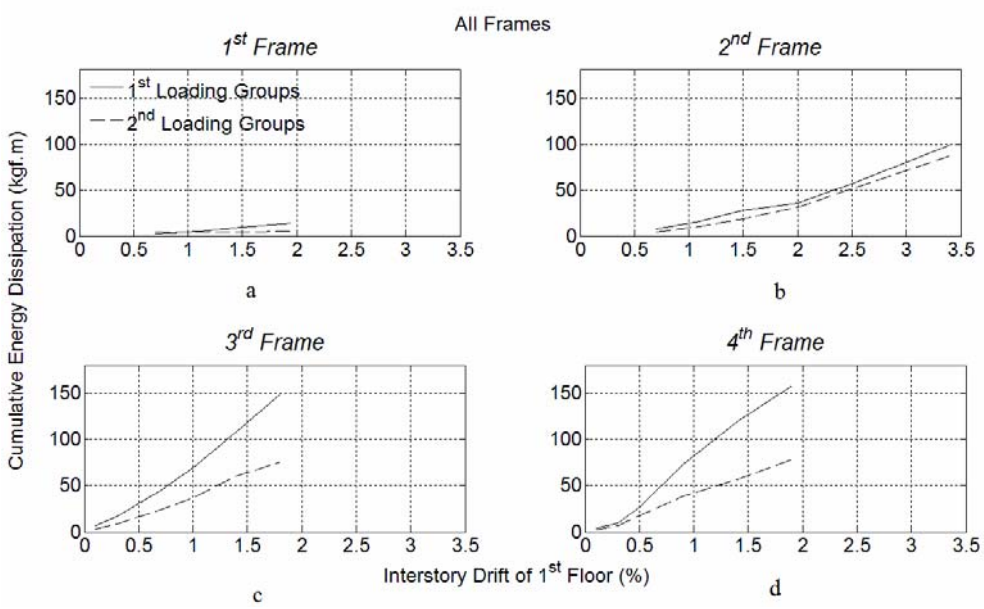

Figure 3.39. First frame dissipated energy in all loading groups

Cumulative dissipated energy of the second frame is presented in Figure 3.39b. As a result of the existing ductile reinforcement design, amount of the dissipated energy is 7 times higher than the maximum value reached by the first frame. Even though still second loading cycles keep the trend of dissipating less energy, difference between the cycles decreased. The amount of absorbed energy in the second loading cycles reached to 87% of the first loading cycles. Similar to the first frame, more energy absorption occurred at higher drift levels.

Cumulative energy absorption by third frame is presented in Figure 3.39c. Similar to the bare frames amount of energy dissipated increased with the increase in the drift. On the other hand, at 1.8% inter-story drift ratio in the first story, frame

absorbed 10.5 and 1.5 times more energy than the first and the second frames, respectively. This result can be explained by the presence of partition walls in the system. However, absorption rates were not sustainable and energy absorbed by the second loading cycles was only about 50% that of first loading cycles.

Cumulative energy absorption by fourth frame is presented in Figure 3.39d. While inter-story drift of the first story reached to 1.9% at the limit, frame absorbed the highest amount of energy among the frames. Peak value is only 5% larger than the energy dissipated by the 3rd frame. Considering that 4th frame had ductile reinforcement detail, dissipated energy is smaller than it is expected. The premature failure of the frame in the 1st story columns caused this result. Energy absorption of second loading cycles reached to %49 of first loading groups.

CHAPTER 4

DYNAMIC TESTS

4.1. Introduction

In this study dynamic tests were conducted to estimate dynamic parameters of the test frames at the end of each loading cycle. Dynamic behavior of the test specimens are discussed thru estimated dynamic parameters which are the natural frequencies, damping and the modal shapes of the frames. Dynamic parameters are estimated by use of the modal analysis methods (He J. and Fu Z.F., 2001). Since dynamic parameters are dependent on the boundary conditions, frames needed to have the support conditions for which the dynamic parameters were aimed to be measured. Therefore static loading setup was detached from the frames to have a free standing frame at the end of each cycle. Dynamic tests (modal tests) were conducted through impact and snap-back excitations. Each excitation type was summarized in Chapter 2. In this chapter measured waveforms and the dynamic parameters of the frames that are obtained by modal analysis will be presented and results discussed.

4.2. Check of Modal Analysis Main Assumptions

In order to use experimental modal analysis methods, main assumptions of modal analysis must be verified. These are the linearity and time invariance of the measured systems.

The first assumption dictates that the measured structure should be linear. Violation of this assumption invalidates mathematical basis of the experimental modal analysis method. Assumption indicates that response of the structure to any combination of simultaneously applied forces, is the sum of the individual responses to each of the forces acting alone. It also implies that frequency response functions (FRF) of the system are independent of excitation amplitudes. If a structure is linear, its behavior can be characterized by a controlled excitation experiment in which forces applied to the

structure have a convenient condition for measurement and parameter estimation rather than being similar to the forces that are actually applied to the structure in its normal environment.

The second assumption dictates that structure should be time invariant. For a chosen force excitation and response location, a linear structure should exhibit identical FRF curves for each measurement. To prove the time invariance by selection of excitation and output locations and testing conditions, a number of measurements is performed with time intervals. Generally, selected FRF measurements are the measurements taken at the begining and the end of the tests of the structure. FRF's obtained by these measurements should be very similar, if not identical, to satisfy the assumption.

In this study to check the linearity of frames, FRF with different intensities were compared with each other to verify whether the estimated FRF were same for measurements with different intensities. Linearity check was applied to the each frame. Considering that the largest deviation from linearity assumption takes place with the heaviest damage in the frames, linearity check of the heavily damaged condition after the last cyclic loading group is presented for each frame. It must be noted that the linearity considered is not the linearity in general understanding but having responses that could be accepted to be linear for dynamic parameter estimation. Linearity check in undamaged condition is also presented for the first frame.

Impact hammer with a soft tip was used for exciting the system (Chapter 2 Section 2.5.2). Typical recorded waveforms of the impulse and the acceleration data and their frequency domain representation are presented in Figure 4.1. As it can be observed from the figure, impact of the hammer created about a 3500N force and given impulse excited the frequency below 50Hz efficiently. It can be observed from the acceleration response that motion died out in 5 seconds. Frequency representation of the acceleration record shows that below 50Hz there are 4 peaks. Each peak is an indication of a possible mode of the system.

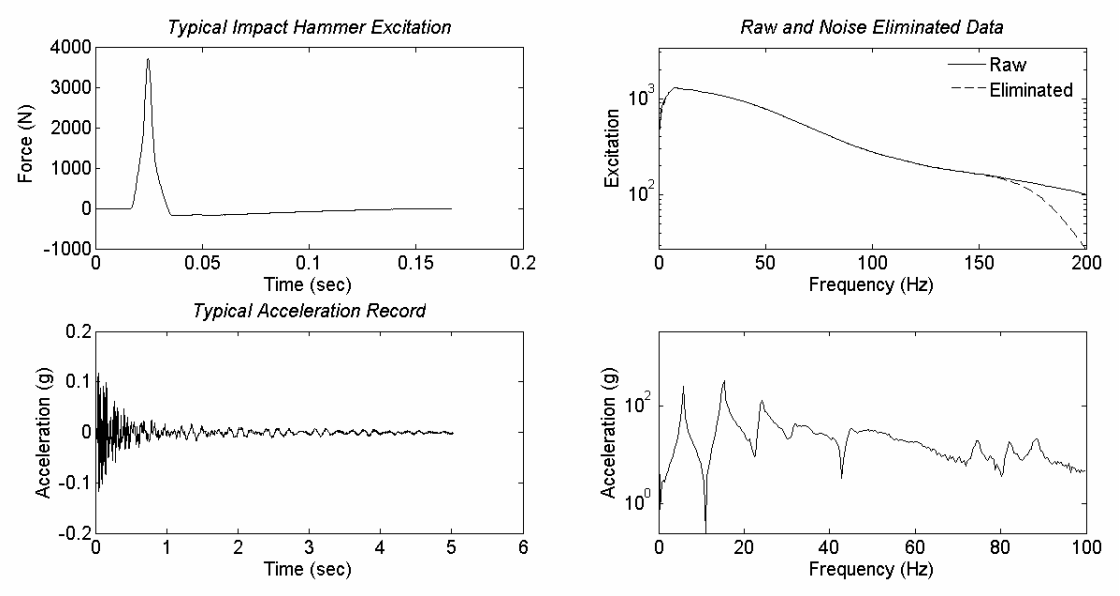

Figure 4.1. Time and frequency domain representations of typical impulse of impact hammer (top) and the acceleration response created in the system (bottom)

Linearity check of the first frame was performed for the records taken at undamaged and heavily damaged conditions. In each case two impacts with different force levels were chosen to observe the differences between FRF. Selected impacts had magnitudes of 2320N and 1960N for undamaged case, Figure 4.2. FRF of the selected impacts showed that system could be accepted linear below 40Hz frequency, Figure 4.3. Calculated FRF of all the frames were based on an impulse given at the fourth floor level and acceleration responses at the levels presented in Figure 2.16 and with the given numbering in the figure. For example H1 represents the FRF for an impact at fourth level with the acceleration response at the 1st position in Figure 2.16. Chosen impact levels for the measurements after last loading group were 2680N and 3920N, Figure 4.4. Considering the repeatability of the FRF below 25Hz, system could be accepted linear up to this level. Observation from the first frame reveals that even though system is damaged heavily, it is acting as linear system below a certain frequency. It should be noted that shape and magnitudes of the peaks in FRF of the system changed position from undamaged to damaged stage. It indicates that even though system could be accepted to be linear below a certain frequency at each damage state for experimental modal analysis purposes, dynamic parameters of the system changes with the level of damage.

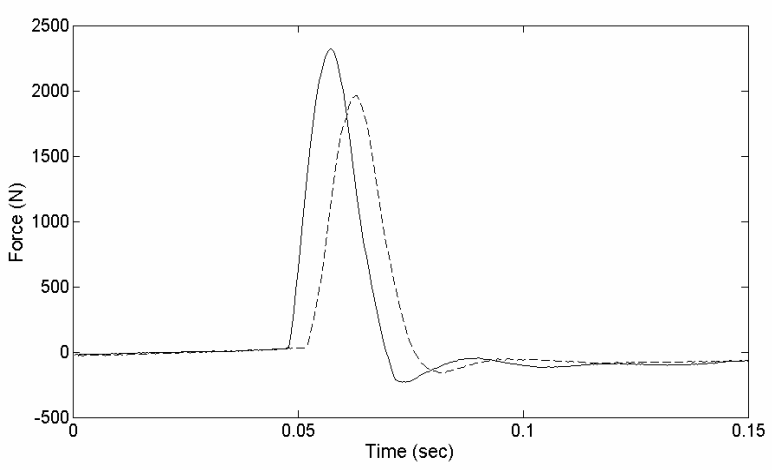

Figure 4.2. Amplitudes of selected impacts, first frame for undamaged case

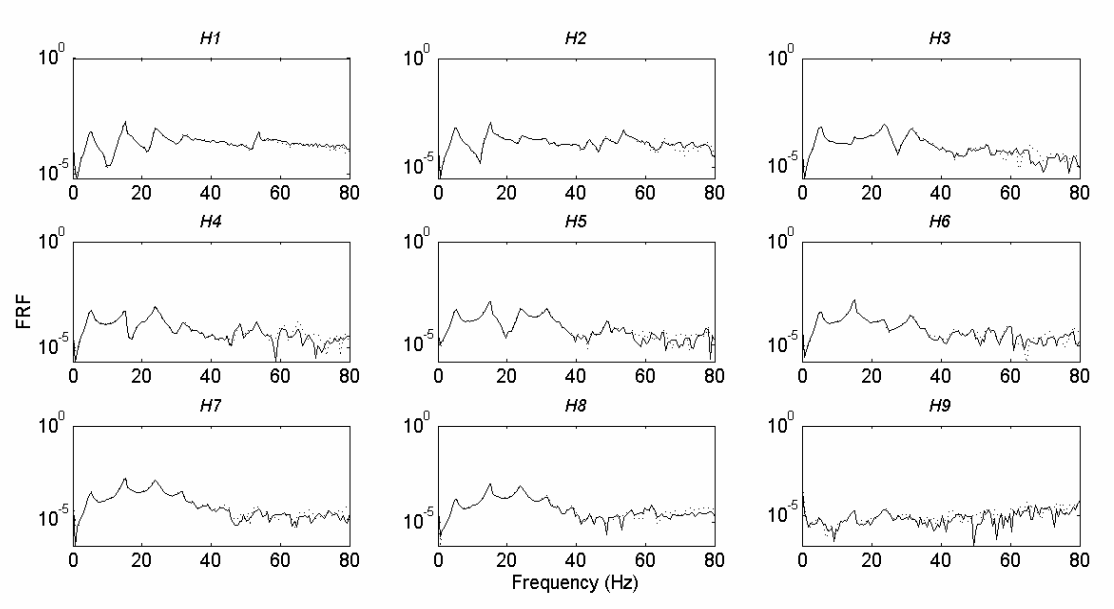

Figure 4.3. FRF of the first frame calculated for each measurement point for the excitations presented in the preceding figure, undamaged case

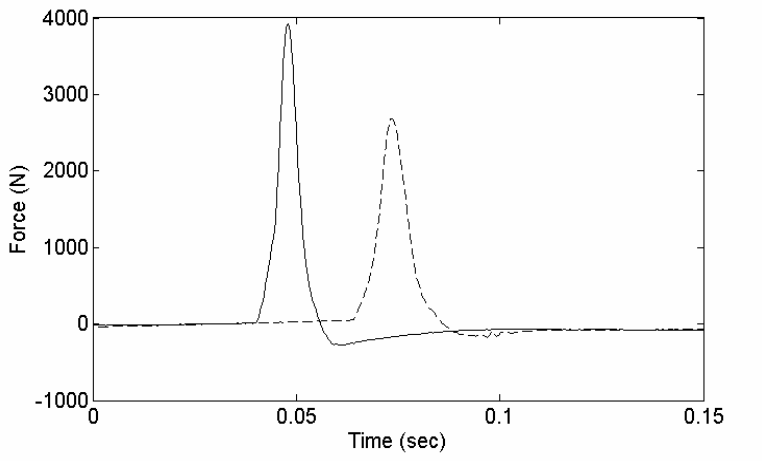

Figure 4.4. Amplitudes of selected impacts, first frame at the end of last loading group

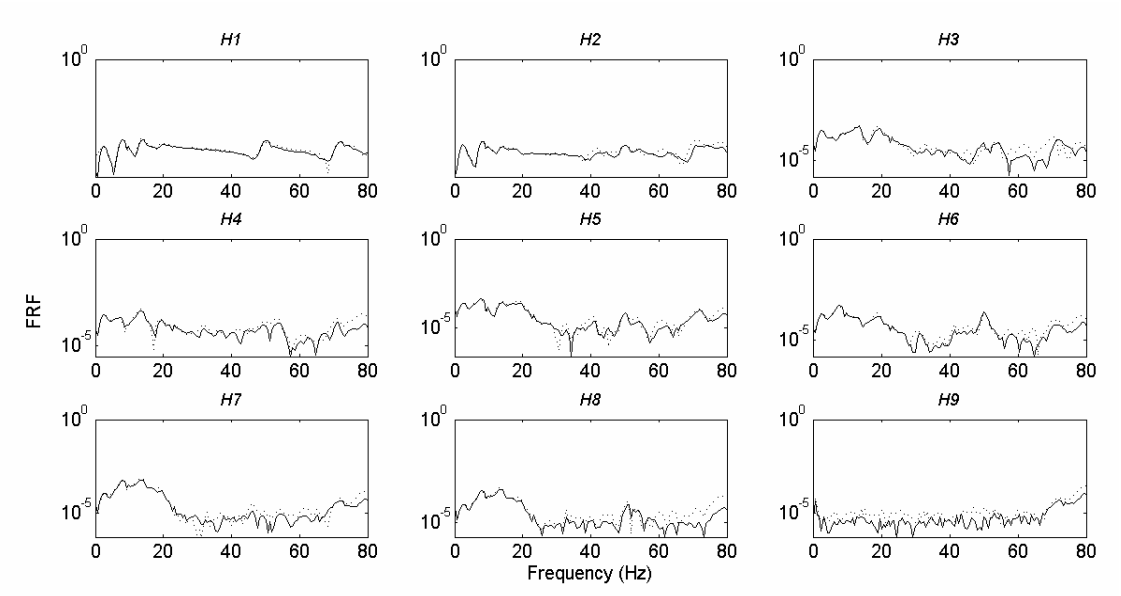

Figure 4.5. FRF of the first frame calculated for each measurement point for the excitations presented in the preceding figure, after last loading group

Linearity check of the second frame was performed for the records taken at the end of sixth loading group. Impulse waveforms of the chosen impacts are presented in Figure 4.6. FRF calculated for each measurement point are compared in Figure 4.7. From the figure, it can be observed that, system has a linear behavior below 20 Hz frequency.

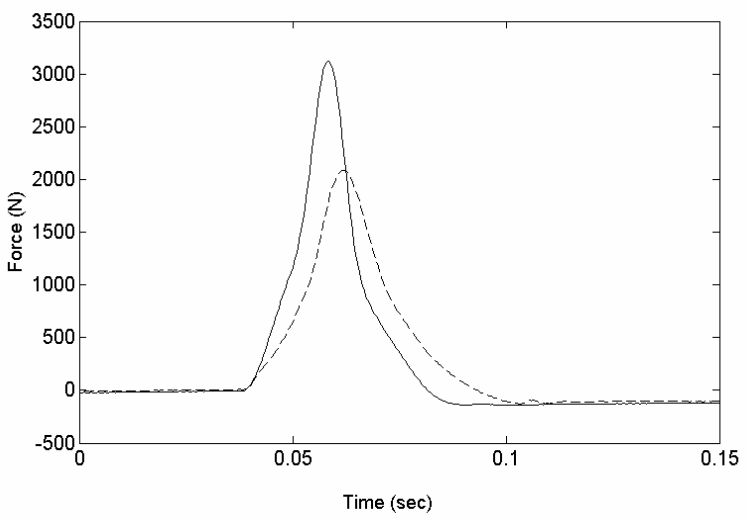

Figure 4.6. Amplitudes of selected impacts, second frame at the end of sixth loading group

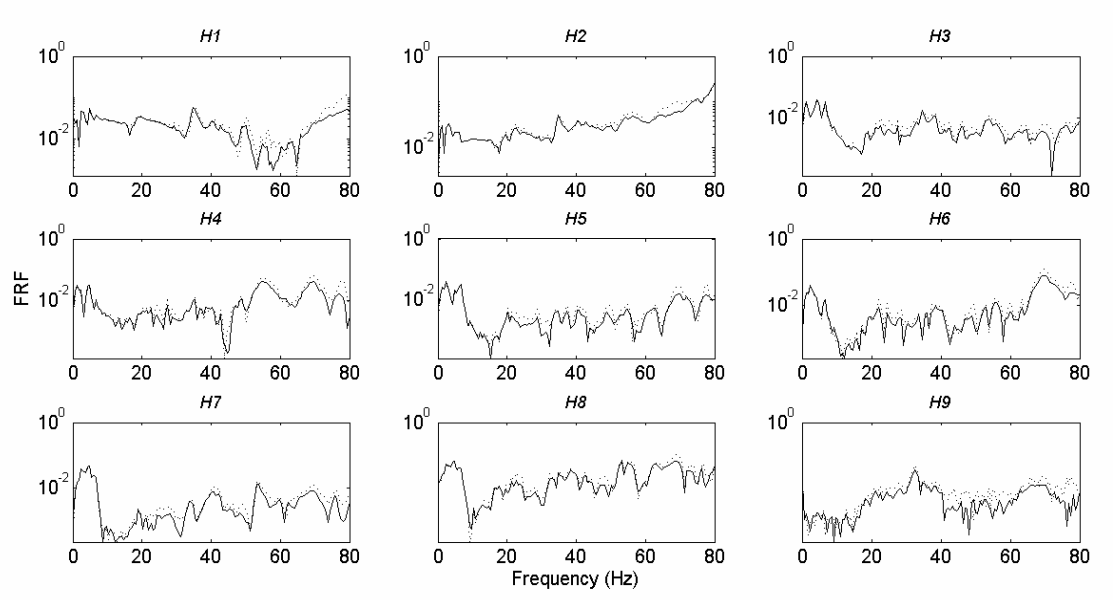

Figure 4.7. FRF of the second frame calculated for each measurement point for the excitations presented in the preceding figure, at the end of sixth loading group

Linearity check of third frame is performed for the records taken at the end of sixth loading group. Impulse waveforms of the chosen impacts are presented in Figure 4.8. Calculated FRF of the impacts for each measurement points are presented in Figure 4.9. As it can observed from the figure frame system is behaving linear below 30Hz.

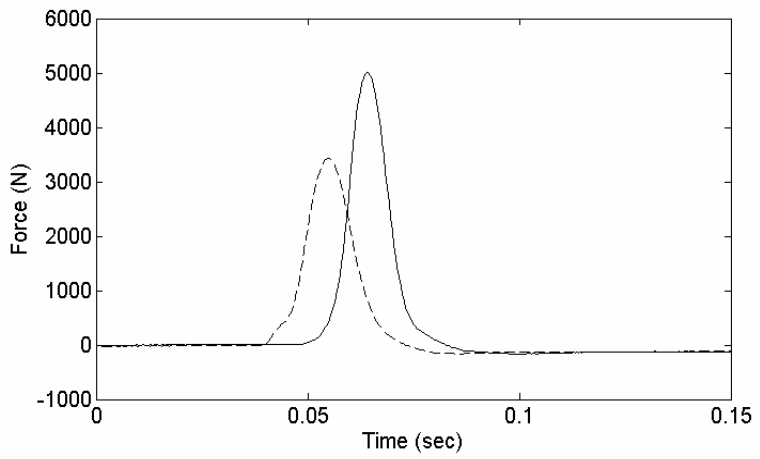

Figure 4.8. Amplitudes of the selected impacts, third frame at the end of sixth loading group

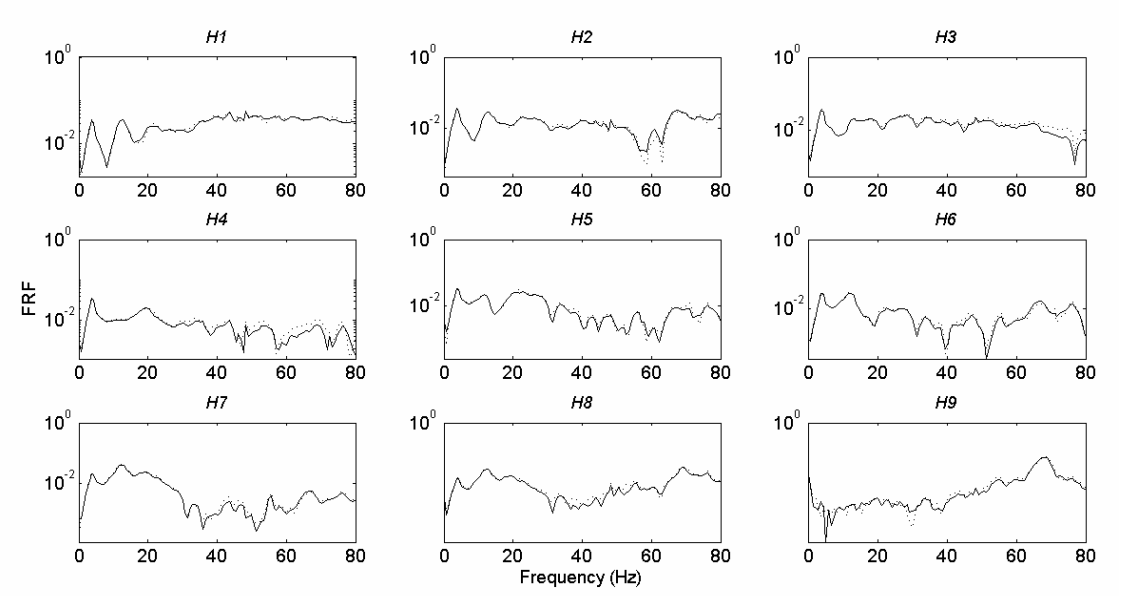

Figure 4.9. FRF of the third frame calculated for each measurement point for the excitations presented in the preceding figure, at the end of sixth loading group

Final linearity check is performed for the fourth frame for the records taken at the end of the sixth loading group. Chosen impulse waveforms are presented in Figure 4.10. As it can be observed from the figure, selected impact amplitudes of the fourth frame have the magnitudes of 4500N and 5400N respectively. FRF calculated for each measurement points are presented in Figure 4.11. From the figure, it can be observed

that the fourth frame system is behaving linear below 30Hz except H8 due to the heavy shear cracks on first story columns and low signal.

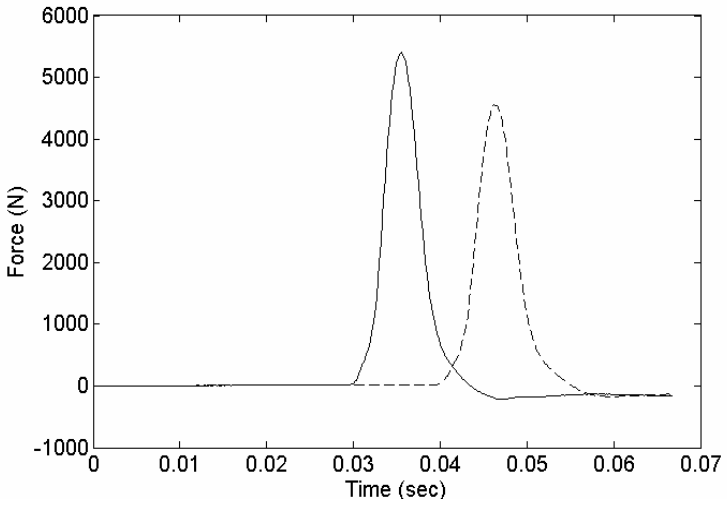

Figure 4.10. Amplitudes of the selected impacts, fourth at the end of sixth loading group

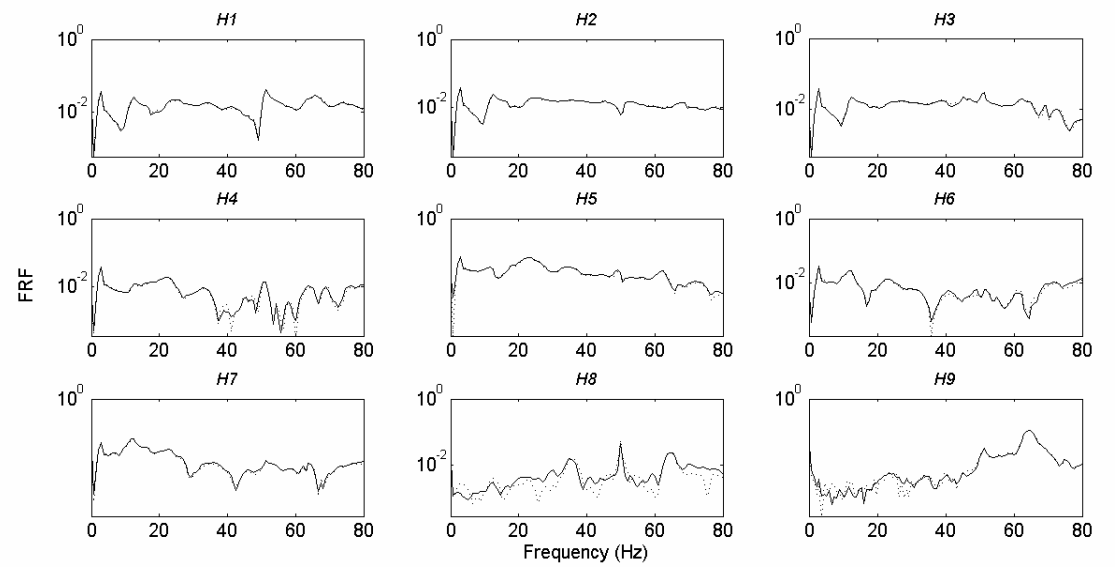

Figure 4.11. FRF of the fourth frame calculated for each measurement point for the excitations presented in the preceding figure, at the end of sixth loading group

Even though frames were damaged, FRF of impact tests exhibited linear behavior in certain frequency intervals. As a result of this observation, it is decided that linearity assumption of modal analysis is valid at these intervals. Therefore, dynamic parameters of systems can be obtained by modal analysis method.

Maximum excitation force that could be given to frames was 5500N. Under such an excitation frames remain in the relatively linear portion of their response. Therefore, in order to excite the frames beyond the linear portion of the hysteresis curves snap-back tests were designed, Chapter 2, Section 2.5.2. For this purpose frames were pulled at the fourth story levels. The drift amount was selected to be half of the maximum drift reached in the fourth story level by the frame in that loading cycle.

It has been observed that Fast Fourier Transforms (FFT) of the snap-back signals have peaks at similar frequencies to impact signals. Encouraged with this observation, out of boldness, it is attempted to feed the FFT signals of the snap-back excitations as a FRF to the algorithm that is used for the estimation of dynamic parameters with the impact data. It is observed that estimated frequencies and the modal shapes with this approach are very similar to parameters obtained from impact excitations. Similar to impact excitations obtained, damping values were out of the physically sensible values and therefore not reported. In order to differentiate FRF obtained by snap-back with the FRF obtained by impact tests, they will be called as the pseudo-FRF.

To observe the response of the system at different levels and repeatability of the behavior, two comparisons are made with the data recorded after the second loading group of the first frame. At this loading stage, first frame system reached to 75% of its lateral load capacity and structural elements of frame system sustained damages.

First set contains two records with initial displacements of 6mm and 12mm at the fourth story, Figure 4.12. Pseudo-FRF of the data show that amplitudes of the peak locations are different and frequencies of the peaks have a trend of sliding to the higher frequency values, Figure 4.13.

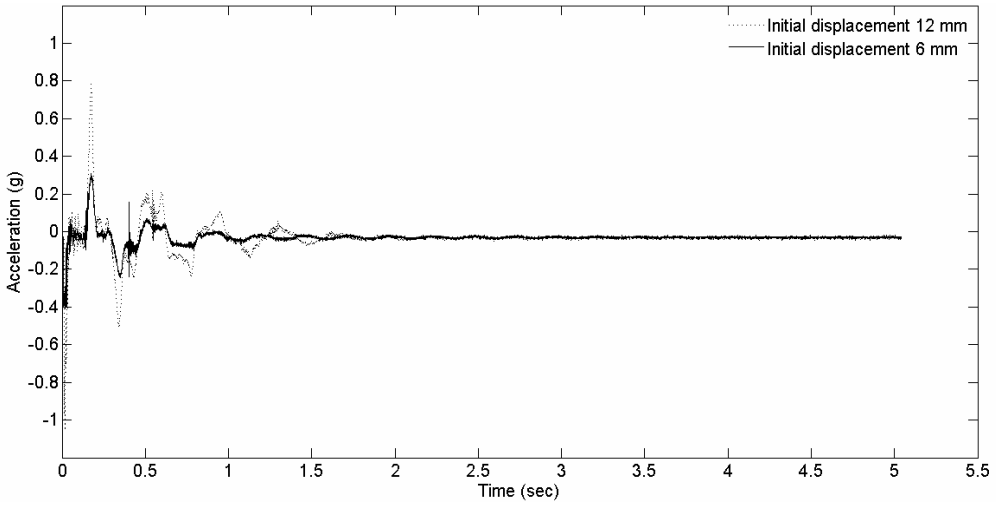

Figure 4.12. Comparison of acceleration response in snap-back tests of the first frame at the end of second loading group

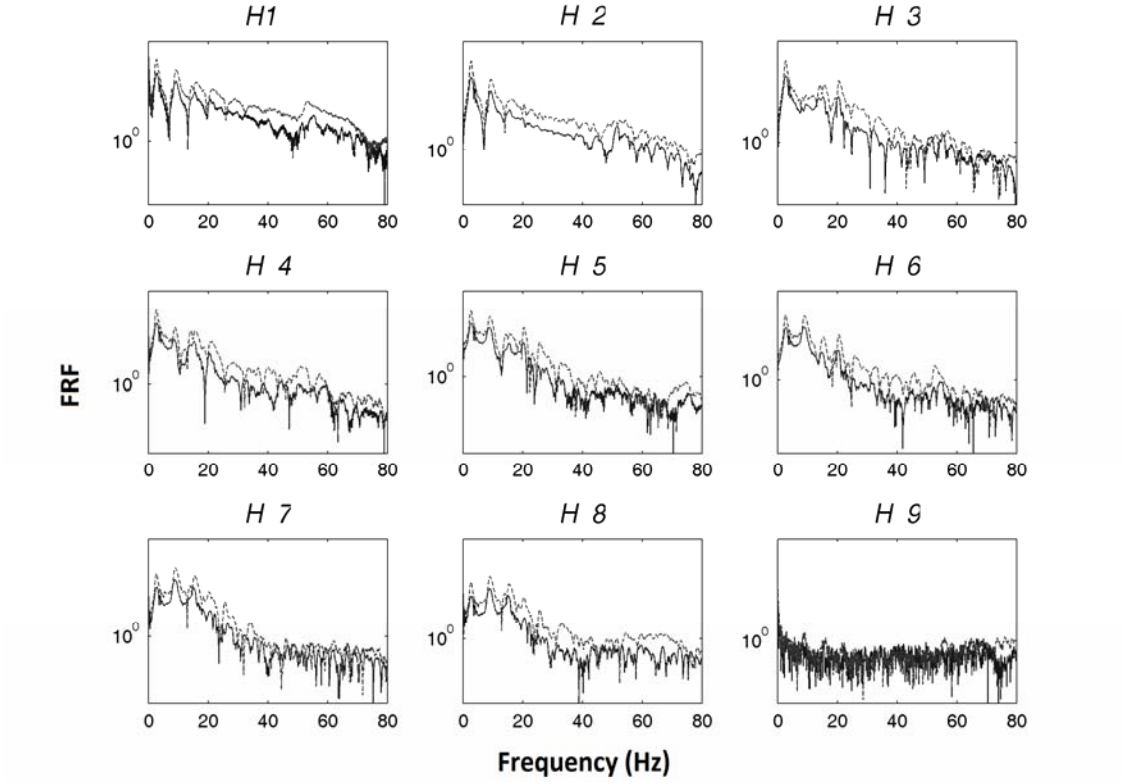

Figure 4.13. Pseudo-FRFs of the first frame calculated for each measurement point after snap-back excitations at the end of second loading group. Solid lines represent 6mm initial displacement and dashed lines represent 12mm initial displacement

Second set is chosen to contain two records with initial displacements of 12mm,

Figure 4.14. Pseudo-FRF of the data showed that up to 40Hz levels both records give

same signal, Figure 4.15. In spite of the existing damage, frame system exhibits a stationary response. Observation revealed that, even though dynamic parameters of the frame changes at different excitation levels, if the excitation level is kept constant system have the same dynamic signature up to a certain frequency. Pseudo-FRF of the 2nd to 4th frames are presented for the heaviest damage levels at Figure 4.16, Figure 4.17, and Figure 4.18, respectively. Except the fourth frame, all frames exhibit the stationary character. After the second cycle, the frequency band of the fourth frame included only the first mode of the system. Pseudo-FRF of fourth frame at the end of first loading group are presented in Figure 4.19.

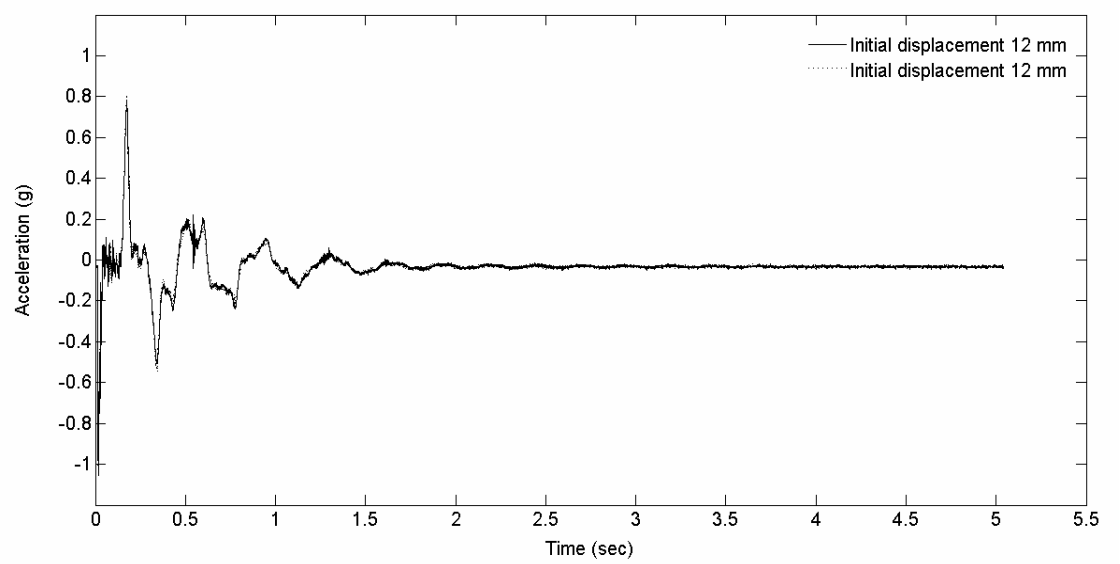

Figure 4.14. Comparison of acceleration response in snap-back tests of the first frame at the end of second loading group

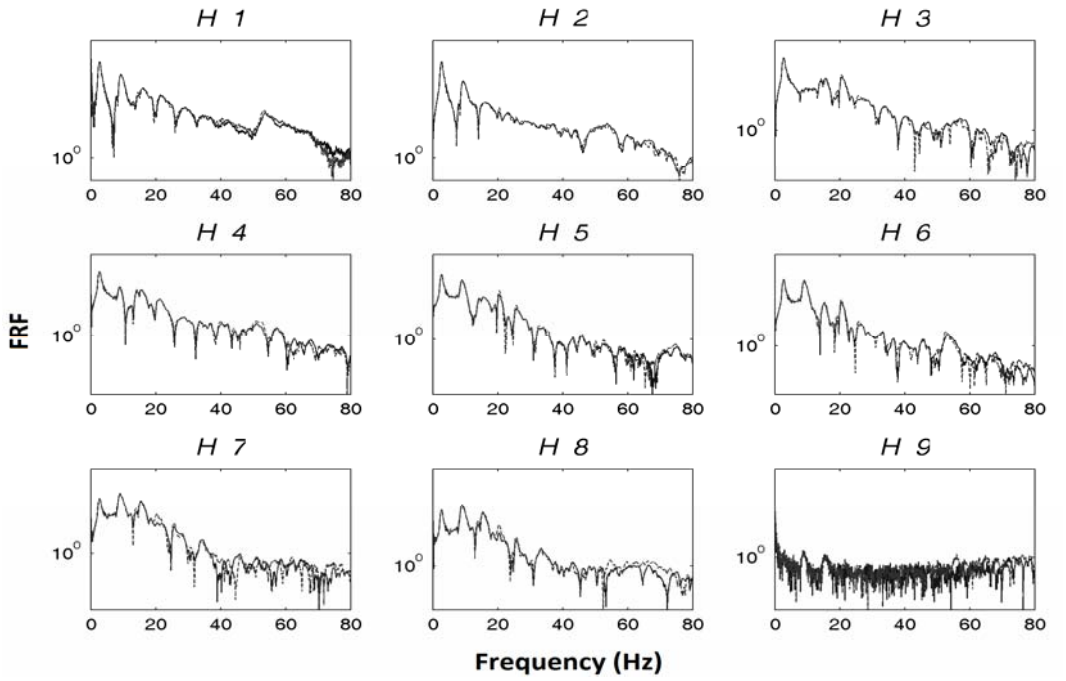

Figure 4.15. Pseudo-FRF of the first frame calculated for each measurement point after snap-back excitations with equal initial displacements at the end of second loading group

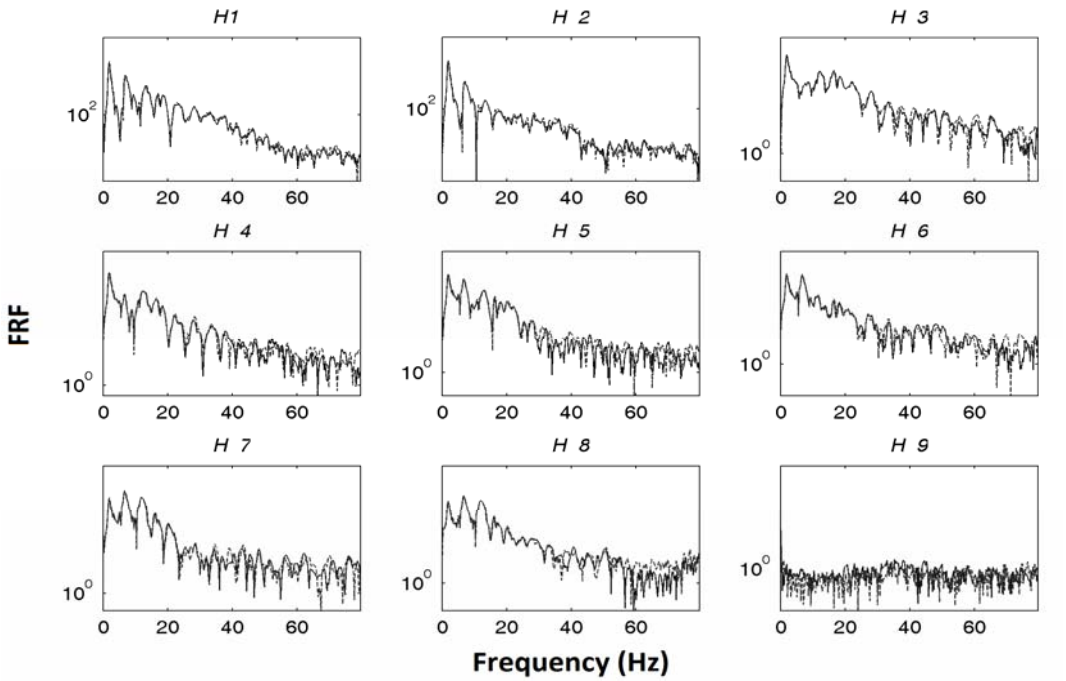

Figure 4.16. Pseudo-FRF of the second frame calculated for each measurement point after snap-back excitations with equal initial displacement at the end of sixth loading group

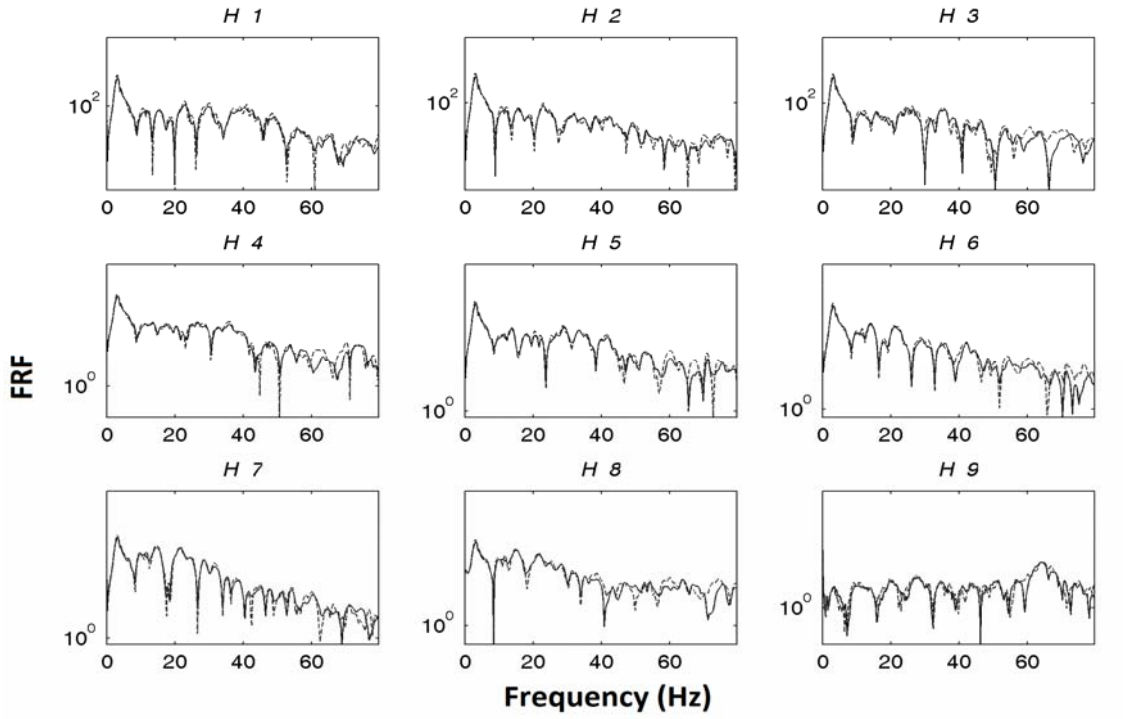

Figure 4.17. Pseudo-FRF of the third frame calculated for each measurement point after snap-back excitations with equal initial displacement at the end of sixth loading group

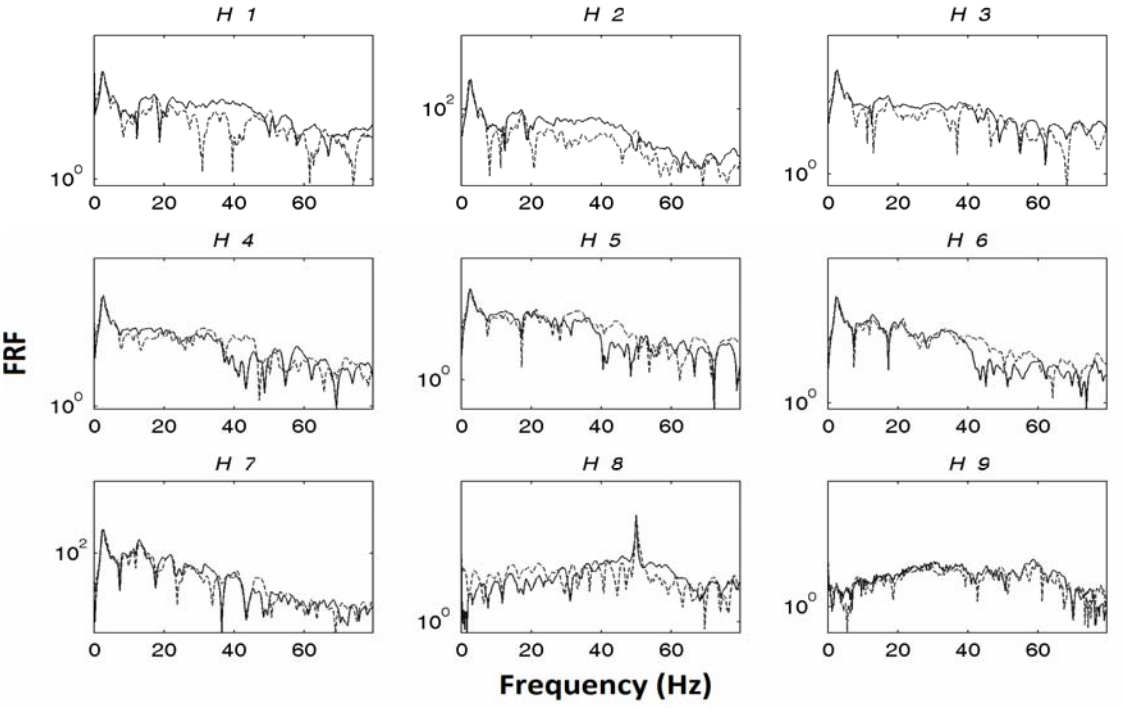

Figure 4.18. Pseudo-FRF of the fourth frame calculated for each measurement point after snap-back excitations with equal initial displacement at the end of sixth loading group

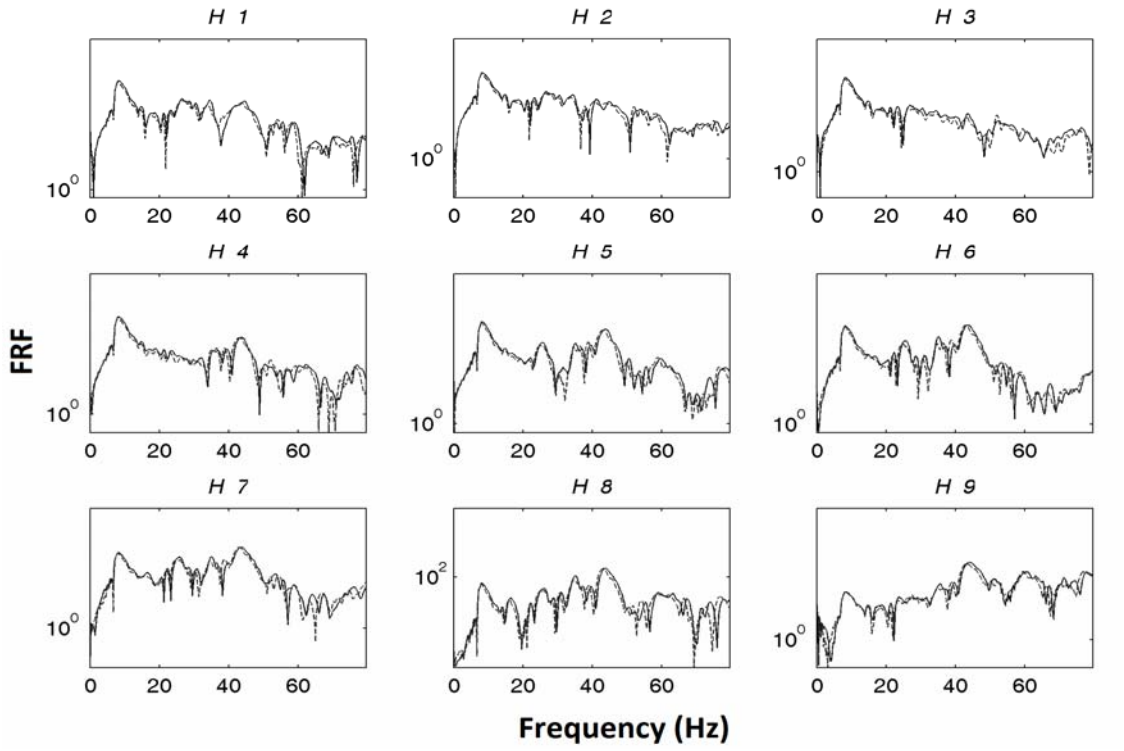

Figure 4.19. Pseudo-FRF of the fourth frame calculated for each measurement point after snap-back excitations with equal initial displacement at the end of first loading group

4.3. Estimation of Dynamic Parameters

Verifying that linearity assumption holds at the frequencies that are including the modes of the system, dynamic parameters of frames were identified by modal analysis methods using impact data. Also observing the steady pseudo-FRF responses exhibited by the snap-back tests at impulses of similar amplitude, modal analysis methods were also used to identify dynamic parameters of the frames at the corresponding excitation levels.

Modal analysis was performed by use of X-Modal computer program. It is an experimental modal analysis program that is able to identify the dynamic parameters from the obtained frequency response functions. Results of both identification approaches are presented below.

4.3.1. Impact Hammer Data

FRF of the first frame for damage levels reached at the end of each loading cycle are presented in Figure 4.20. Since strongest signal was recorded at 4th story for all of the frames, this signal is used for presentation purposes in the figure. Presented FRF of the first frame showed that dynamic characteristics were changing with damage. As it can be observed from the figure, undamaged case of first frame had four sharp peak points, which varies between 5 to 35Hz. At the end of first loading group, although it is still possible to observe four modes of system, sharpness of peak points softens and shifted towards origin. In this stage, dominant frequencies varied between 5 to 25Hz levels. FRF of the later loading groups had a similar trend with the first loading group. Finally, at the end of fourth loading group, dominant frequencies were varying between 2 to 20Hz. Shift of the peaks of FRF indicates the reduction of stiffness in the frames. And softening of the peak points is an indication of increase in damping.

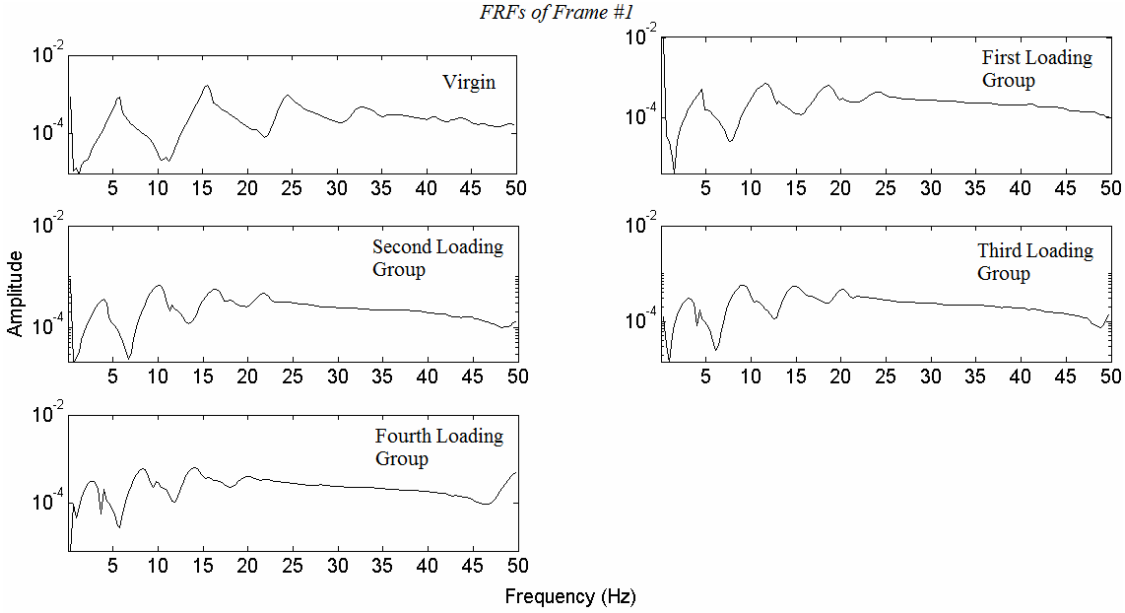

Figure 4.20. Calculated FRFs for the fourth story of the first frame for all loading groups

FRF of the second frame are presented in Figure 4.21. As it can be observed from the Figure 4.20 and Figure 4.21, change of the dynamic parameters of the second

frame had a similar behavior with the first frame. Frequencies of the peaks decreased and the sharpness softened.

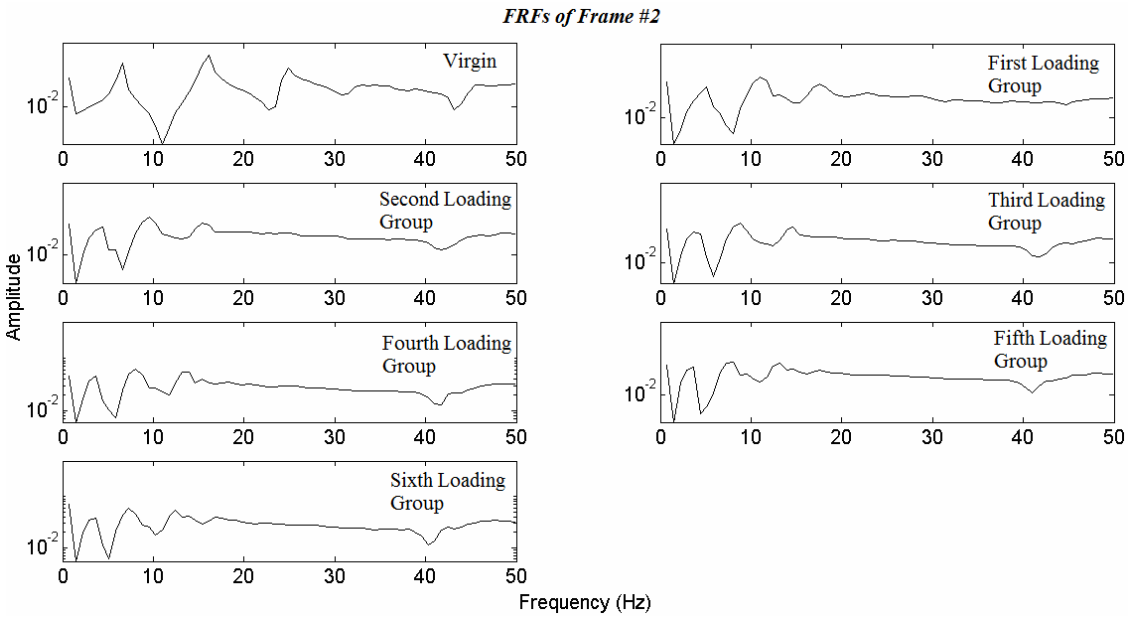

Figure 4.21. Calculated FRF for the fourth story of the second frame for all loading groups

FRF of third and fourth frames are presented in Figure 4.22 and Figure 4.23, respectively. From the figures, it can be observed that at higher damage levels, new peaks appeared. At the undamaged case of third frame, the first dominant frequency was at 16Hz levels. This value reduced almost one half at the end of the following loading group and at the end of the last loading it was about 3Hz. This decrease is much higher than the decrease in the bare frames at which frequency of the first mode decreased to one third of the undamaged state. In spite of the appearance of new peaks at the higher damage levels and shifting of these frequencies towards origin, FRF of third frame had a continuous transformation.

Different from third frame FRF, fourth frame had a sudden change at the end of fourth loading group which can be observed from the figure. Fourth loading group is the group at which heavy diagonal cracks formed at the top of the 1st story columns. On the other hand, frames with infill walls had a similar transformation with the first two frames in softening of the peaks. In other words damping increased with damage.

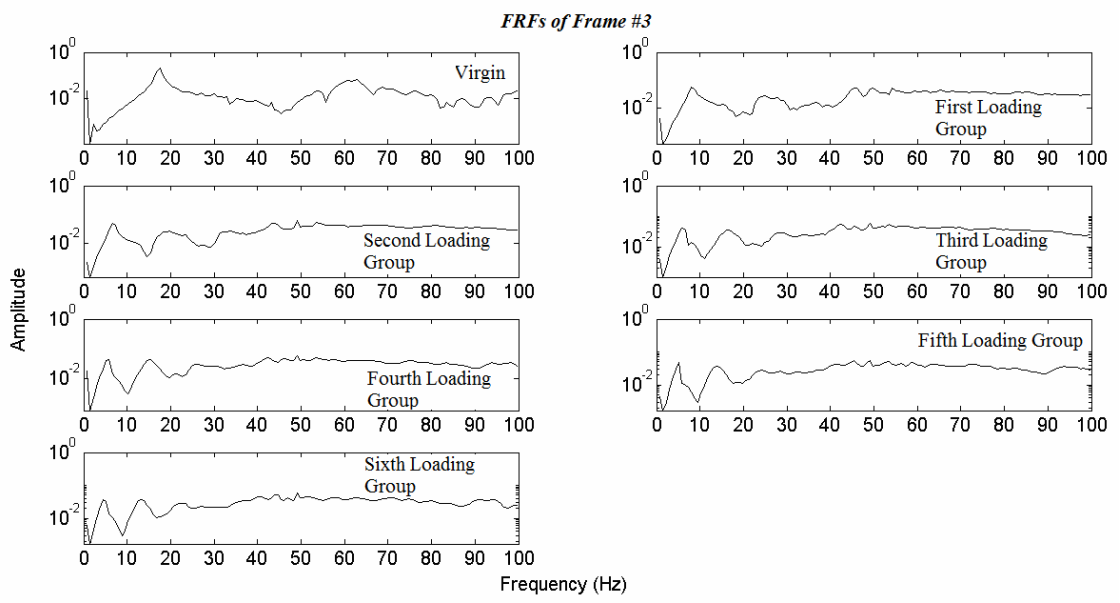

Figure 4.22. Calculated FRF for the fourth story of the third frame for all loading groups

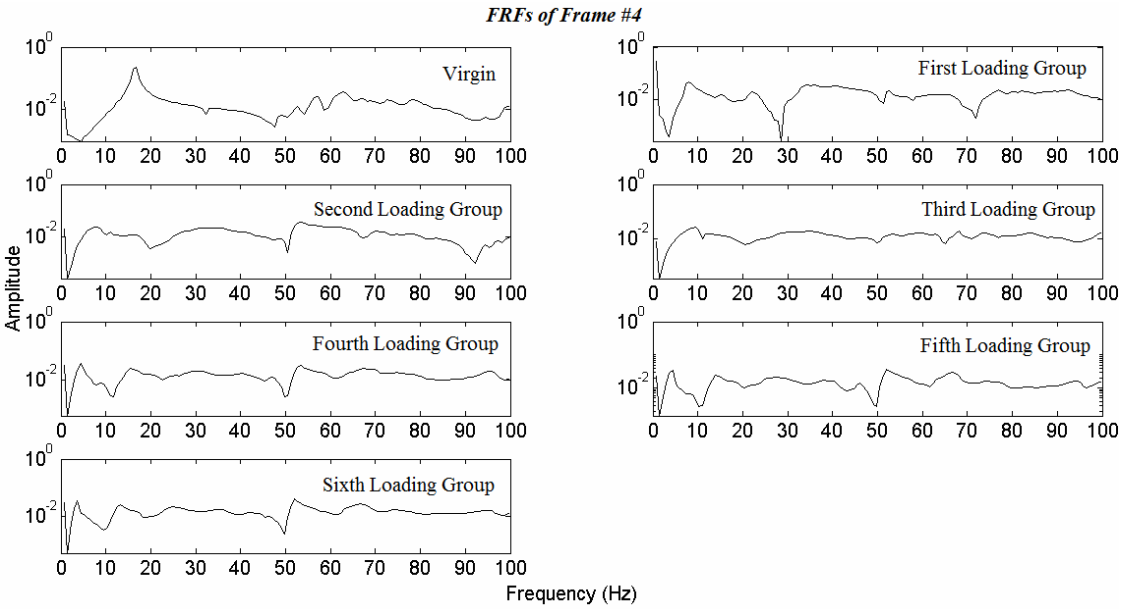

Figure 4.23. Calculated FRF for the fourth story of the fourth frame for all loading groups

Dominant frequencies and corresponding modal shapes of these dominant frequencies are determined by application of complex mode indicator function to the obtained FRF. Even though it is possible to determine damping values with this estimation method, after investigation of the damping values obtained it is decided that estimated damping values are not realistic. Thus, damping results are not reported.

Dominant frequencies of the first and second frames are presented in Table 4.1 and Table 4.2, respectively. As it can be observed from the tables, dominant frequencies did not differentiate from frame to frame with increasing damage in the system. This situation can be explained by the existence of similar physical properties, except the reinforcement detailing and concrete strengths, with each other. It is also observed that frequency decrease of higher modes were steeper.

Table 4.1. Dominant frequencies of the first frame

LEVEL	*DOMINANT FREQUENCIES, HZ*			
	#1	#2	#3	#4
Undamaged	5.1	14.9	23.9	31.6
After 1st Loading Group	3.4	10.6	17.4	22.8
After 2nd Loading Group	2.6	9.1	15.0	20.4
After 3rd Loading Group	2.1	8.1	13.8	19.1
After 4th Loading Group	1.9	7.5	13.0	18.6

Table 4.2. Dominant frequencies of the second frame

LEVEL	*DOMINANT FREQUENCIES, HZ*			
	#1	#2	#3	#4
Undamaged	5.7	15.1	24.0	31.6
After 1st Loading Group	3.8	9.7	16.0	21.2
After 2nd Loading Group	2.6	8.0	14.0	19.0
After 3rd Loading Group	2.3	7.2	12.9	17.6
After 4th Loading Group	1.9	6.5	11.9	16.6
After 5th Loading Group	1.8	6.2	11.4	16.1
After 6th Loading Group	1.7	5.8	10.8	15.5

Figure 4.24 presents the change in the dominant frequencies of the bare frames graphically. In this figure x-axis represents increasing inter-story drift ratios at the first story of frames. From the figure it can be inferred that the behavior of frequencies can be expressed by a decaying function. The first dominant frequency at 1% and 2% inter-story drifts were 0.48 and 0.35 times that of the undamaged cases for the first and second frames, respectively.

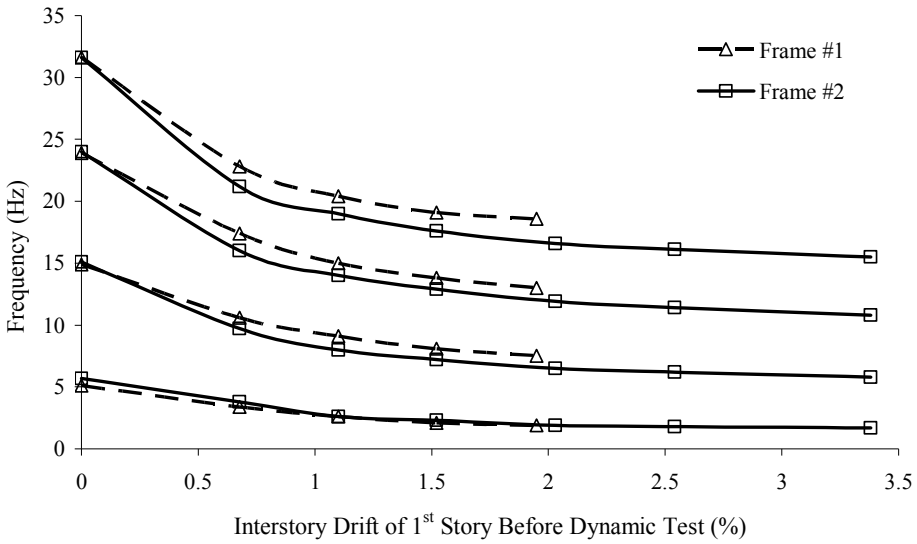

Figure 4.24. Change of dominant frequencies for the first and second frames

Dominant frequencies of the frames with infill walls are presented in Table 4.3 and Table 4.4. Similar to the bare frames, these frames had same physical properties except concrete and mortar strengths and the reinforcement detailing. First dominant frequencies of the frames stayed close to each other in spite of the increasing damage. On the other hand, unlike the observed close follow up in the bare frames, there was a clear deviation of the values in the second dominant frequency. Difference of the frequencies in the second mode diminished after the heavy damage in the first floor of the fourth the frame.

Table 4.3. Dominant frequencies of the third frame

LEVEL	*DOMINANT FREQUENCIES, HZ*			
	#1	#2	#3	#4
Undamaged	16.6	-	-	-
After 1st Loading Group	7.2	23.1	44.9	-
After 2nd Loading Group	5.8	17.6	31.5	-
After 3rd Loading Group	4.8	14.7	26.4	-
After 4th Loading Group	4.4	13.6	24.7	-
After 5th Loading Group	3.9	12.2	22.6	-
After 6th Loading Group	3.6	11.6	20.3	-

Table 4.4. Dominant frequencies of the fourth frame

LEVEL	*DOMINANT FREQUENCIES, HZ*			
	#1	#2	#3	#4
Undamaged	15.7	-	-	-
After 1st Loading Group	7.2	33.5	-	-
After 2nd Loading Group	5.5	27.0	-	-
After 3rd Loading Group	5.2	26.3	-	-
After 4th Loading Group	3.4	14.1	-	-
After 5th Loading Group	2.8	12.8	-	-
After 6th Loading Group	2.4	11.8	-	-

Figure 4.25 presents the comparison of the change in dominant frequencies for the third and fourth frames. It can be observed that the dominant frequencies decayed with increasing damage in the system.

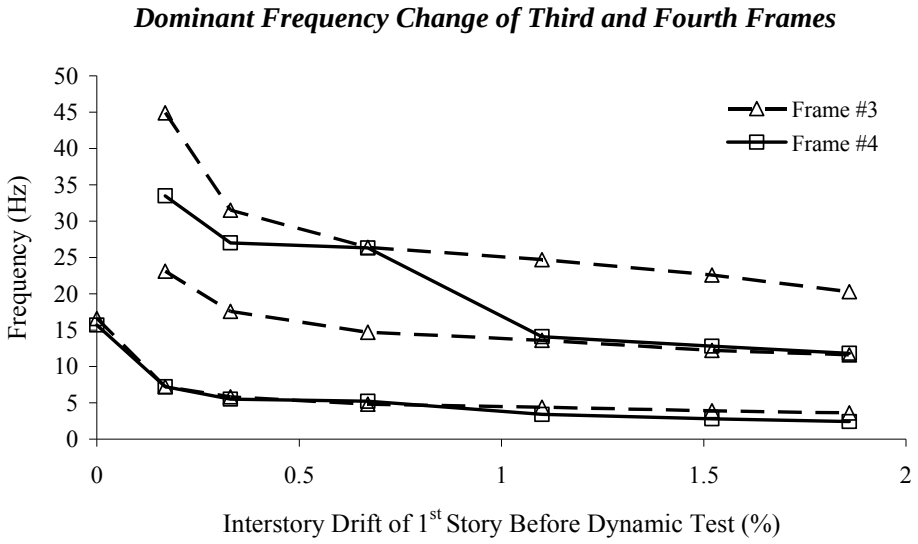

Figure 4.25. Variation of dominant frequencies for the frames with infill walls

Lastly, modal shapes of dominant frequencies at the end of each loading group are presented. Calculated shapes for each frame is shown separately. Afterwards, comparisons of modal shapes between the first and third frames will be discussed.

Modal shapes are normalized to permit a comparison. For this purpose, displacement in the fourth floor of first and second modes are normalized to 10 units and displacements of the third floor of third and fourth modes are normalized to 5 units.

As it can be observed from Figure 4.26, modal shapes of the first frame did not change significantly with increasing damage. Change in the first mode was smaller than the upper modes.

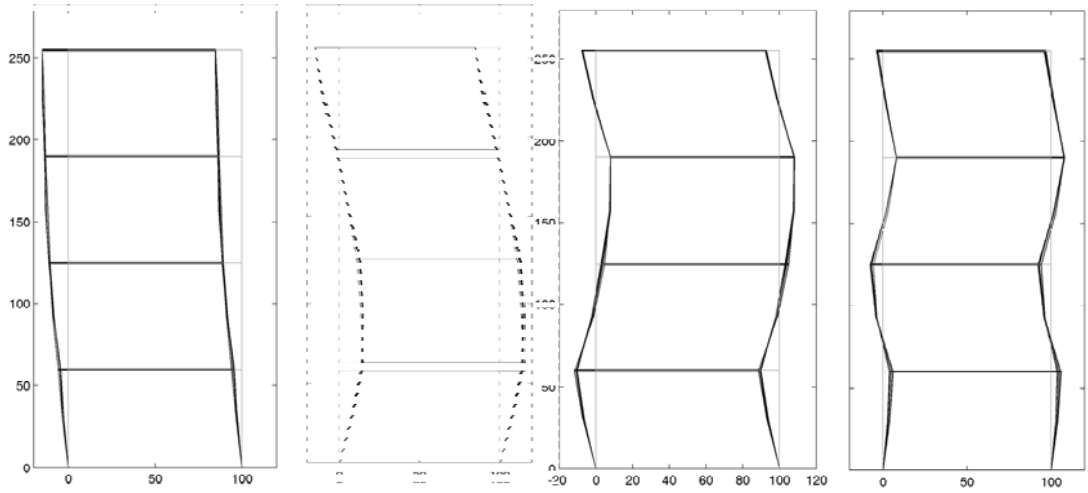

Mode #1 Mode #2 Mode #3 Mode #4

Figure 4.26. Modal shapes of the dominant frequencies of first frame for first to fourth columns of Table 4.1 respectively

Even though variations of the modal shapes of the second frame were similar to the first frame, variations in the second frame was stronger, Figure 4.27. This situation can be explained by the increased damage levels due to the higher drifts attained.

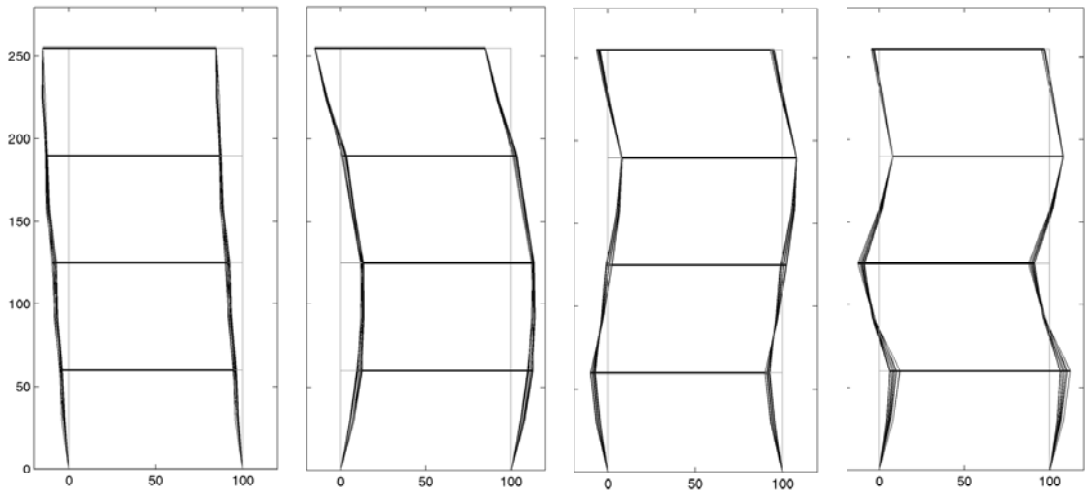

Mode #1 Mode #2 Mode #3 Mode #4

Figure 4.27. Modal shapes of the dominant frequencies of second frame for first to fourth columns of Table 4.2 respectively

Higher modes of the third frame were unavailable due to the difficulty in exciting these modes. Therefore modal shapes of the first three dominant frequencies were estimated only, Figure 4.28. For second and third dominant frequencies no data was available at the undamaged case for the same reason as well. Similar to the bare frames mode shapes of first dominant frequency was lightly effected from increasing damage. For the second and third modal shapes, effect of damage was stronger.

Again due to the excitation problem and increased effect of nonlinearities only modal shapes of the first two dominant frequencies of the fourth frame were estimated Figure 4.29. As it can be observed from the figure modal shapes exhibited significant change at the end of fourth loading group. Change can be observed at the columns of first story with sharp corners. The sharp corners were not result of a physical condition; it was caused by the resolution of data gathered. Considering the observed damage rather than the middle of the column, jump in the shape should be taking place at the top portion (heavily sheared portion) of the column.

It should be noted that the dynamic test set-up permitted the observation lateral movement of the frames only. Therefore presented data is blind to any vertical movement taking place in the frames. Barred with this limitation, variations of the modal shapes of the bare frames and the frames with infill walls are presented in Figure 4.30. In order to present the change in modal shapes, three different modal shapes of first and the third frame are chosen. These are undamaged case and after the cycles with 4mm (0.7% inter-story drift) and 11mm (1.9% inter-story drift) story drifts at the first story. Presented modal shapes are normalized to have the same value at the first story. Change in the horizontal sway of the frames indicated that mode shape varied to reflect the softening in the 1st story.

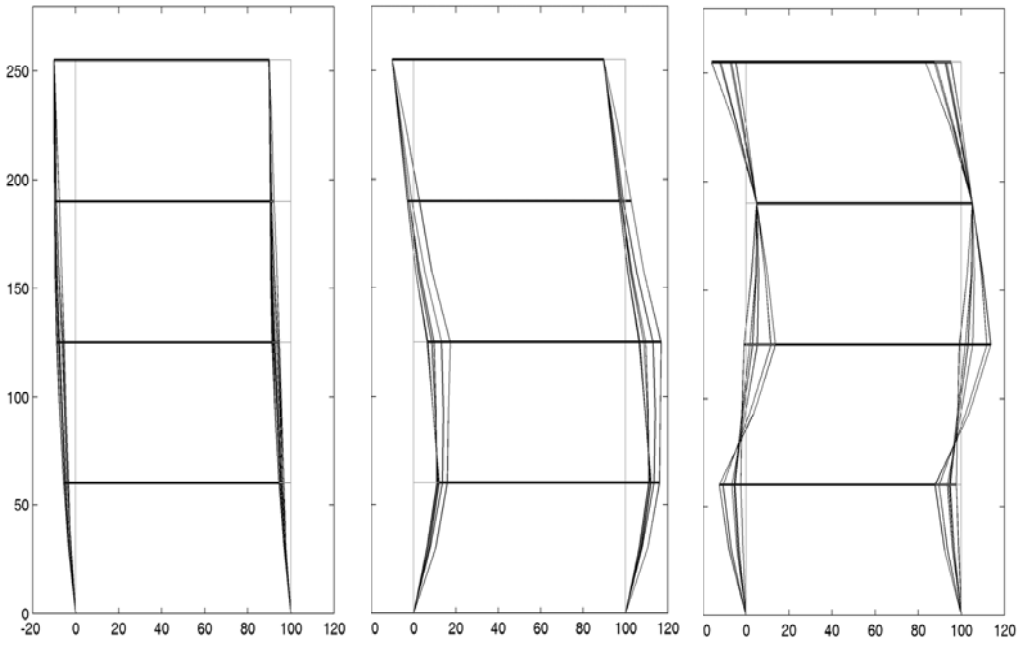

Figure 4.28. Modal shapes of the dominant frequencies of third frame for first to third columns of Table 4.3 respectively

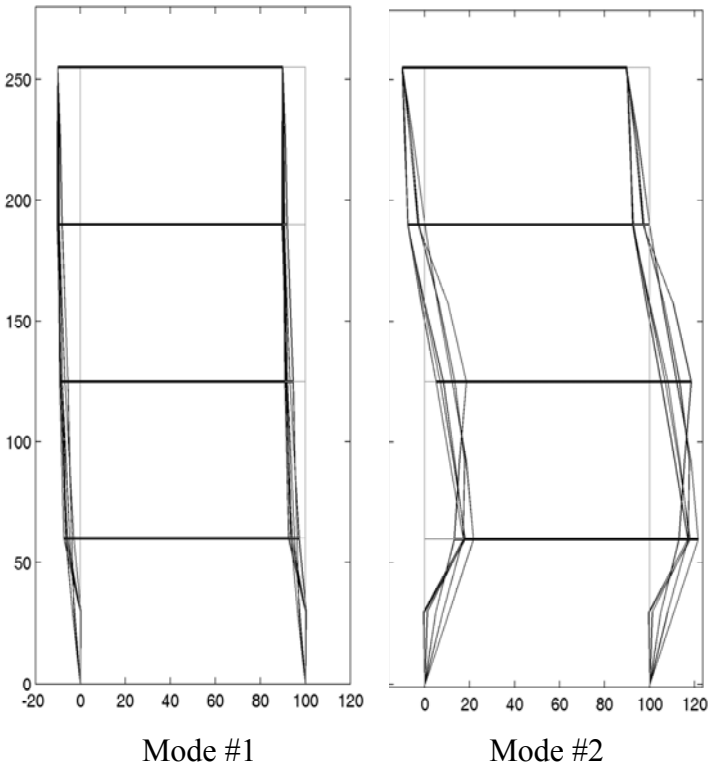

Figure 4.29. Modal shapes of the dominant frequencies of fourth frame for first and second columns of Table 4.4 respectively

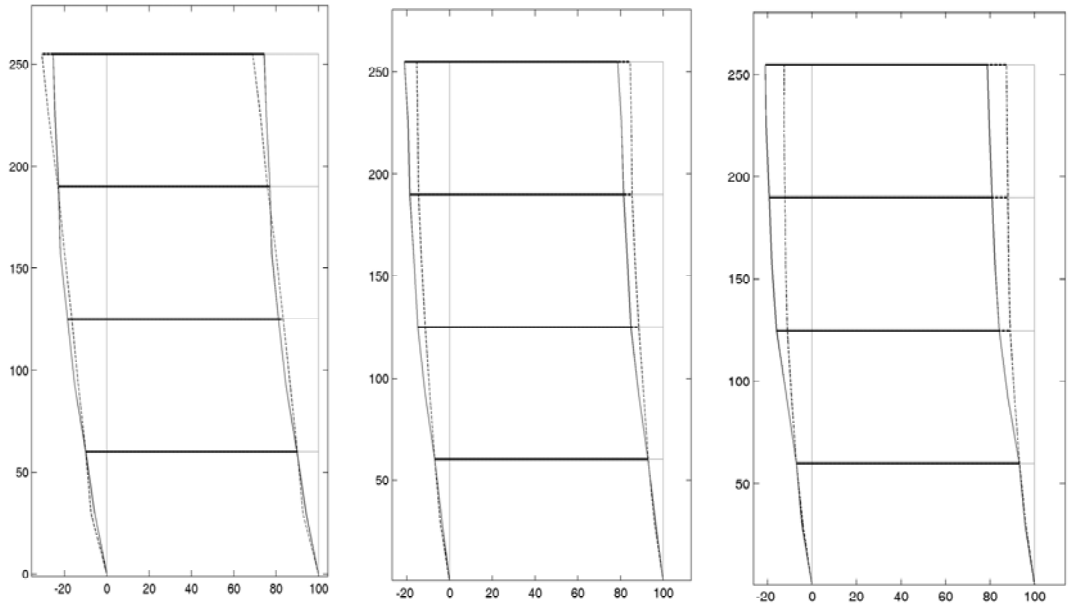

Figure 4.30. Normalized first modes of 1st and 3rd frames at undamaged condition and after 4mm and 11mm drifts at the 1st story. Dashed lines indicates the modes of 3rd frame

4.3.2. Dynamic Variable Estimation by Snap-back Tests

In this section dynamic variables of frames determined by the utilization of the modal analysis method to snap-back test data is presented and results are discussed. As it was mentioned at Section 4.3.1, when frames were excited by strong excitations at similar magnitudes steady frequency responses were obtained at certain frequency ranges. Considering this behavior and the FFT trace of the signals, it is assumed that system frequencies and the modal shapes of the frames could be approache with modal analysis methods. It should be noted that dynamic parameters obtained will be representing the system characteristics in the applied excitation levels.

Dominant frequencies of the first frame at the end of each loading group by snap-back test data is presented in Table 4.5. It should be noted that with the increase of damage new frequency peaks with modal shapes similar to parent mode were observed. Only frequencies of the modes that were steady with minor modifications to their parent mode shapes were listed in the table. In order to compare these frequencies with the frequencies obtained from impact tests, Figure 4.31 is presented. As it can be observed from the figure, dominant frequencies of the frame reach to higher values with

increasing inter-story drift ratios compared to frequencies obtained with the impact test. On the other hand, change in the dominant frequencies of first two modes was at negligible levels.

Table 4.5. Estimated dominant frequencies of the 1st frame by snap-back tests

LEVEL	*DOMINANT FREQUENCIES, HZ*			
	#1	#2	#3	#4
Undamaged	-	-	-	-
After 1st Loading Group	2.9	10.5	16.9	22.7
After 2nd Loading Group	2.4	8.1	15.5	20.6
After 3rd Loading Group	2.2	8.2	16.2	26.0
After 4th Loading Group	2.0	7.8	19.2	25.1

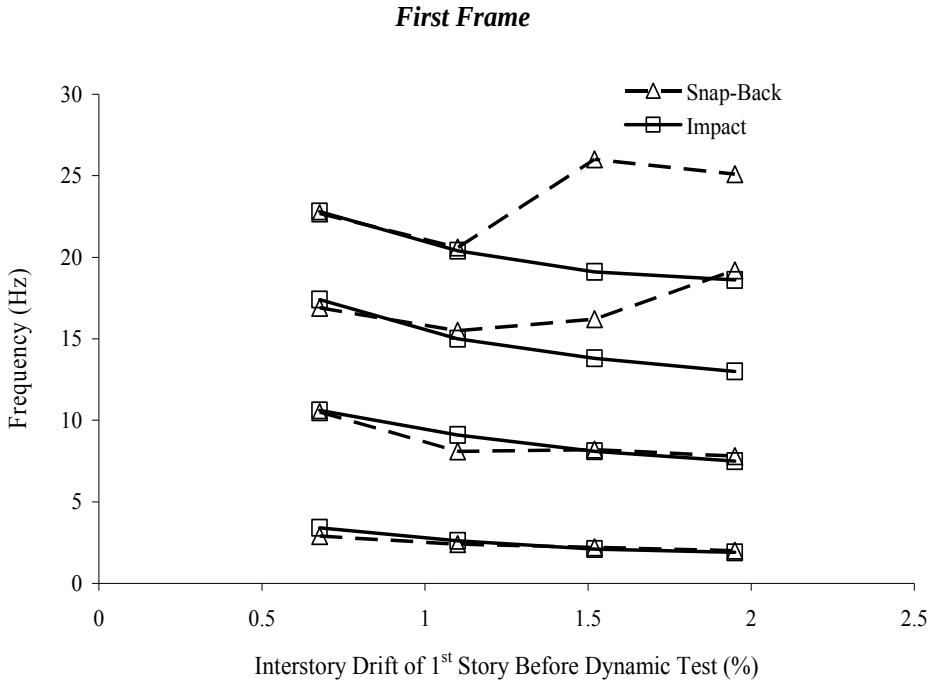

Figure 4.31. Comparison of the dominant frequencies obtained by impact and snap-back tests for the 1st frame

Estimation of the dominant frequencies of the second frame at the end of each loading group by snap-back test data is presented in Table 4.6. As observed in the first frame with the increase of damage, new frequency peaks with modal shapes similar to parent modes were observed. Again only frequencies of the modes that were steady with minor modifications to their parent modes were listed in the table. Comparisons of the frequencies obtained by snap-back and impact tests are presented in, Figure 4.32.

Similar to the first frame, with increasing inter-story drift ratios at the first floor, frequencies estimated from snap-back excitations was higher than values obtained from impact excitations. Again the change in the dominant frequencies of first two modes was at negligible levels. In both of the bare frames variations in the 2nd and 3rd modes were comparatively small as well. Accepting that the first two modes of the system dominates its dynamic behavior, estimation of the dynamic parameters by impact tests could be accepted as the system parameters with minor effect on the dynamic behavior.

Table 4.6. Estimated dominant frequencies of the 2nd frame by snap-back tests

LEVEL	*DOMINANT FREQUENCIES, HZ*			
	#1	#2	#3	#4
Undamaged	-	-	-	-
After 1st Loading Group	3.0	9.9	16.4	23.4
After 2nd Loading Group	2.6	8.8	14.9	24.5
After 3rd Loading Group	2.2	8.0	13.8	28.3
After 4th Loading Group	2.0	7.4	12.8	17.6
After 5th Loading Group	1.9	7.2	12.7	-
After 6th Loading Group	1.8	6.6	16.4	-

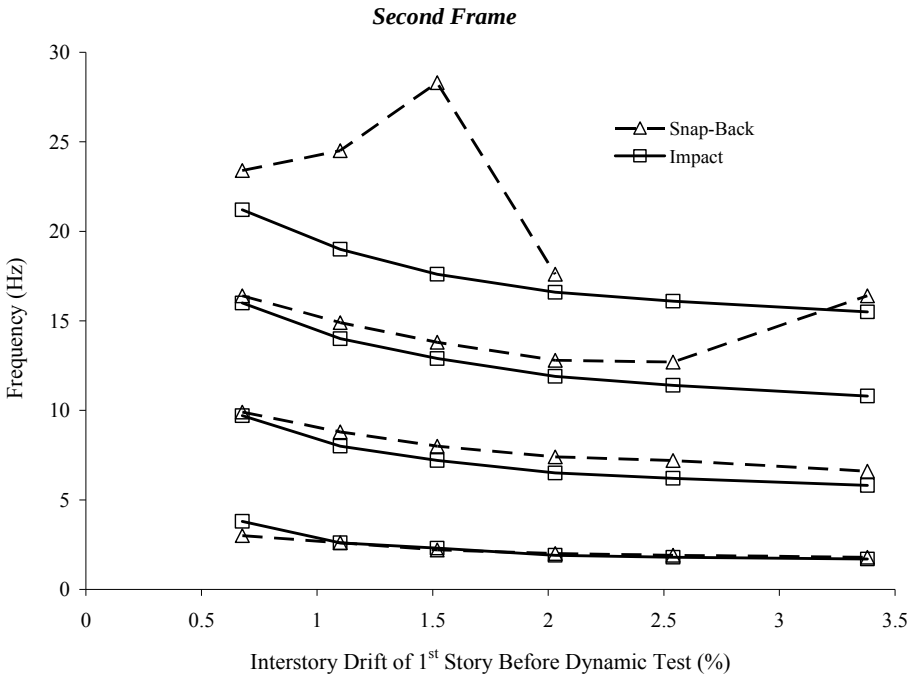

Figure 4.32. Comparison of the dominant frequencies obtained by impact and snap-back tests for the 2nd frame

Estimation of the dominant frequencies of the frames with infill walls at the end of each loading group by using snap-back test data are presented in Table 4.7 and

Table 4.8 for the frames 3 and 4 respectively. Unlike the bare frames, a healthy estimation of dominant frequencies was not possible beyond the first dominant frequency. The dominancy of the first mode signal to the measured data did not permit the observation of higher modes. Utilizing the available information, comparison of the frequencies estimated by snap-back and impact data are presented in Figure 4.33 and Figure 4.34 for frame 3 and 4 respectively. Except a deviation in the second cycle of 4th frame frequency values estimated by the snap-back tests were lower than the values estimated by impact tests.

Finally it can be concluded that obtained frequency values from the FRFs of each frame by snap-back excitations generally showed similarities with the ones from the impact hammer tests especially at the first modes.

Table 4.7. Estimated dominant frequencies of the 3rd frame by snap-back tests

LEVEL	*DOMINANT FREQUENCIES, HZ*			
	#1	#2	#3	#4
Undamaged	-	-	-	-
After 1st Loading Group	7.0	-	-	-
After 2nd Loading Group	5.0	-	-	-
After 3rd Loading Group	4.5	-	-	-
After 4th Loading Group	3.6	-	-	-
After 5th Loading Group	3.0	-	-	-
After 6th Loading Group	2.6	-	-	-

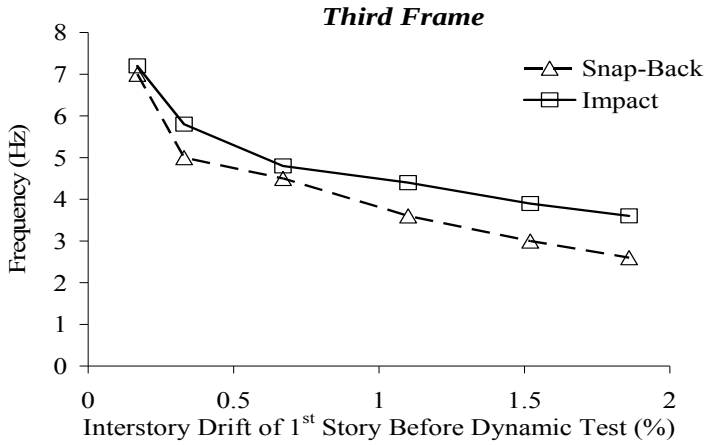

Figure 4.33. Comparison of the dominant frequencies obtained by impact and snap-back tests for the 3rd frame

Table 4.8. Estimated dominant frequencies of the 4th frame by snap-back tests

LEVEL	*DOMINANT FREQUENCIES, HZ*			
	#1	#2	#3	#4
Undamaged	-	-	-	-
After 1st Loading Group	7.4	-	-	-
After 2nd Loading Group	6.2	-	-	-
After 3rd Loading Group	4.1	-	-	-
After 4th Loading Group	3.3	-	-	-
After 5th Loading Group	2.8	-	-	-
After 6th Loading Group	2.4	-	-	-

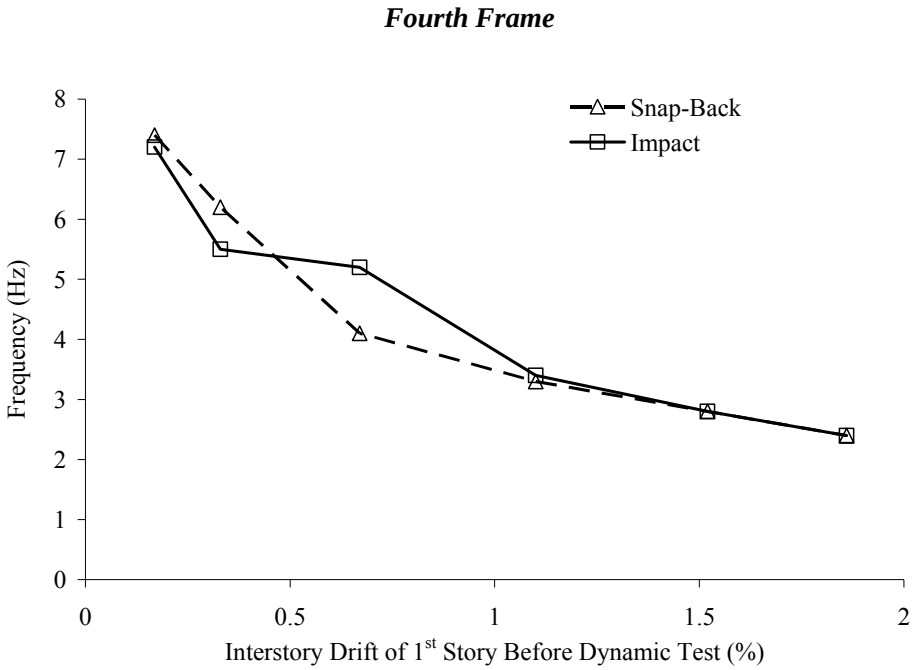

Figure 4.34. Comparison of the dominant frequencies obtained by impact and snap-back tests for the 4th frame

CHAPTER 5

CONCLUSIONS

5.1. Summary and Evaluation of Test Results

The most important test results may be listed as follows:

- If maximum lateral load carrying capacities of frames with and without partition walls are compared, frames with partition wall resisted up to 3 times higher total lateral loading. On the other hand, partition walls in third and fourth frames provided a 12 fold increase of stiffness. As a result, it can be stated that partition walls could increase lateral loading capacity and stiffness of RC frames significantly.
- Higher shear capacity of the fourth frame infill walls and relatively different strength of frames ended up creating different failure mechanism of the partition walls and frame elements of the third and fourth frames. In this respect, fourth frame partition walls kept their share in load carrying throughout the tests and the soft story resulted in the end which is a result of having shear-compression failure at the top ends of the first story columns. Interestingly even though fourth frame had a ductile reinforcement detailing, it failed at similar drifts with the relatively brittle third frame..
- If the total energy dissipation of the frames are compared, it can be seen that the second frame dissipated 2.5 times more energy than the first frame. It should be note that this comparison was made at the end of the fourth cycle group where test of the first frame stopped. Otherwise if the total energy dissipated at the end of the tests are compared the second frame dissipated 7 times more energy. On the other hand fourth frame, which also have a reinforcement detailing for ductile behavior, dissipated only 1.05 times more energy than non-ductile designed third frame. If the energy dissipation of frames with and without infill walls is considered, it is observed that fourth frame dissipated 1.5 times more energy than second

frame and third frame dissipated 10.5 times more energy than the first frame. As it can be inferred from the results that ductile design of reinforcement and presence of partition walls on frame systems have a significant effect on increasing the energy dissipation amounts.

- Estimation of dominant frequencies by impact hammer data has revealed that the dominant frequencies decreased when damage levels of systems were increasing. Although a significant change in the first dominant frequency was not observed between ductile designed first frames and non-ductile designed second frame, first dominant frequencies of third and fourth frames showed a deviation after formation of the heavy damage in the first story columns of the fourth frame.
- Even though first stories of the first and second frames reached 1.9% and 3.4% inter-story drift ratios respectively, it was observed that the obtained modal shapes at the end of each cycle group did not exhibit a significant difference than the previous modal shapes of the cycle groups. However, this condition differed for modal shapes of frames with partition walls. Except the first mode, modal shapes of the frames with infill walls changed significantly. Soft story effect has shown itself on the modal shapes. Especially for the fourth frame the heavy shear cracks that occurred in the joint zones at the end of fourth cycle group had a big impact.
- In spite of the occurred damages on the frame systems, at the end of each cycle group it was observed that data gathered can be used for modal parameter estimation purposes with experimental modal analysis procedures.

Test results indicate that under an earthquake motion ductile design of reinforcement enables a higher deformation capacity and energy dissipation in the bare frame. In this respect ductile reinforcement design will be beneficial for the structure without infill walls. On the other hand, partition walls in the openings of the frames may dominate the behavior and even if the structure has ductile reinforcement design, it might not guarantee an expected ductile failure mechanism due to the complex interaction mechanism between frame and partition walls.

5.2. Recommendations

Damage occurred in the frames with partition walls causes the concentration of drift to the lower stories and causes failure in these stories. Definition of methods to spread the drifts to other stories without limiting the positive effects of partition walls can be very useful to mitigate the earthquake risk in frames with infill walls.

Partition walls have the potential of causing premature failures in the perimeter elements of frames, thereby, causes earlier collapses. Procedures to define safe designs against premature failure should be developed.

In order to prevent collapse of a structure during an earthquake, structure should provide the drift demanded by the earthquake. Amount of the drift demanded based on the natural period of the structure. Partition walls cause reductions both in structural period and the drift capacity of the structures. These two competing behaviors should be investigated closely to utilize it for mitigation of earthquake behavior of existing gravity designed RC frames.

REFERENCES

TSE. 2005. Specification for masonry units-Part 1: Clay masonry units. *Turkish Standards Institute.* Designation: TS EN 771-1. Ankara.

DBYBHY. 2007. Specification for Structures to be Built in Disaster Areas. *Bayındırlık ve İskan Bakanlığı.* Ankara.

Fajfar, P. and Dolsek, M. 2008. The Effect of Infills on the Seismic Response of a Four-Storey Reinforced Concrete Frame – A Deterministic Assessment. *Engineering Structures,* Vol. 30, p.1991-2001.

Negro, P. and Colombo, A. 1997. Irregularities Induced by Non-Structural Masonry Panels in Framed Buildings. *Engineering Structures*, Vol. 19, No. 7, p. 576-585

Mehrabi, A. B., Shing, P. B., Schuller M. P. And Noland J. L. 1996. Experimental Evaluation of Masonry-Infilled RC Frames. *Journal of Structural Engineering (ASCE),* Vol. 122, No. 3, p. 228-237

Mosalam, K. M., White R. N. and Gergely P. 1997. Static Response of Infilled Frames Using Quasi-Static Experimentation. *Journal of Structural Engineering (ASCE*), Vol. 123, No.11, p. 1462-1469

Lee, H. S. and Woo, S. W. 2002. Effect of Masonsry Infills on Seismic Performance of a 3-Storey R/C Frame with Non-Seismic Detailing. *Earthquake Engineering and Structural Dynamics*, Vol. 31, p. 353-378

Al-Chaar, G., Issa, M. and Sweeney S. 2002. Behavior of Masonry-Infilled Nonductile Reinforced Concrete Frames. *Journal of Structural Engineering (ASCE)*, Vol. 128, No. 8 p.1055-1063

Pujol, S. and Fick, D. 2010. The Test of a Full-Scale Three-Story RC Structure with Masonry Infill Walls. *Engineering Structures,* Vol. 32, p. 3112-3121

He, J. and Fu, Z. F. 2001 Modal Analysis. *Butterworth-Heinemann*

X-MODAL. 2007. Modal Analysis Software. *University of Cicinnati Str. Dyn. Lab.*

APPENDIX A

DETAILS OF THE FRAME LOADING MECHANISM AND THE SUPPORT FRAMES

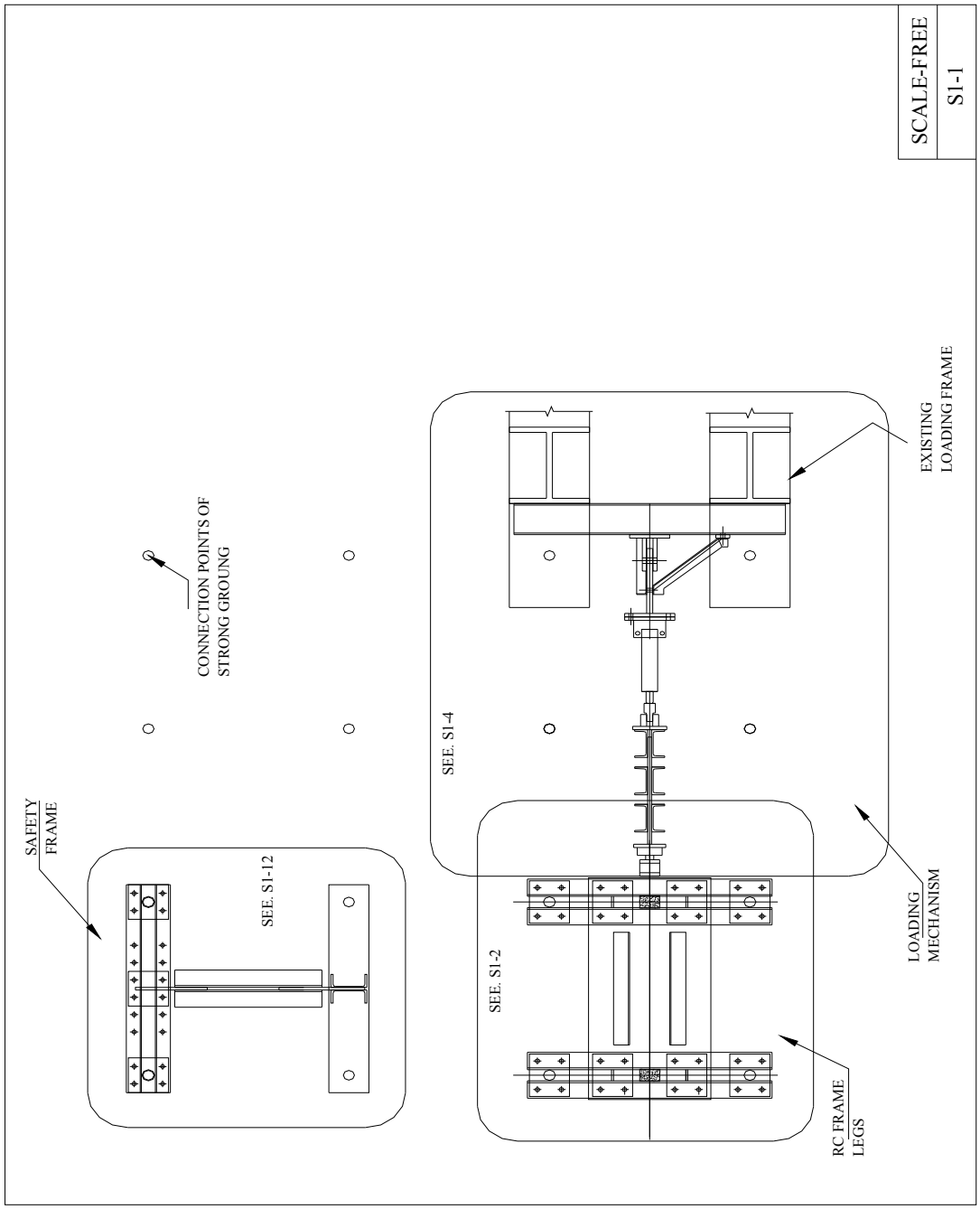

Figure A.1. Frame plan layout

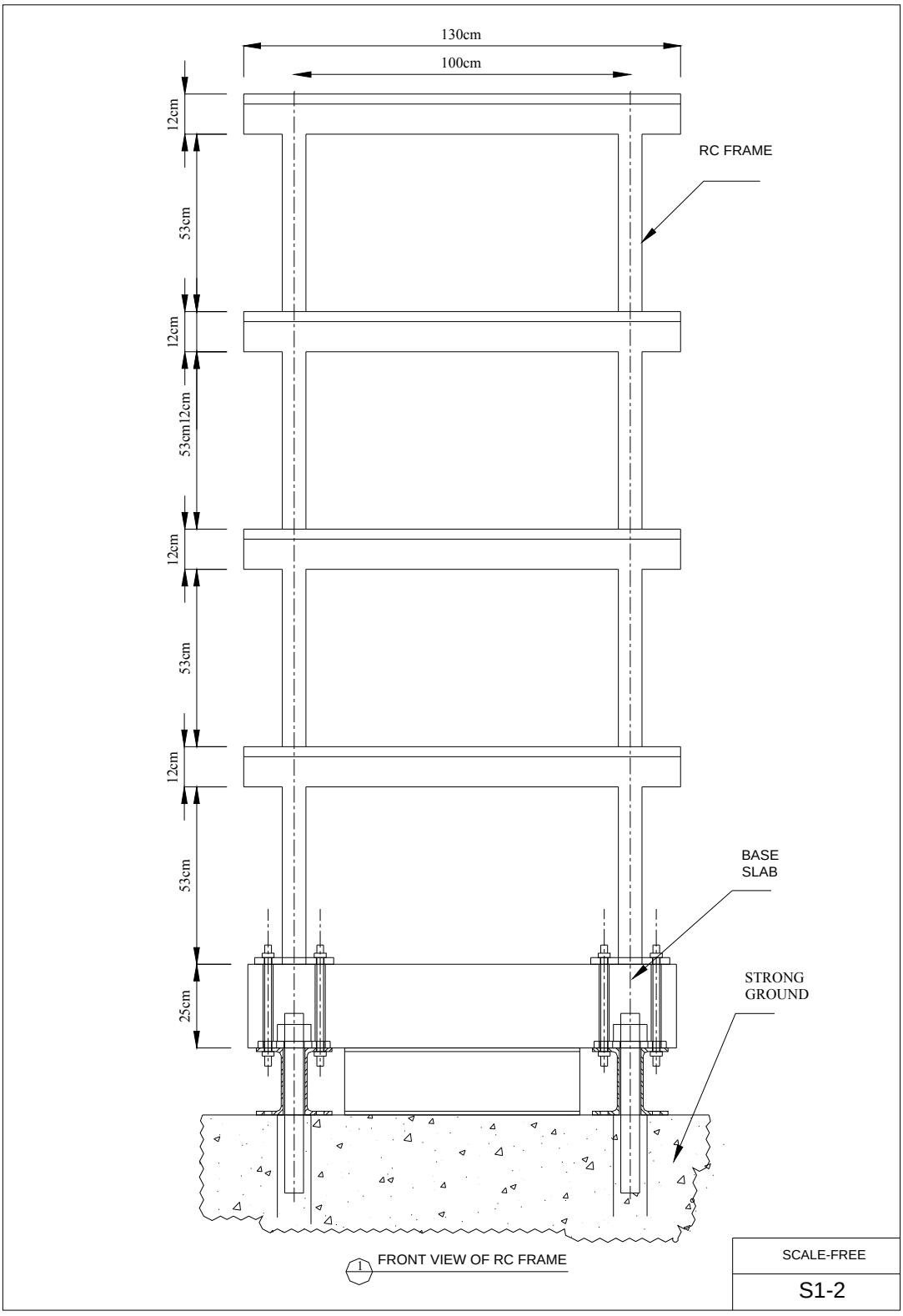

Figure A.2. Frame dimensions and ground connection

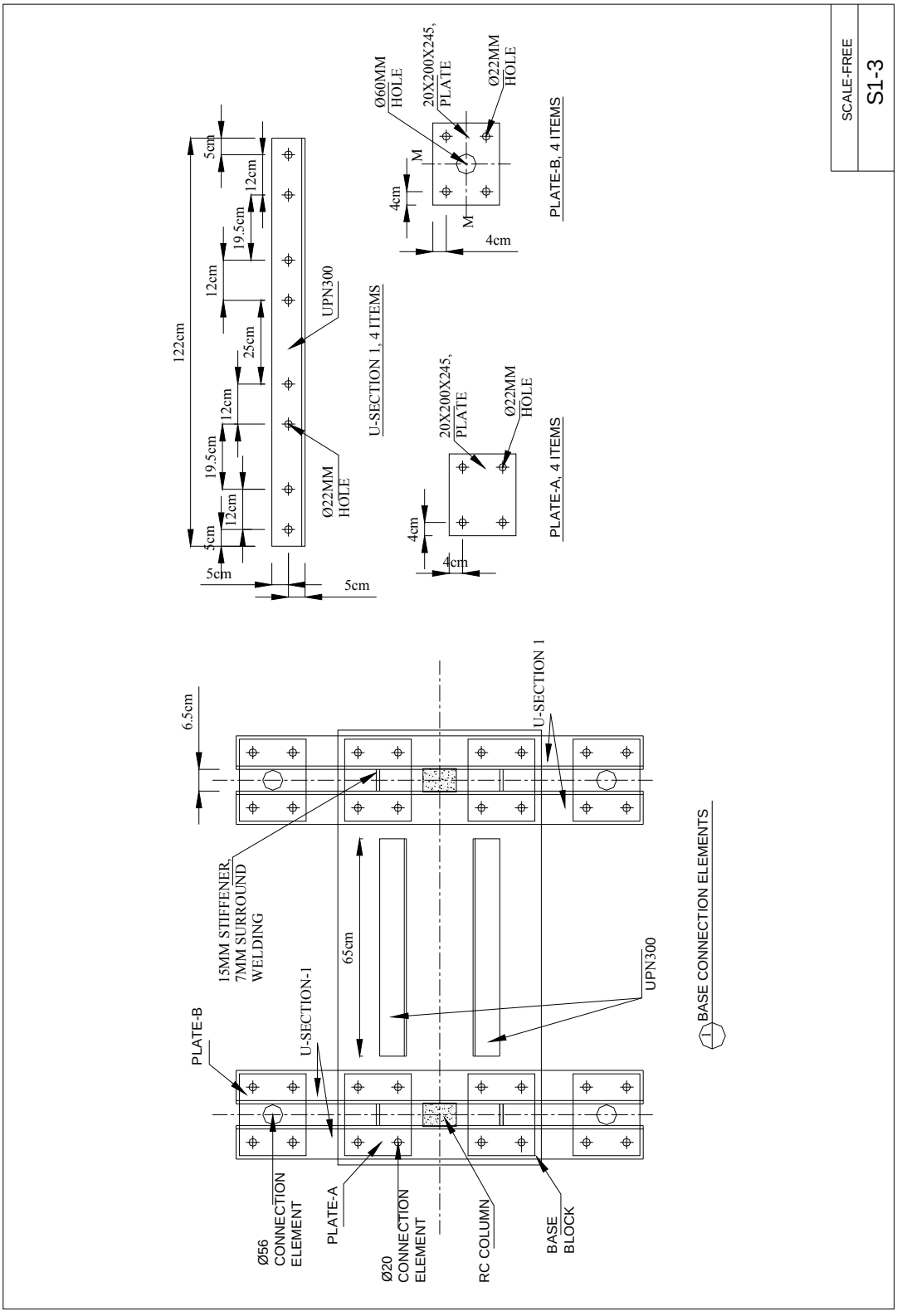

Figure A.3. Support details of frame base

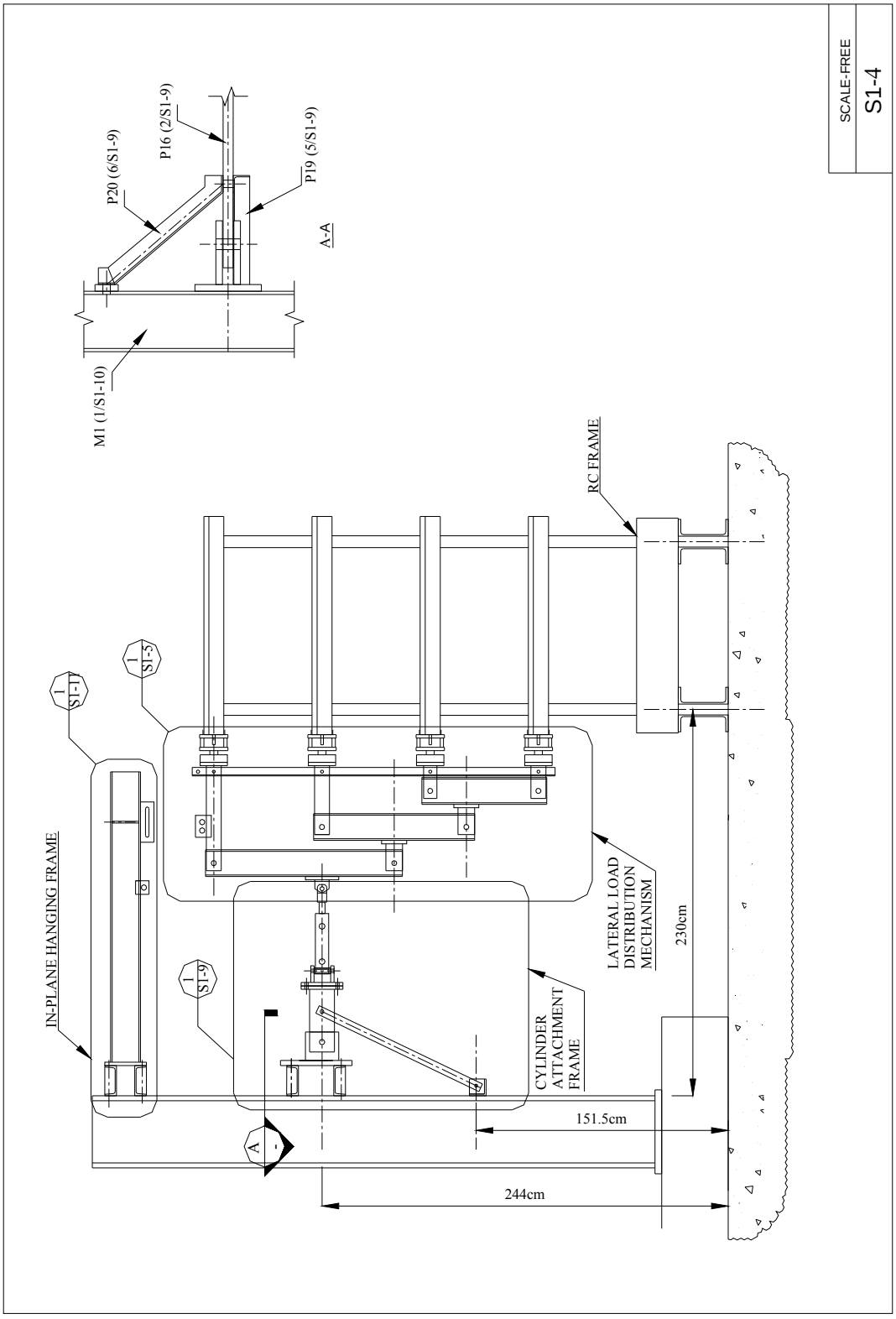

Figure A.4. In-plane hanging frame and lateral loading mechanism

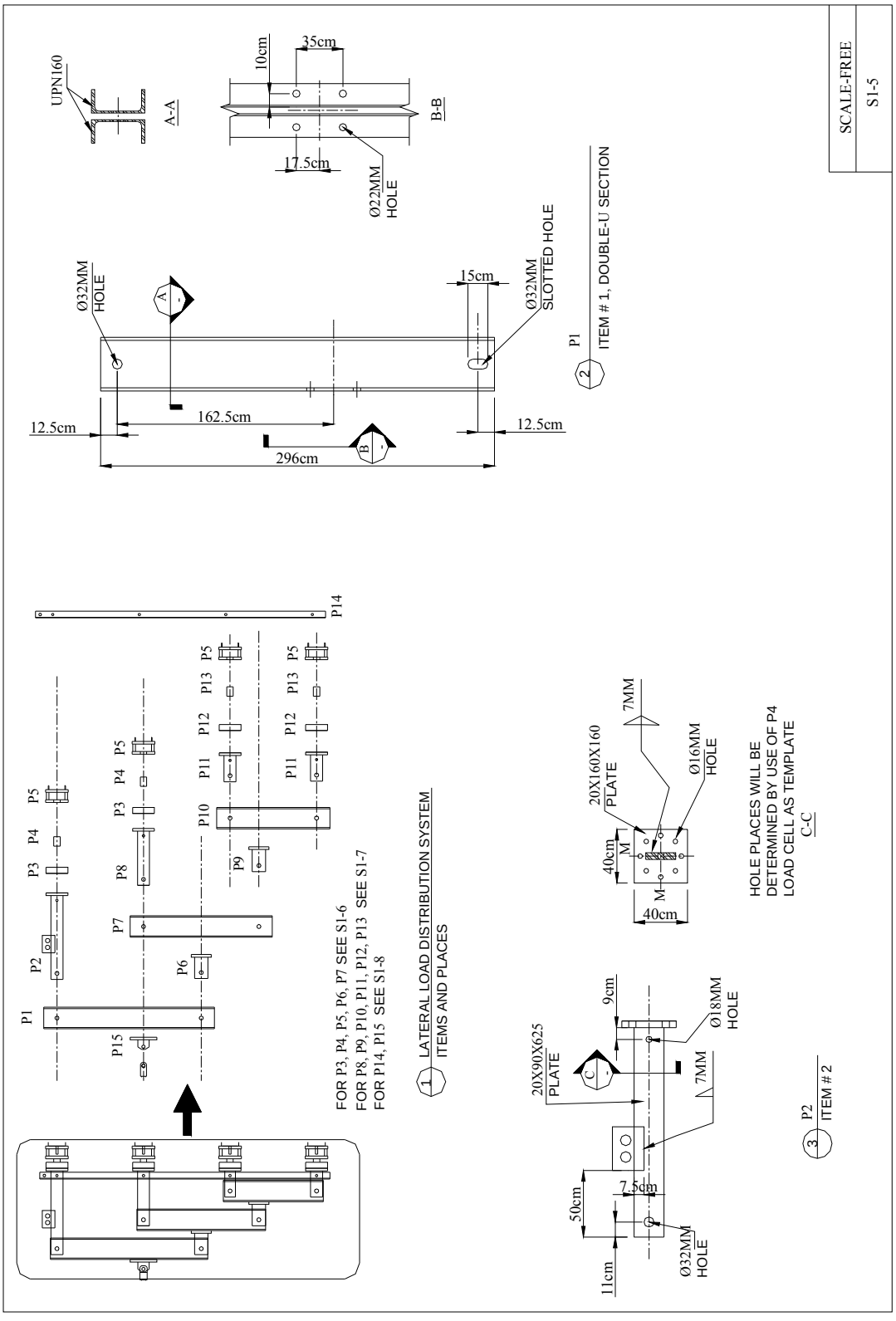

Figure A.5. Lateral load distribution system and its components

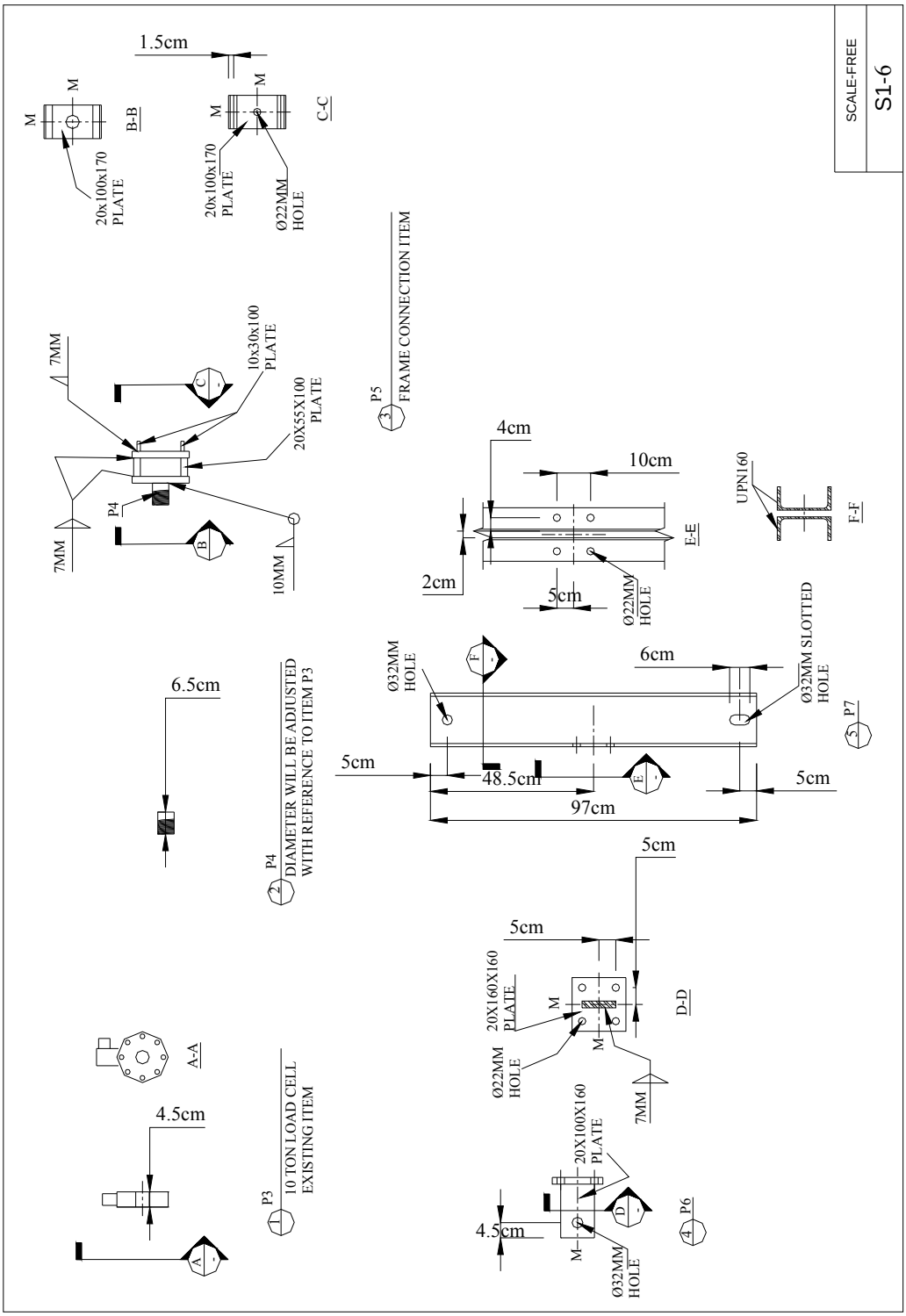

Figure A.6. Components of lateral load distribution system

(cont. on next page)

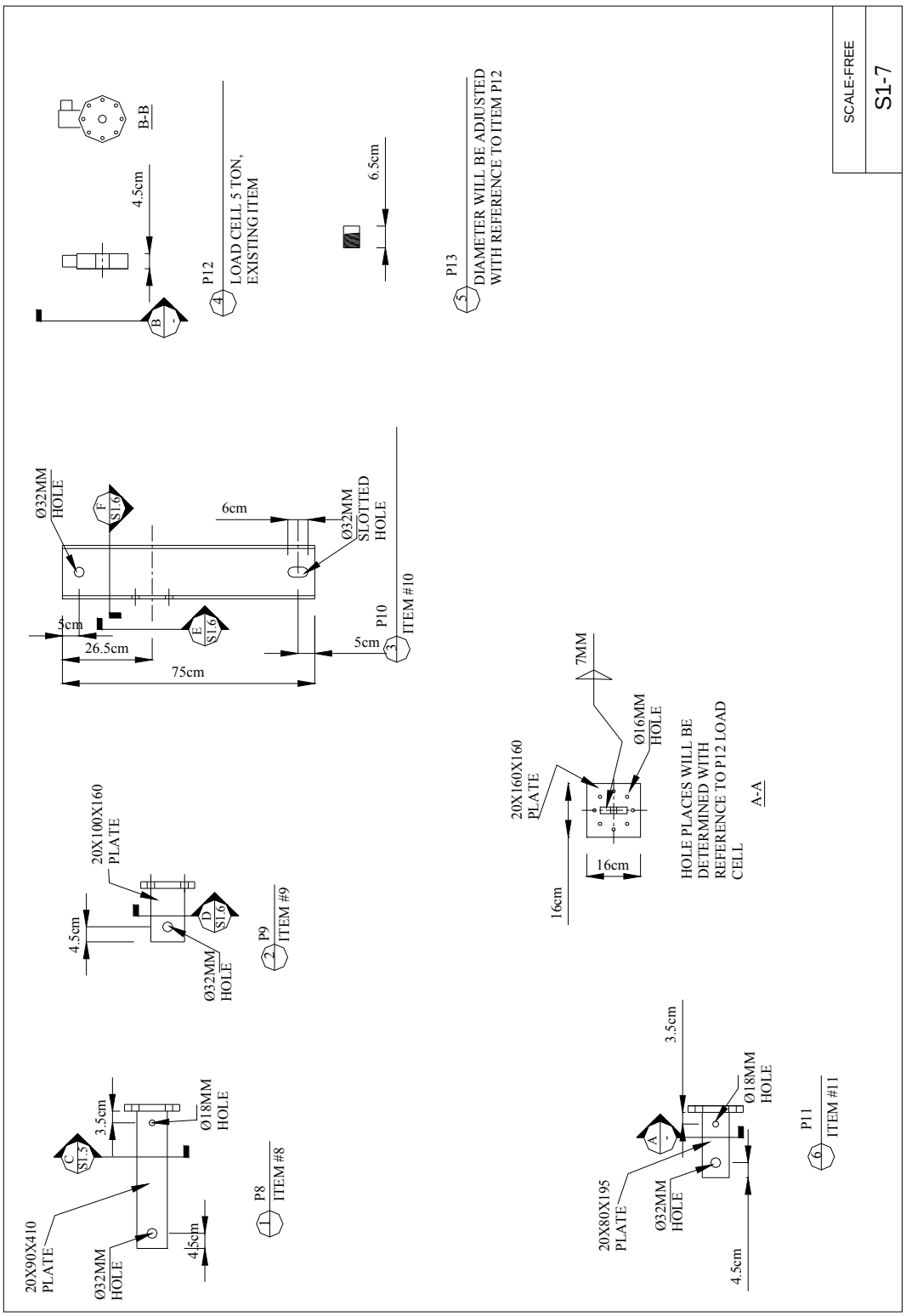

Figure A.7. (cont.)

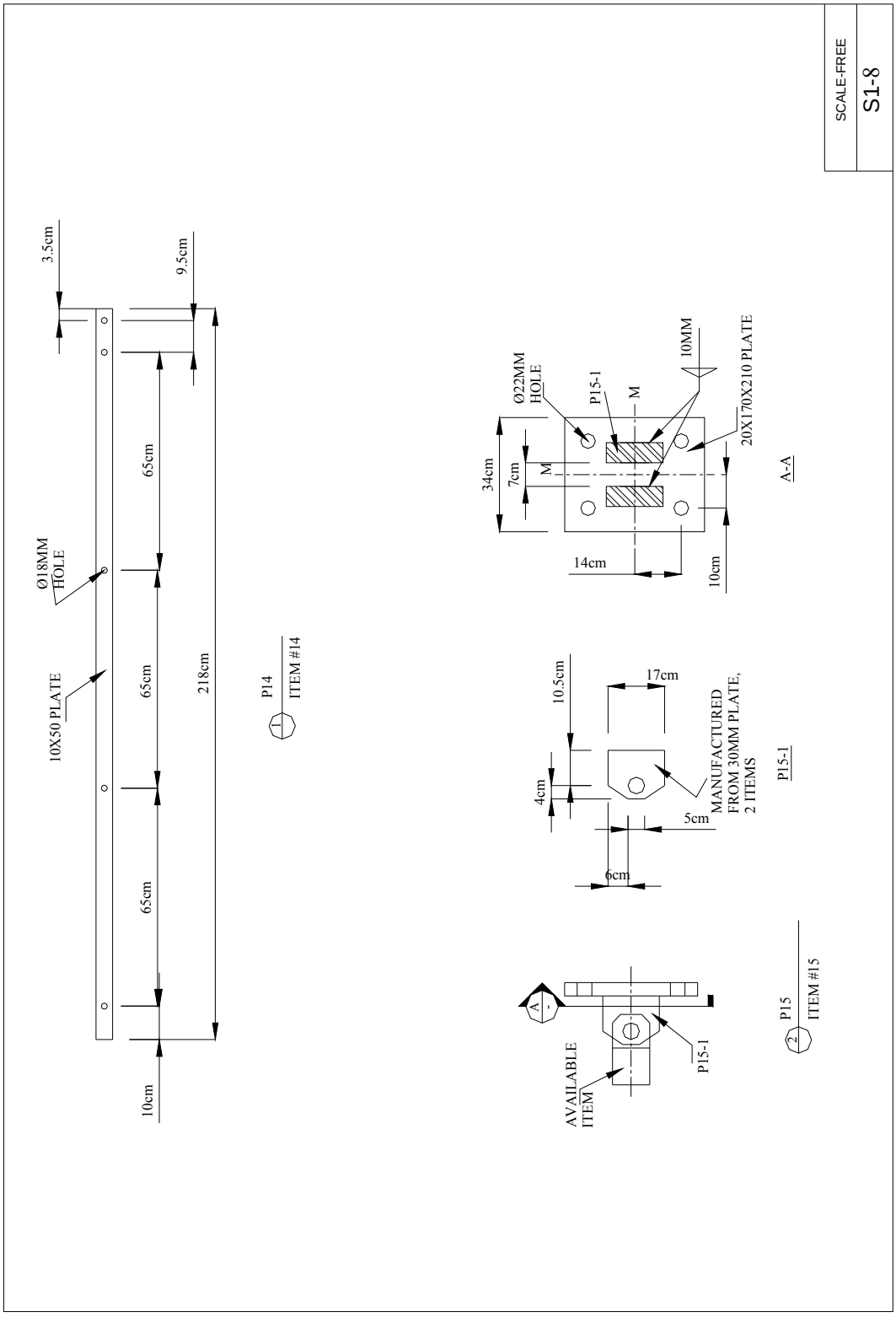

Figure A.8. (cont.)

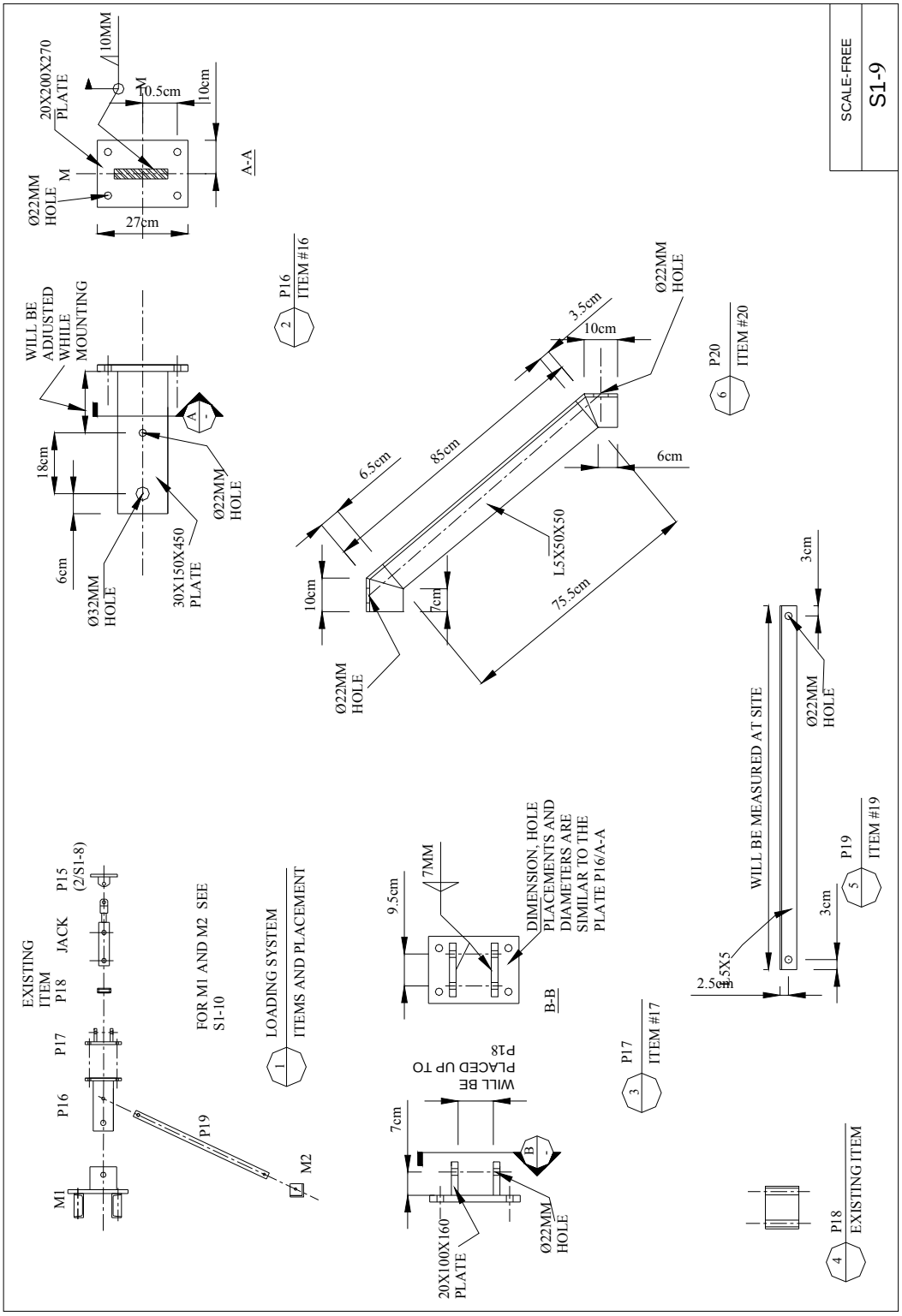

Figure A.9. Components of cylinder attachment frame

(**cont. on next page)**

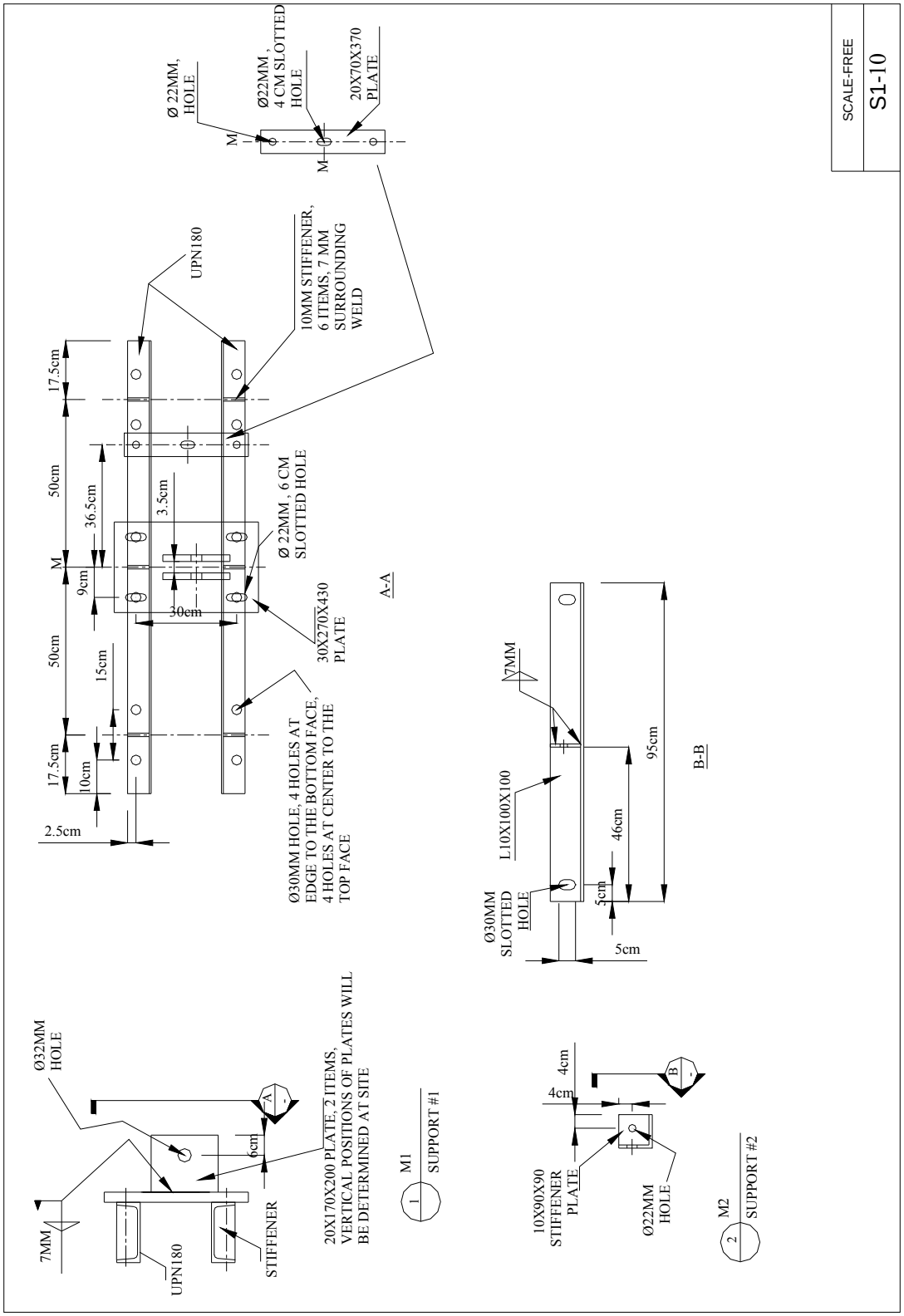

Figure A.10. (cont.)

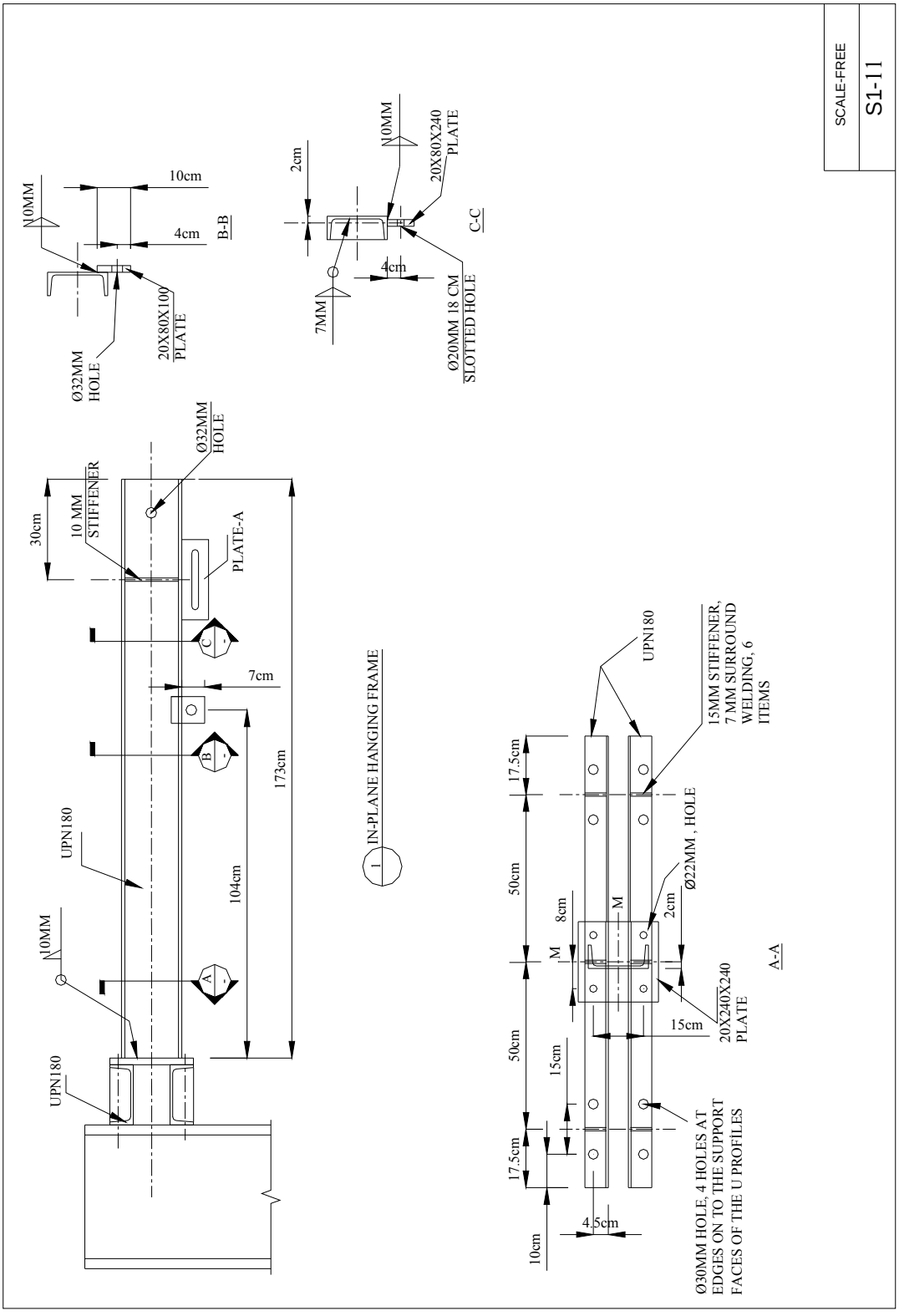

Figure A.11. Components of in-plane hanging frame

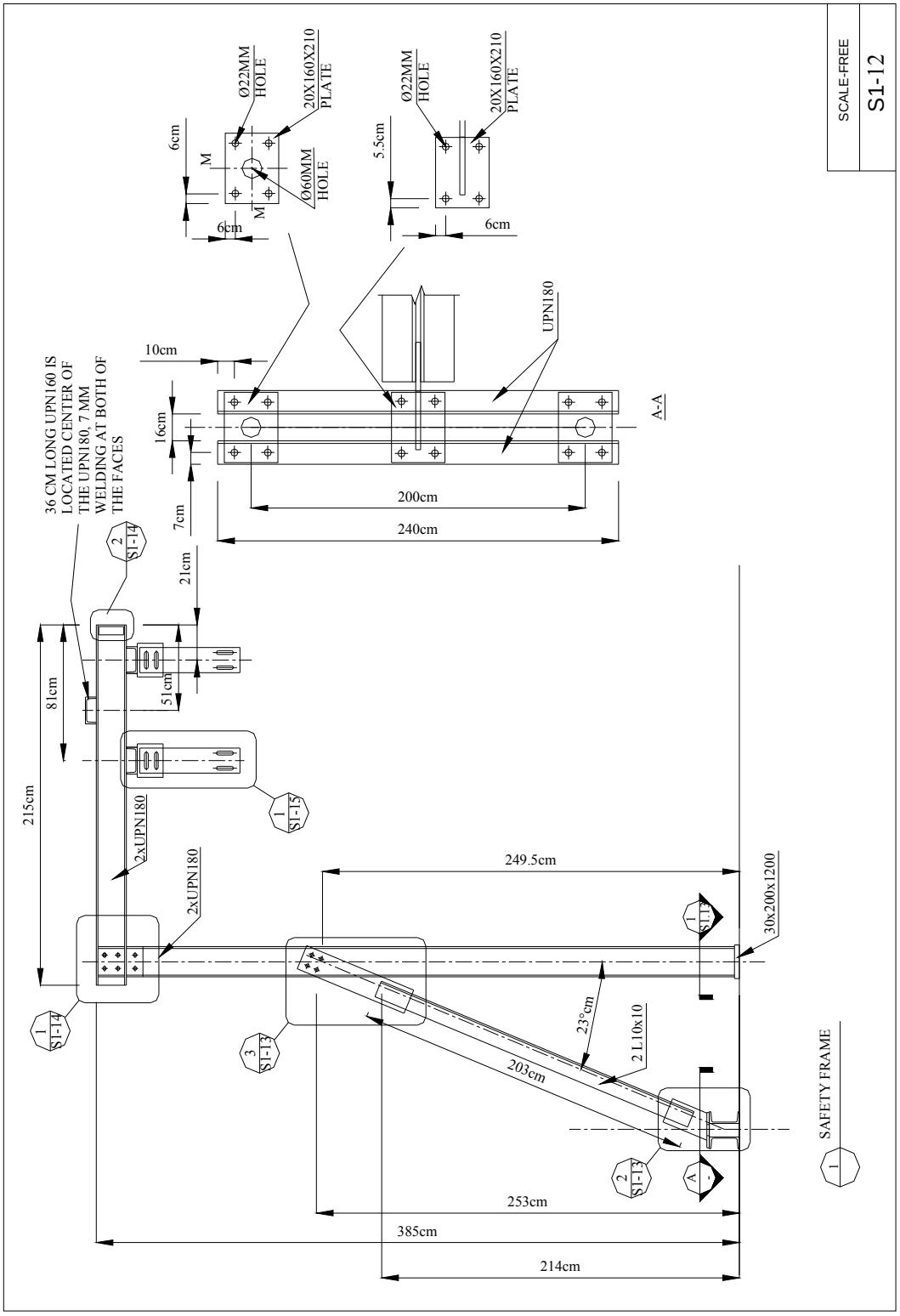

Figure A.12. Safety frame

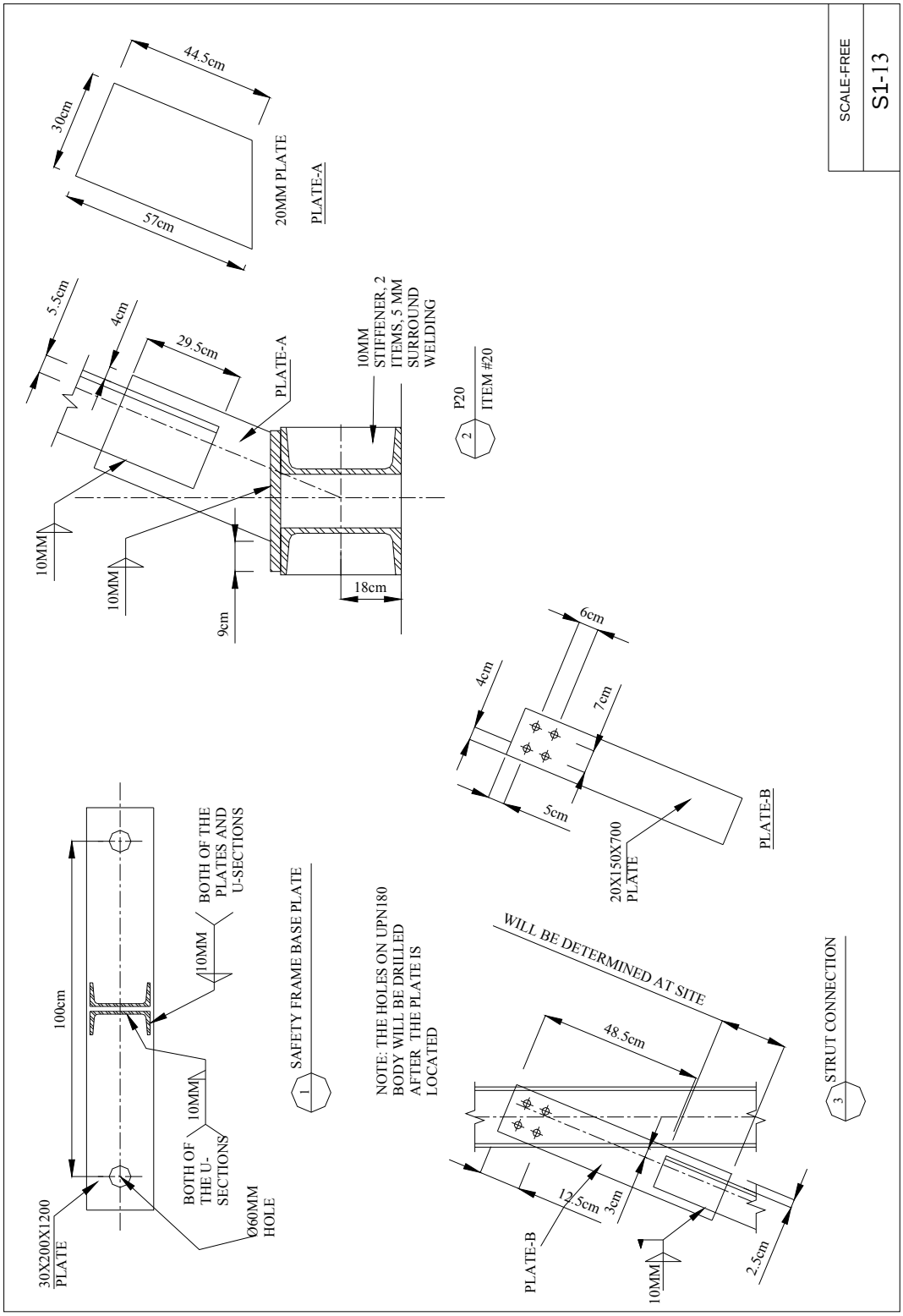

Figure A.13. Components of safety frame

(cont. on next page)

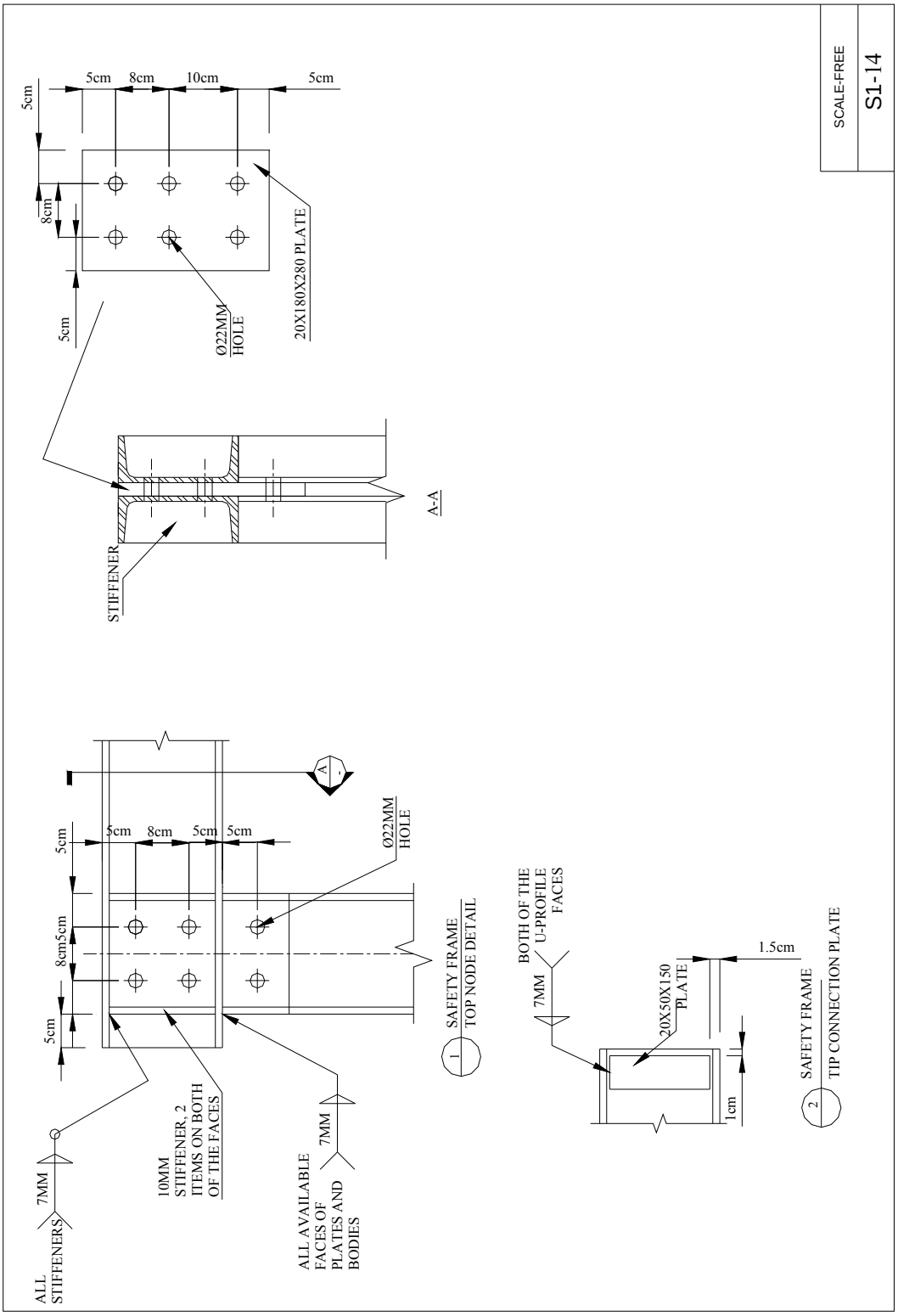

Figure A.14. (cont.)

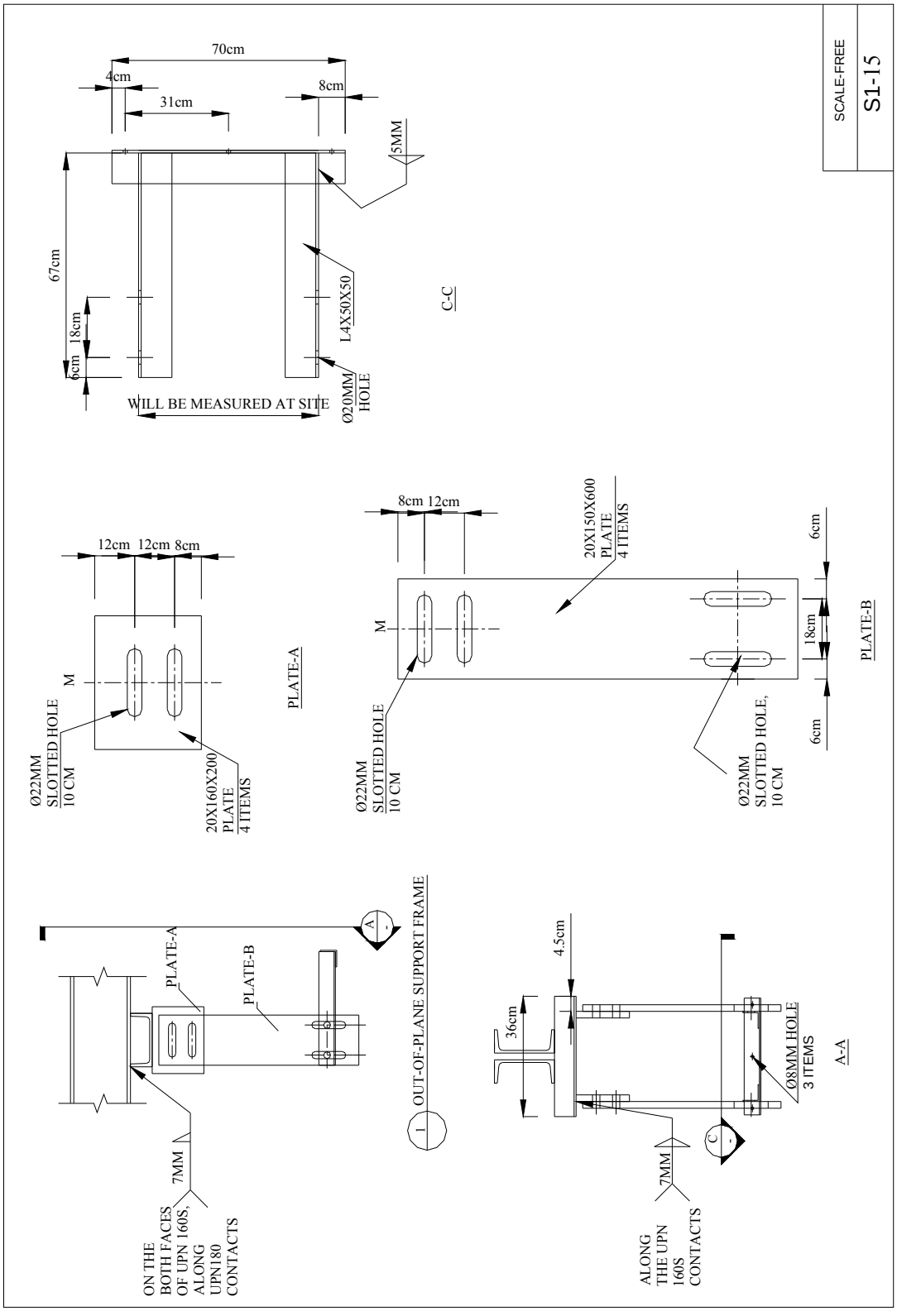

Figure A.15. Out-of-plane support frame and components of it

(cont. on next page)

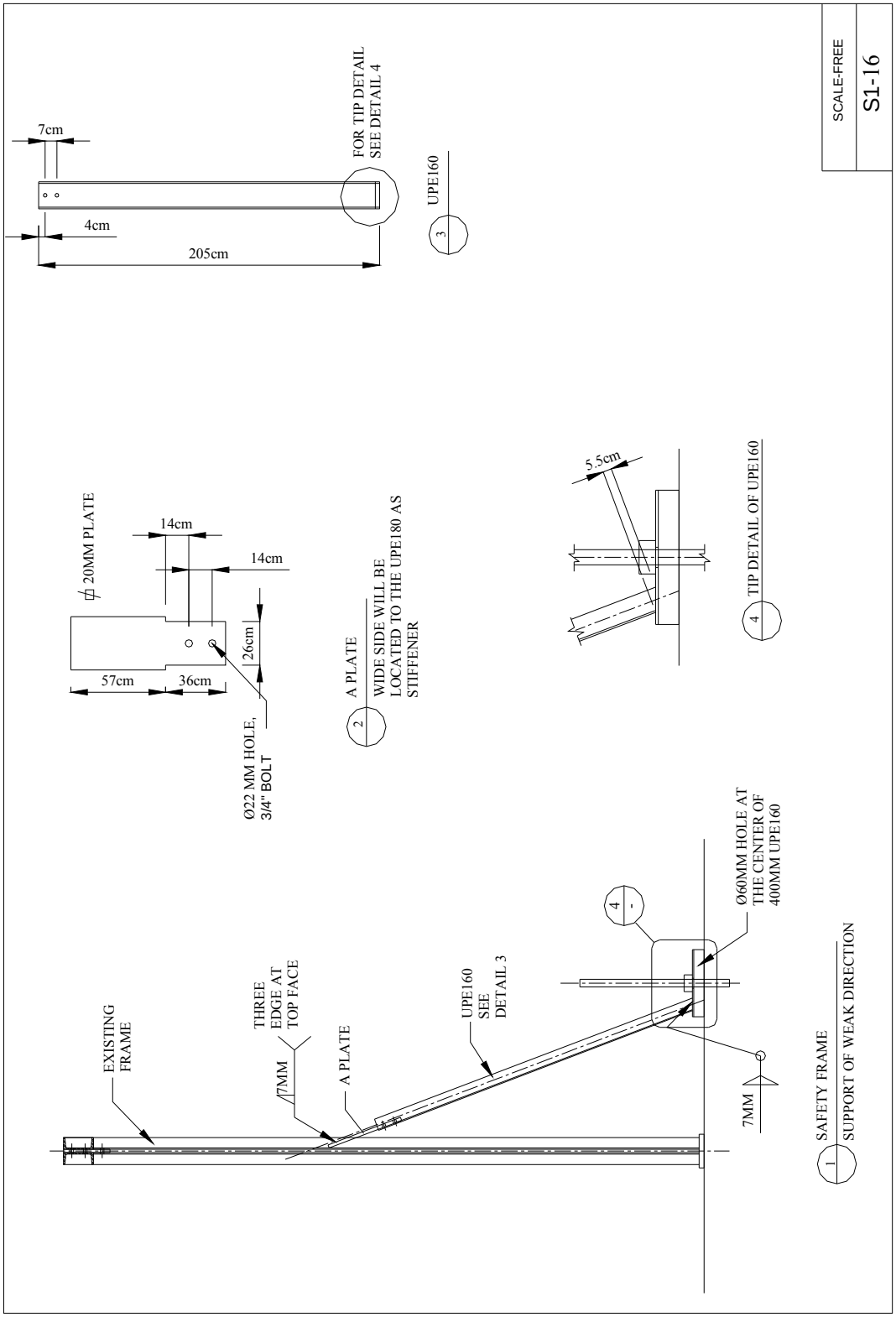

Figure A.16. (cont.)

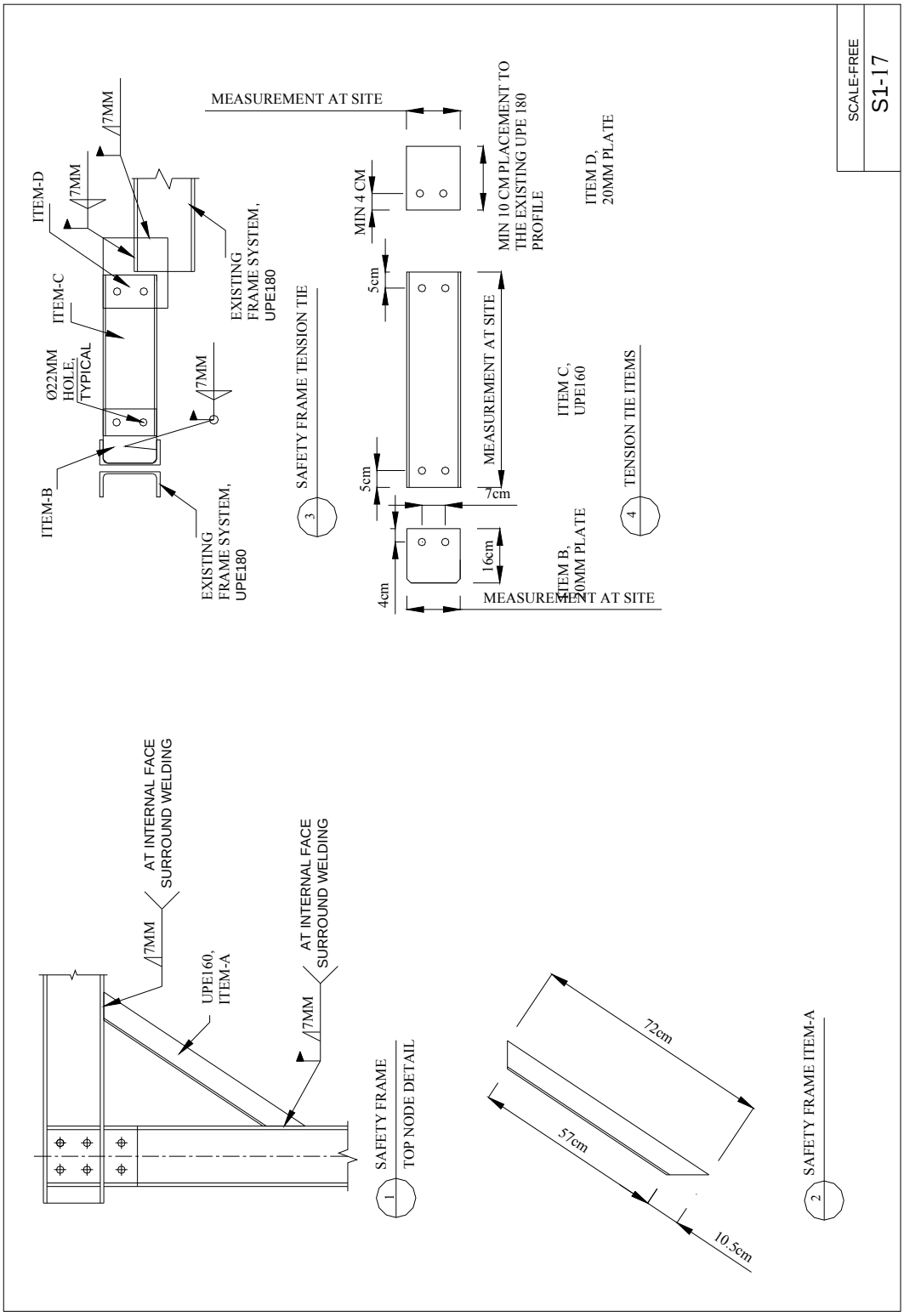

Figure A.17. (cont.)

APPENDIX B

TECHNICAL SPECIFICATIONS OF INSTRUMENTATIONS

B.1 Load Cell:

1. Trademark- Model: Honeywell-41A
   Loading Range: +/- 22650 kgf
   Sensitivity: 2264 kgf / V

2. Trademark - Model: Honeywell-41A
   Loading Range: +/- 9060 kgf
   Sensitivity: 906 kgf / V

3. Trademark - Model: Honeywell-41
   Loading Range: +/- 4530 kgf
   Sensitivity: 906 kgf / V

B.2 Accelerometer:

1. Trademark - Model: PCB-333B42
   Sensitivity: 500 mV / g
   Frequency Range: 0.5 to 3000 Hz
   Maximum Acceleration: +-10g

2. Trademark -Model: PCB-393B04
   Sensitivity: 1000 mV/g
   Frequency Range: 0.06 to 450 Hz
   Maximum Acceleration: +-5g

3. Trademark -Model: PCB-356A16 (Tri axial)
   Sensitivity: 100 mV / g
   Frequency Range: 0.5 to 5000 Hz
   Maximum Acceleration: +-50g

B.3 Linear Variable Displacement Transducer (LVDT) and Resistive Linear Position Transducer (RLPT):

1. Trademark - Model: OPKON- LPM-100-B-10K-S
   Measurement Range: +/-50 mm
   Sensitivity: 0.1 V / V.mm

2. Trademark - Model: OMEGA- LD600
   Measurement Range: +/-50 mm
   Sensitivity: 6 mV / V.mm

3. Trademark - Model: OMEGA- LD600
   Measurement Range: +-100 mm
   Sensitivity: 2 mV / Vmm

B.4 Strain Gauge:

1. Trademark: TML
   Type: QFLA-5-11
   Maximum Unit Elongation: 3%
   Measurement Length: 5 mm

2. Trademark: TML
   Type: QFLK-1-11
   Maximum Unit Elongation: 3%
   Measurement Length: 1 mm

3. Trademark: TML
   Type: YFLA-5
   Maximum Unit Elongation: 15 %
   Measurement Length: 5 mm

APPENDIX C

Crack Patterns

C.1 First Frame Crack Patterns

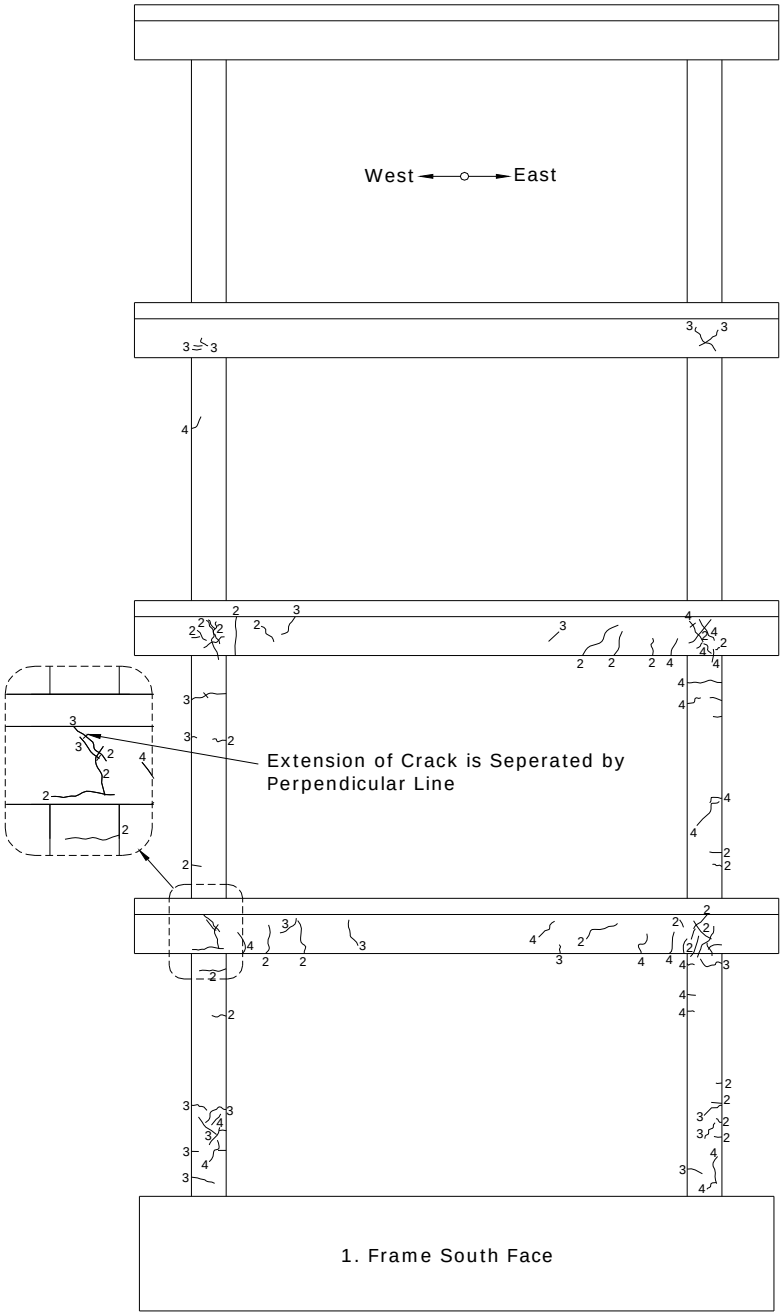

Figure C.1. First frame south face crack patterns

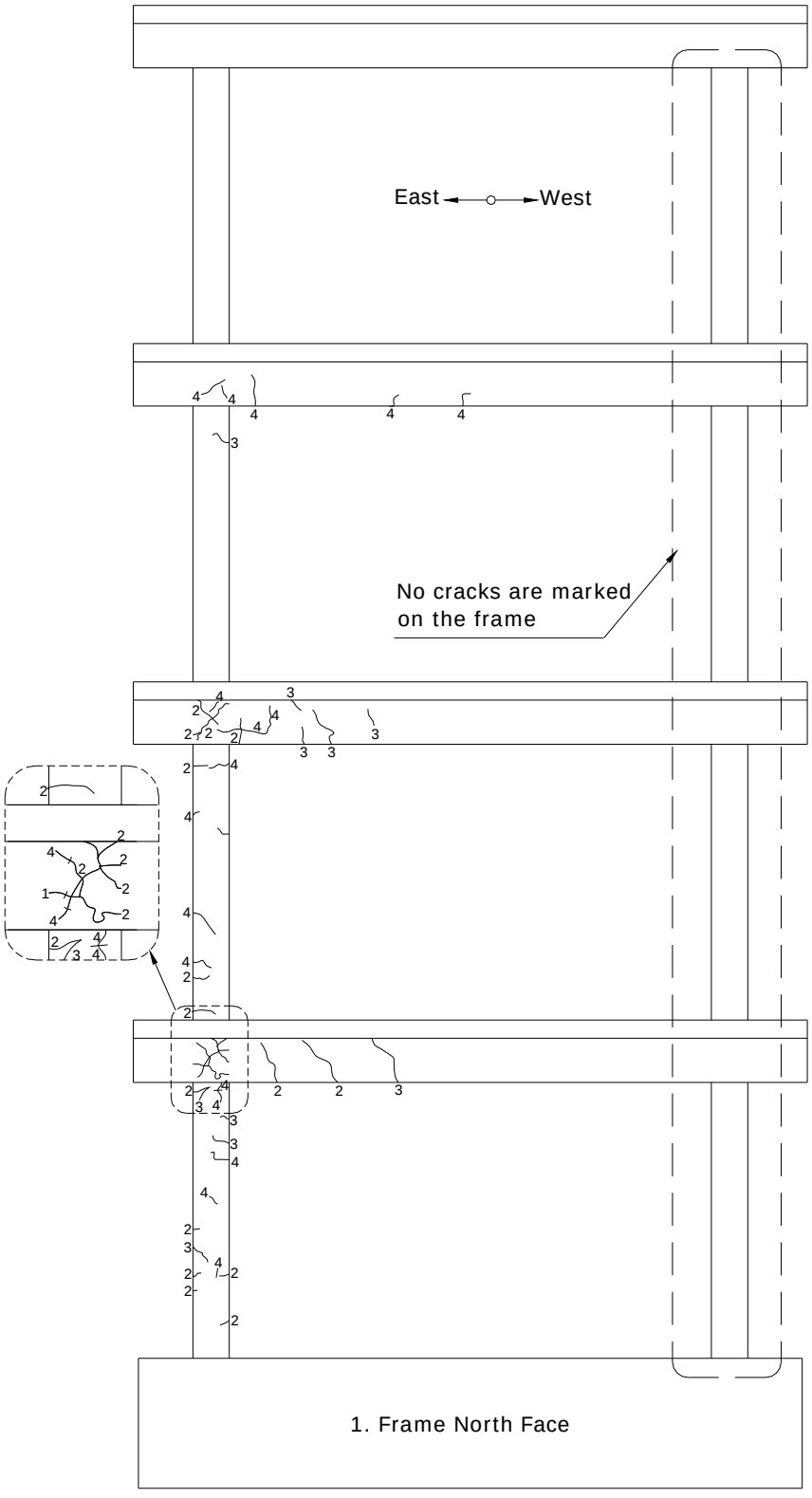

Figure C.2. First frame north face crack patterns

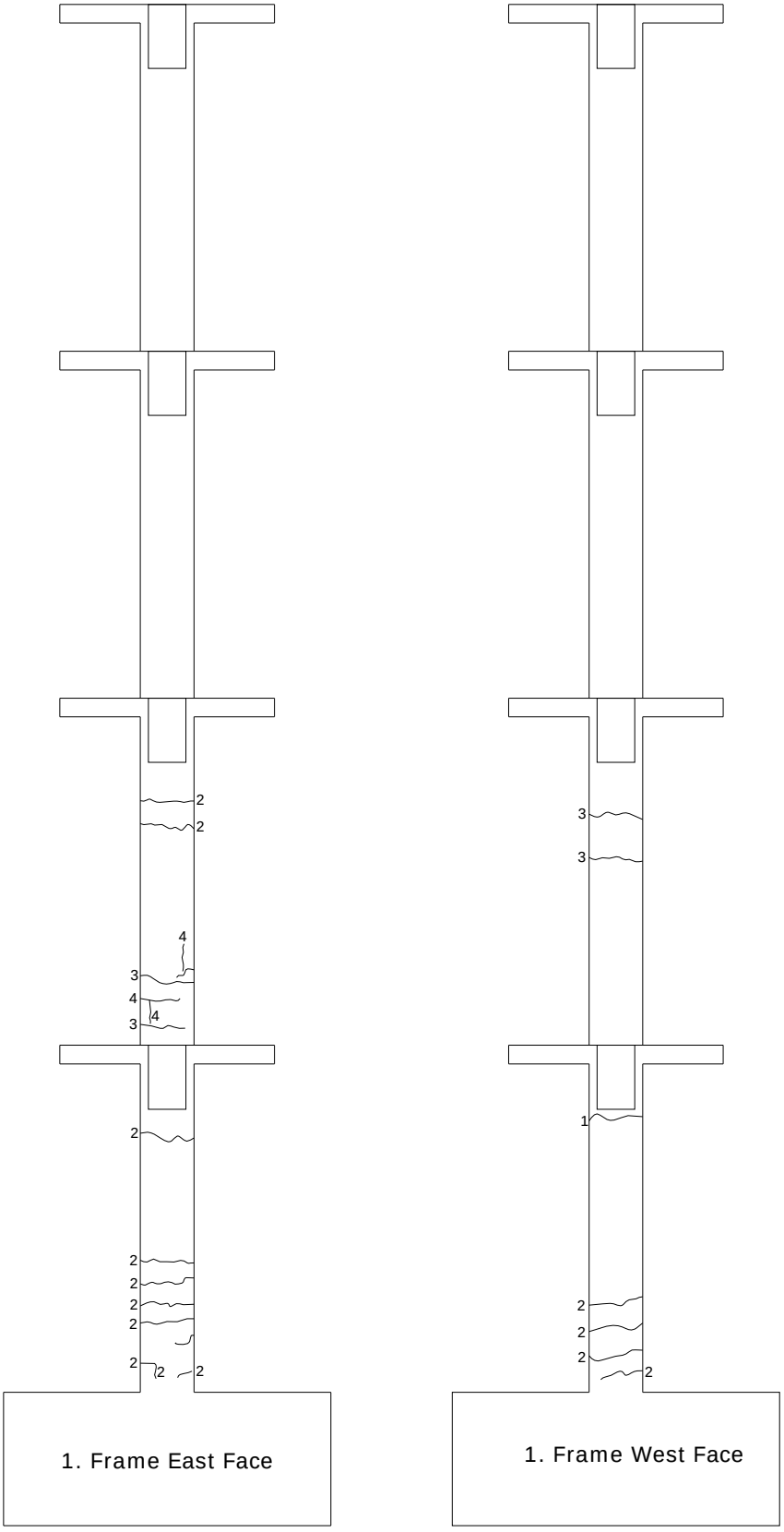

Figure C.3. First frame east (left) and west (right) face crack patterns

C.2 Second Frame Crack Patterns

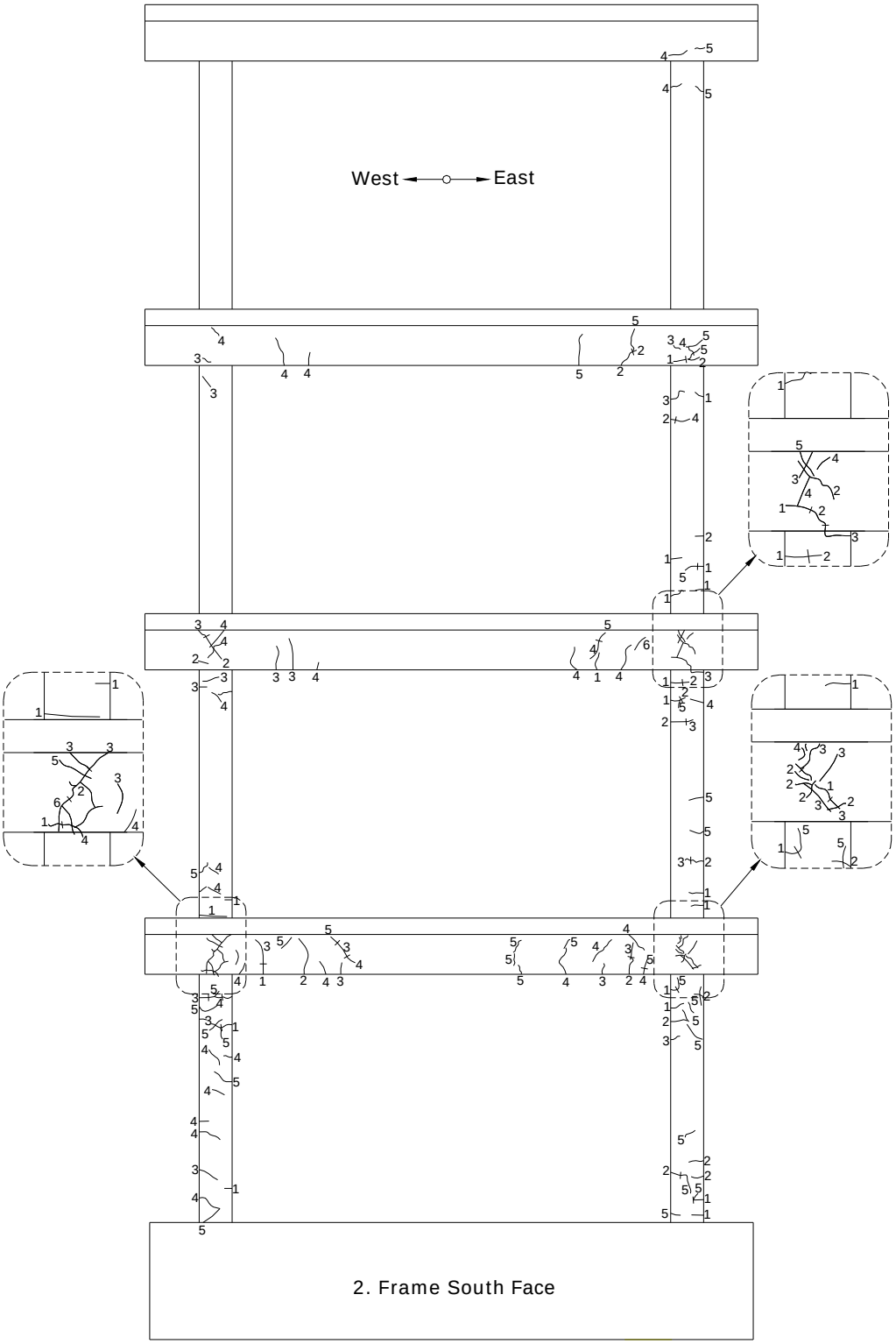

Figure C.4. Second frame south face crack patterns

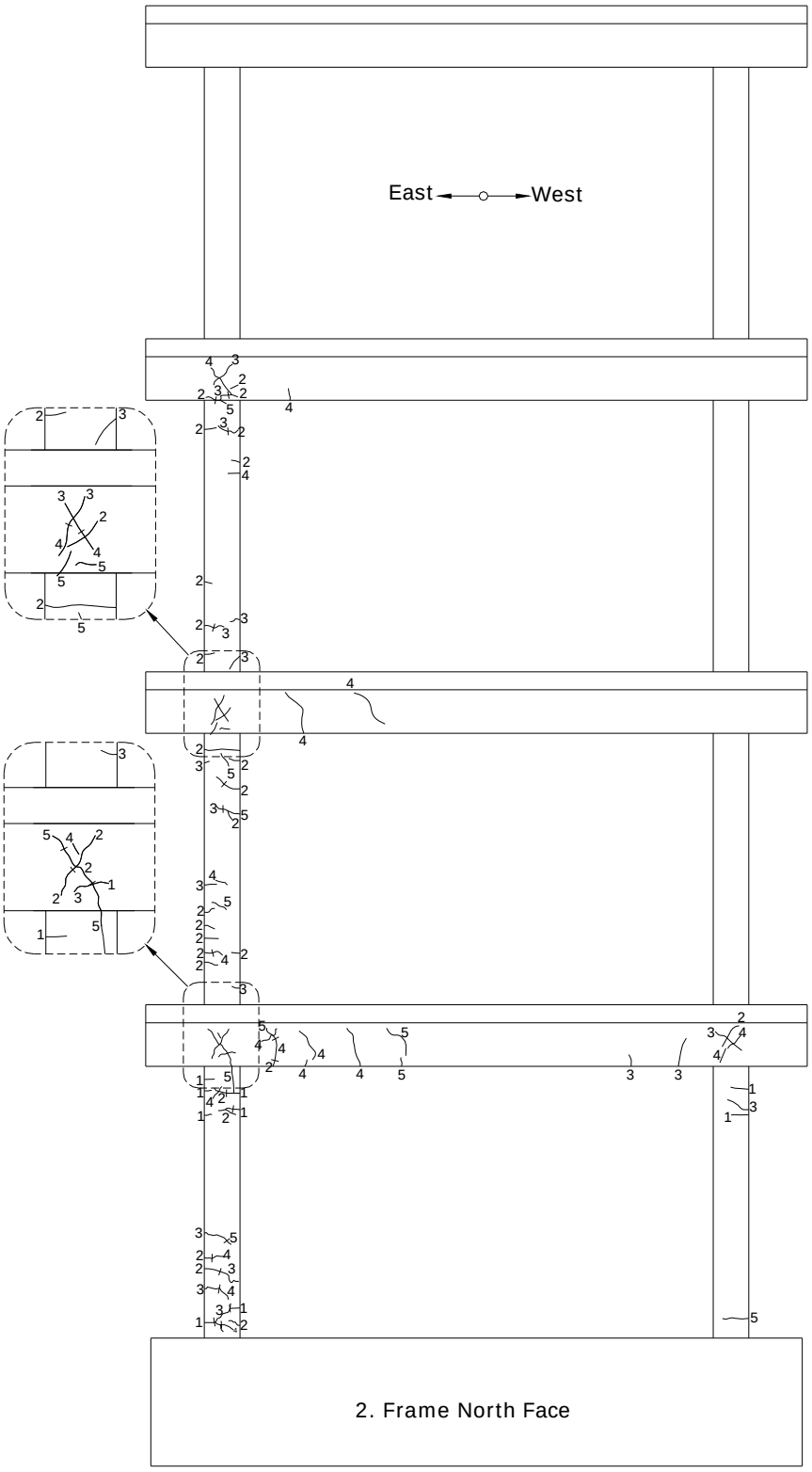

Figure C.5. Second frame north face crack patterns

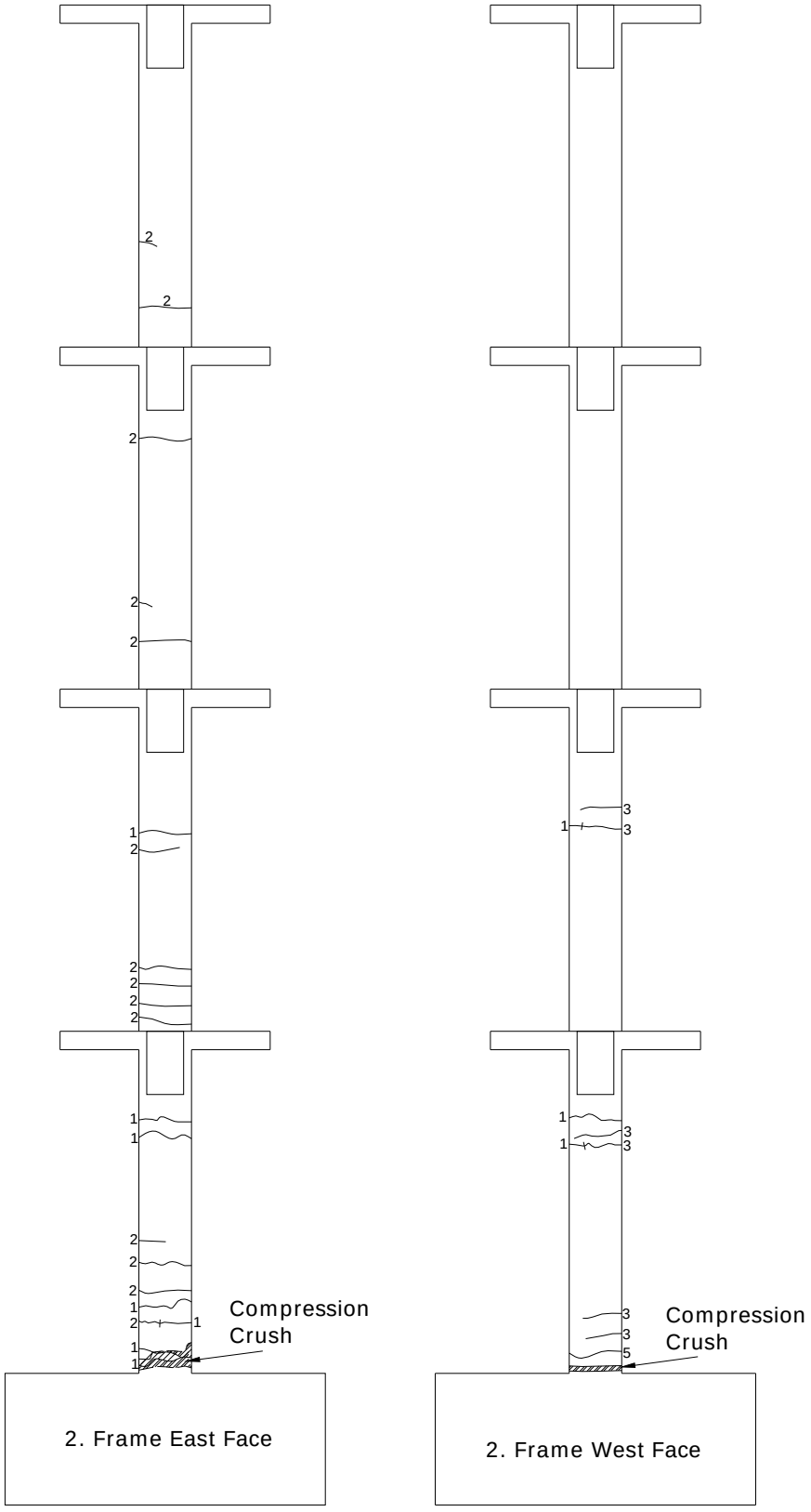

Figure C.6. Second frame east (left) and west (right) face crack patterns

C.3 Third Frame Crack Patterns

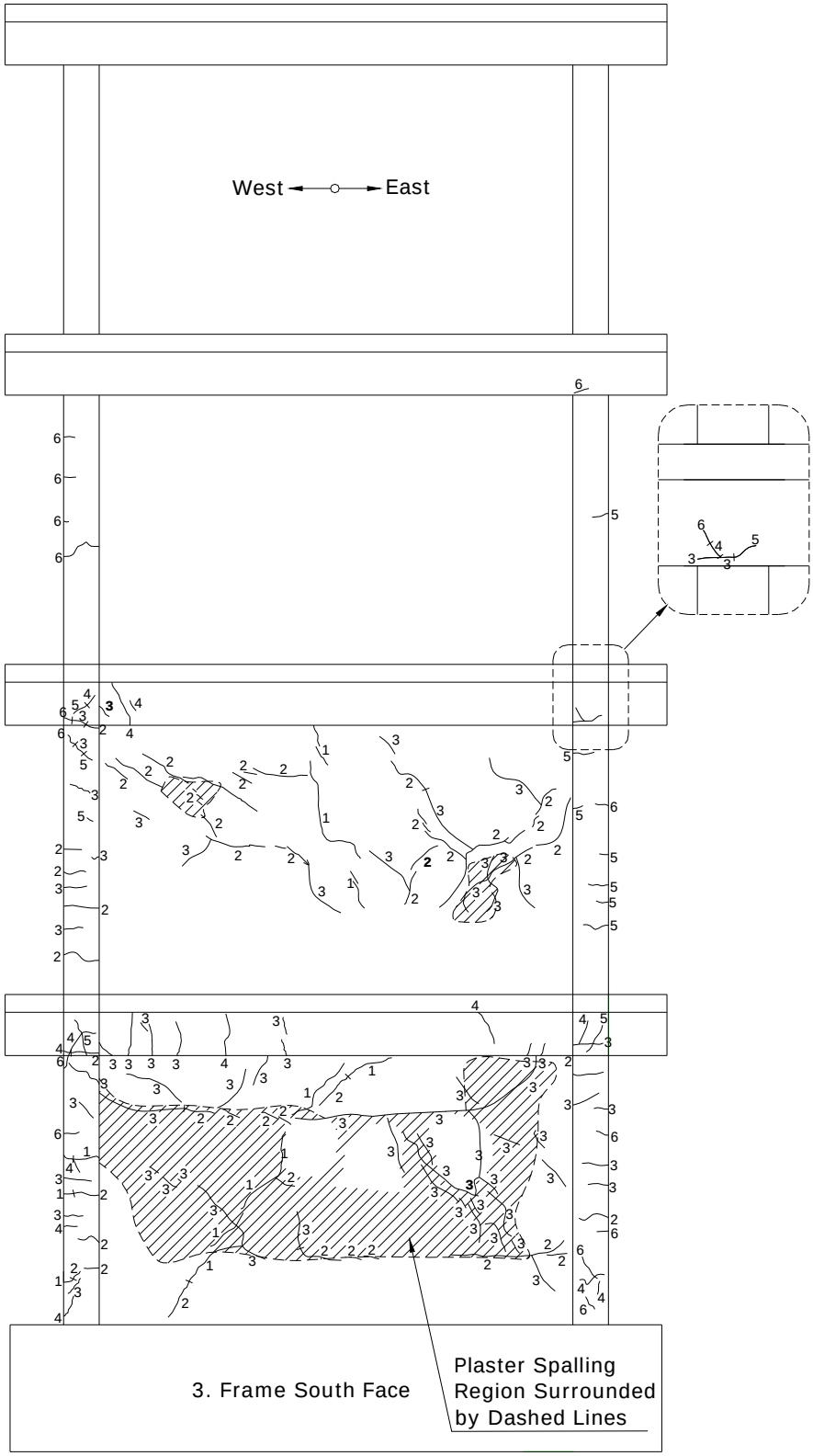

Figure C.7. Third frame south face crack patterns

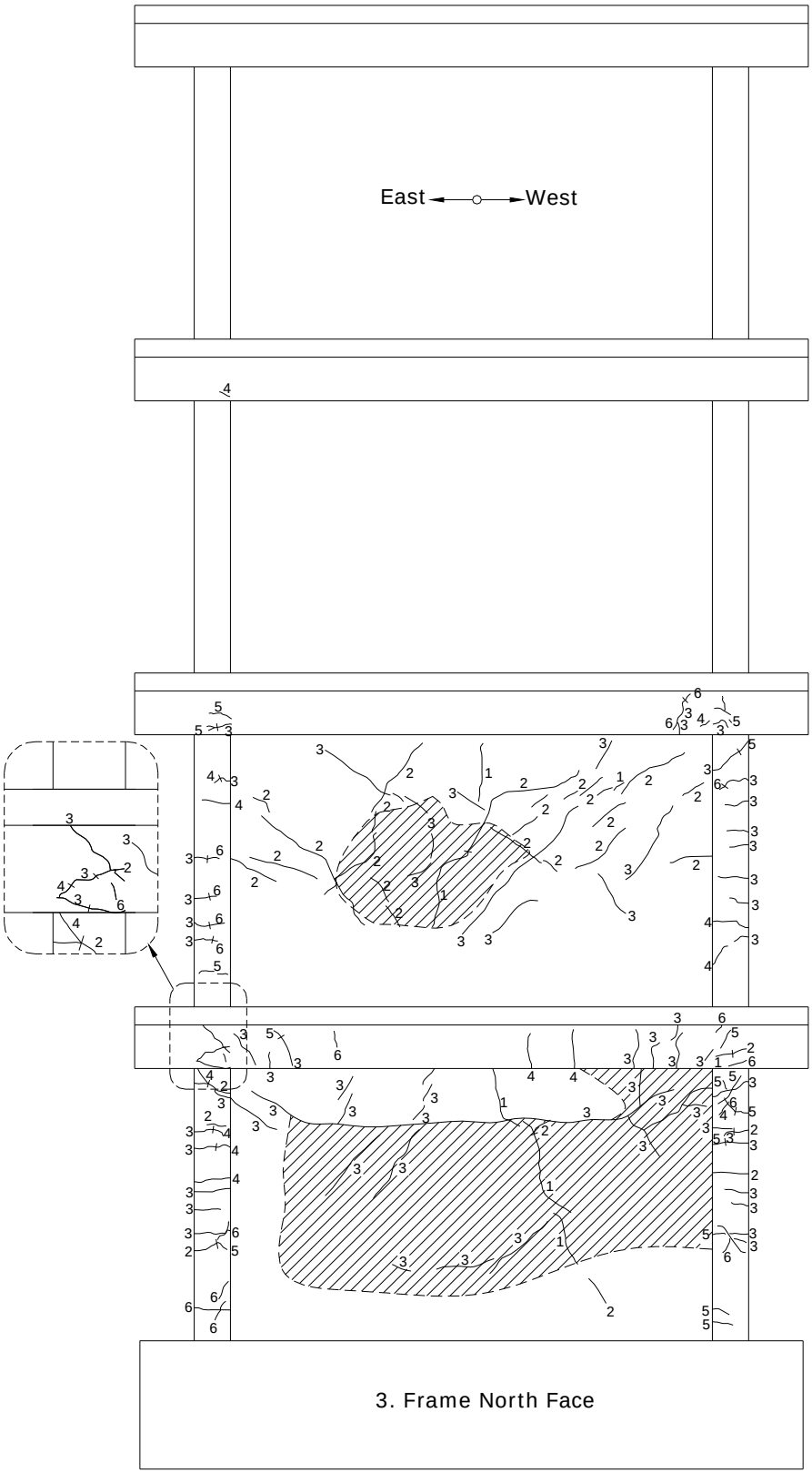

Figure C.8. Third frame north face crack patterns

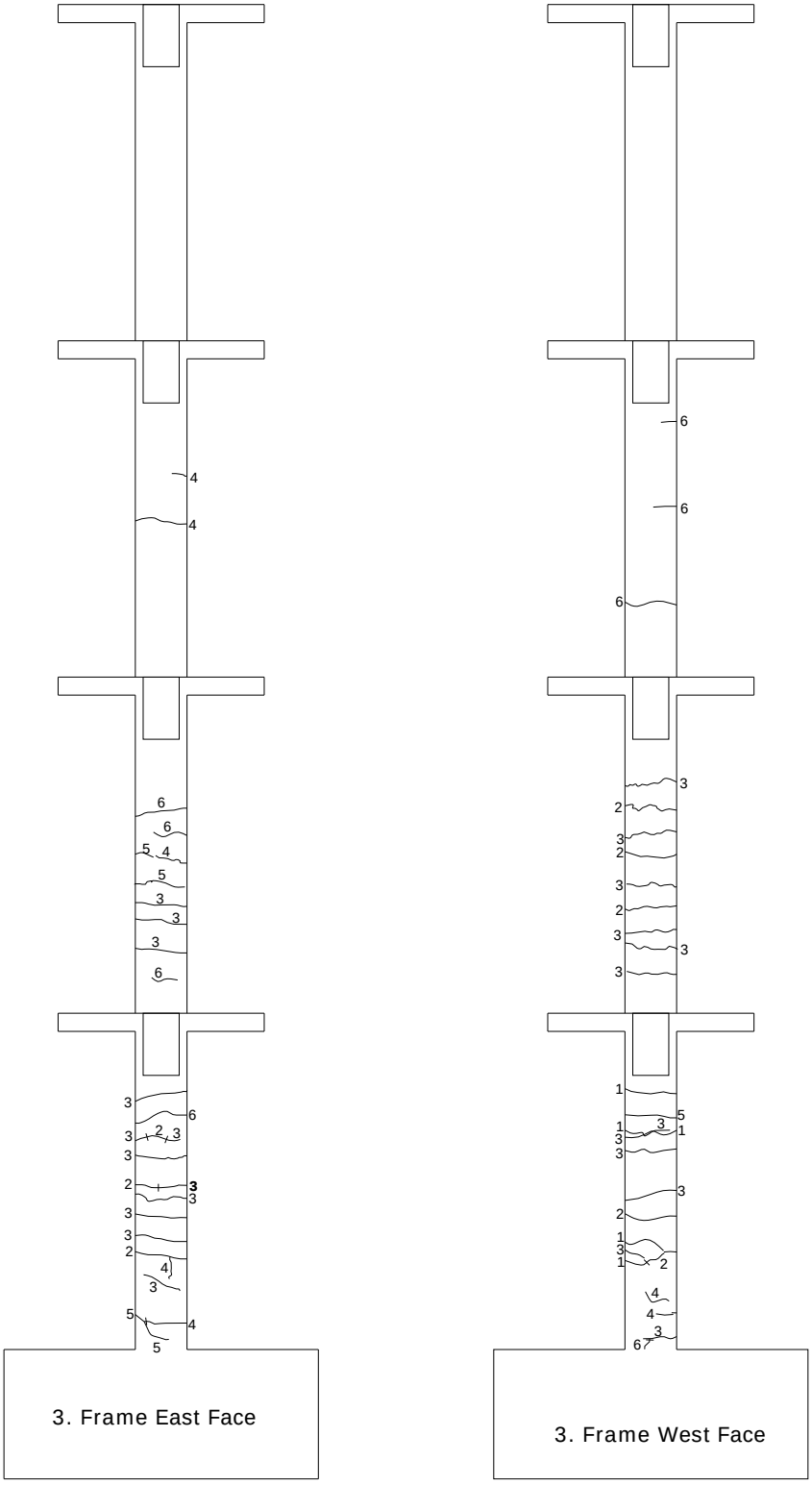

Figure C.9. Third frame east (left) and west (right) face crack patterns

C.4 Fourth Frame Crack Patterns

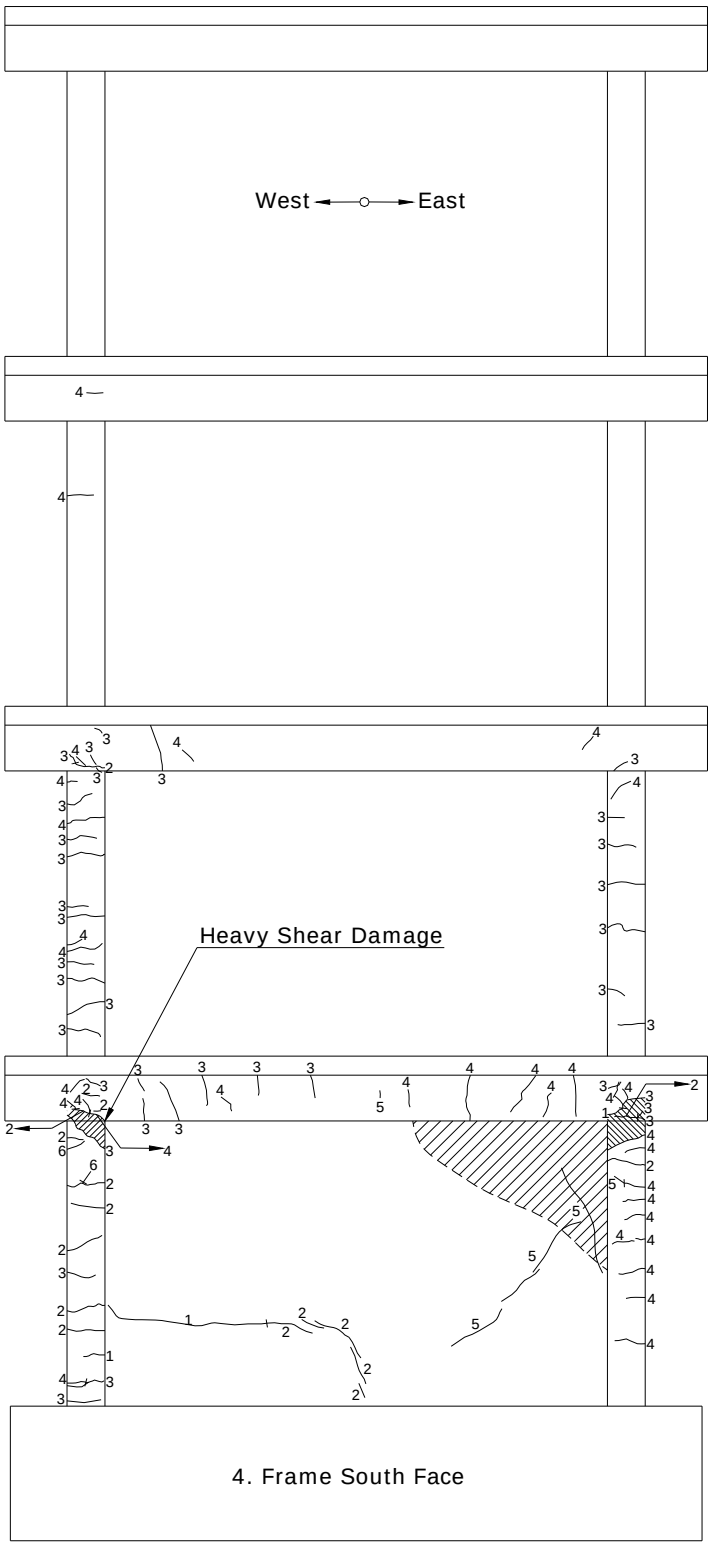

Figure C.10. Fourth frame south face crack patterns

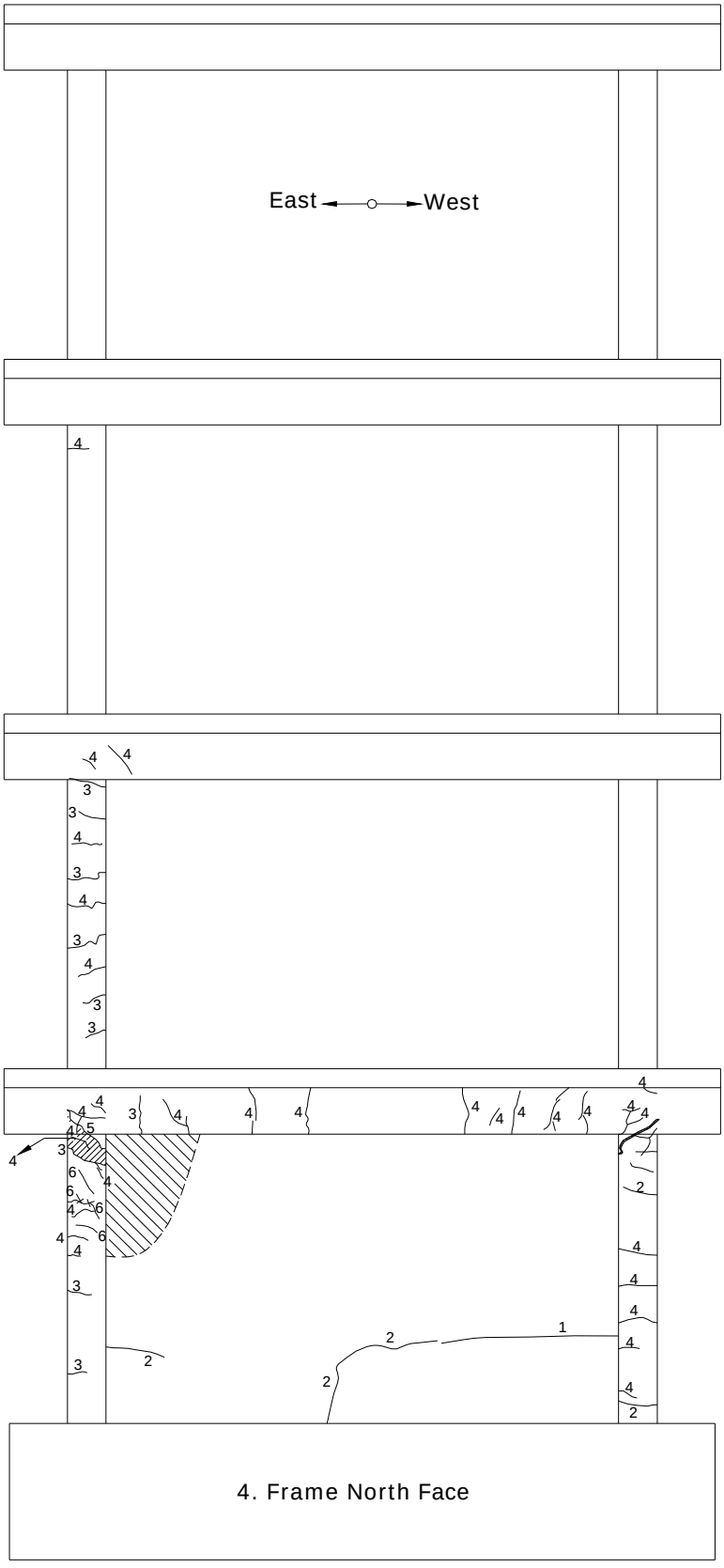

Figure C.11. Fourth frame north face crack patterns

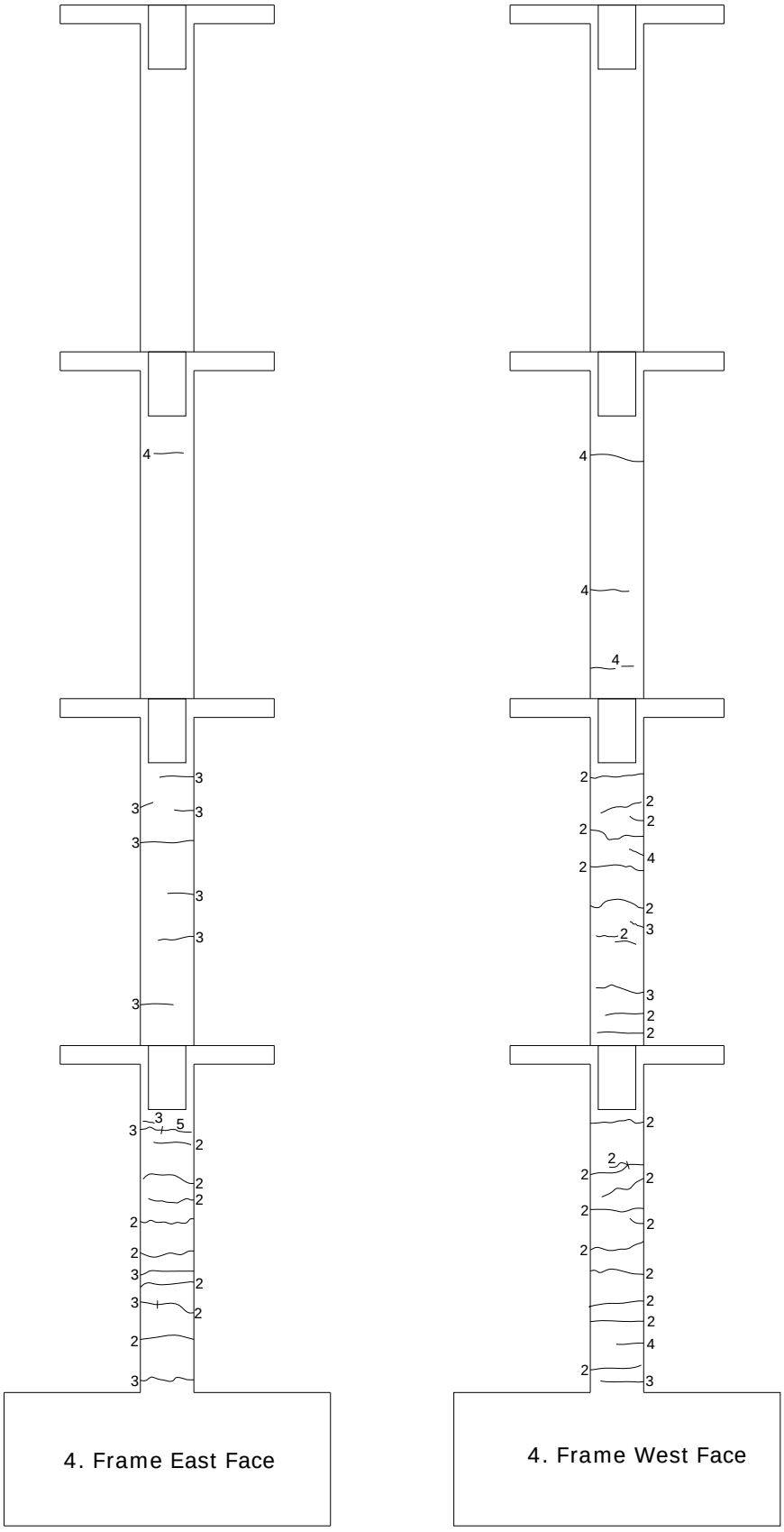

Figure C.12. Fourth frame east (left) and west (right) face crack patterns